

# **AN EXPERIMENTAL STUDY OF MIDDLE-EAR VIBRATIONS IN GERBILS**

Department of Biomedical Engineering  
McGill University  
Montréal, Québec

August 2009

A thesis submitted to the Faculty of Graduate Studies and Research in partial  
fulfilment of the requirements of the degree of

Master of Engineering

© Shruti Nambiar, 2009

## ABSTRACT / RÉSUMÉ

The Mongolian gerbil has been widely used in middle-ear research, as it is low in cost and has easily approachable middle-ear structures. The goal of this study was to present vibration measurements of the gerbil tympanic membrane. A single-point laser Doppler vibrometer was used to measure displacement frequency responses in twelve gerbils at multiple points on the tympanic membrane. A sinusoidal sweep excitation was used to perform the vibration measurements. Displacements at the umbo, normalized with respect to the sound pressure level measured near the tympanic membrane, are presented over the frequency range from 0.2 to 10 kHz, and compared with measurements published in the literature. Displacements at multiple locations on the pars flaccida and pars tensa are also presented, and the variability and repeatability of the measurements are investigated.

La gerbille de Mongolie est de plus en plus utilisée dans la recherche sur l'oreille moyenne, car elle est peu coûteuse, et les structures de son oreille moyenne sont facilement accessibles. Le but de cette étude est de présenter des mesures de vibrations du tympan de la gerbille. Des réponses fréquentielles des déplacements furent acquises à l'aide d'un vibromètre à laser Doppler Polytec, dans douze gerbilles à plusieurs points sur le tympan. Un stimulus à balayage sinusoïdal fut employé. Des déplacements à l'umbo, normalisés par le niveau de pression acoustique mesuré près du tympan, sont présentés dans la gamme de fréquence de 0.2 à 10 kHz, et comparés aux mesures publiées dans la littérature. Des déplacements à plusieurs endroits sur le pars flaccida et le pars tensa sont aussi présentés, et la variabilité et la répétabilité des mesures sont étudiées.

## ACKNOWLEDGEMENTS

I express my deepest gratitude and thanks to my supervisor, Professor W. Robert J. Funnell for his guidance throughout the years of my Masters. His patience, comments and teaching have made this thesis possible. I deeply appreciate his cooperation and willingness to review multiple drafts of this manuscript at short notice and late hours. His ethics, professionalism, integrity and research intellect have provided me precious learning both professionally and personally.

I thank my co-supervisor Dr. Sam J. Daniel, for his help and support throughout the course of my thesis work. I also thank Sophia and Dan for their assistance and valuable input during my days with the gerbils.

The love, support and encouragement from my dear husband, Ratish and my beloved family members have always enabled me to withstand challenges both at work and in life. I dedicate my work to them.

This thesis would not have been a real fulfillment without the backing and cooperation from my friends and colleagues.

I humbly offer this work to the almighty God whose blessings allow me to bring purpose to the life He has granted me.

This work was supported by the Canadian Institutes of Health Research, the Fonds de recherche en santé du Québec, the Natural Sciences and Engineering Research Council Canada, the Montréal Children's Hospital Research Institute and the McGill University Health Centre Research Institute.

# TABLE OF CONTENTS

<b>CHAPTER 1: INTRODUCTION</b>	<b>1</b>
1.1 Background	1
1.2 Research objectives	2
1.3 Thesis outline	3
<b>CHAPTER 2: THE AUDITORY SYSTEM</b>	<b>4</b>
2.1 Introduction	4
2.2 Overview of hearing	4
2.2.1 Physics of sound	4
2.2.2 Perception of sound	4
2.3 Human middle ear	6
2.3.1 Tympanic membrane	6
2.3.2 Ossicles	8
2.3.3 Other middle-ear structures	9
2.4 Gerbil middle ear	10
2.5 Middle-ear mechanics	11
2.5.1 Axis of rotation	11
2.5.2 Role of the middle ear	12
2.5.2.1 Surface area ratio	13
2.5.2.2 Ossicular lever ratio	13
2.5.2.3 Tympanic-membrane curvature	14
<b>CHAPTER 3: PREVIOUS STUDIES</b>	<b>15</b>
3.1 Introduction	15
3.2 Non-gerbil studies	15
3.2.1 Introduction	15
3.2.2 Tympanic membrane vibration patterns	15

3.2.3 Ossicular motion	18
3.2.4 Middle-ear cavity	20
3.3 Gerbil studies	21
3.3.1 Static pressure deformations	21
3.3.2 Vibration measurements	23
3.3.3 Finite-element models	28
3.4 Conclusion	30
<b>CHAPTER 4: MATERIALS AND METHODS</b>	<b>32</b>
4.1 Introduction	32
4.2 Specimen preparation	32
4.3 Experimental set-up	34
4.3.1 Acoustical system	34
4.3.2 Fixation device	37
4.3.3 Laser Doppler vibrometer	39
4.3.3.1 The principles of LDV	39
4.3.3.2 Hardware and software	43
4.4 Overview of measurements	43
4.4.1 Sound pressure level	45
<b>CHAPTER 5: RESULTS</b>	<b>47</b>
5.1 Introduction	47
5.2 Vibrations at the umbo	47
5.2.1 Displacement frequency response	47
5.2.2 Inter-specimen variability	49
5.2.3 Repeatability	50
5.2.4 Open/closed bulla configuration	59
5.2.5 Comparison with previous studies	63
5.3 Manubrial vibrations	66

5.4 Pars-flaccida vibrations	73
5.5 Pars-tensa vibrations	75
<b>CHAPTER 6: CONCLUSION</b>	<b>82</b>
6.1 Summary	82
6.2 Future work	84
<b>REFERENCES</b>	<b>86</b>

# CHAPTER 1

## INTRODUCTION

### 1.1 Background

Hearing loss can be defined as a total or partial inability to hear sound in one or both ears. It has been estimated that about one tenth of the world population suffers from mild or worse hearing loss (Swanepoel, 2008). It is also one of the most common abnormalities present at birth and, if undetected at the early stages, can impede speech, language and cognitive development. Hence, there is an increasing demand for early diagnosis of such defects.

The middle ear plays a major role in hearing and is often the site of infections, pathologies, congenital defects and other problems that contribute to hearing loss. The middle ear consists of an air-filled cavity, a tympanic membrane (TM), and a chain of bones connecting the TM to the inner ear, as well as ligaments, muscles and other structures. Any defect in this pathway would lead to hearing impairment. Better understanding of middle-ear mechanics will allow better diagnosis and treatment of middle-ear disorders. For this purpose, many groups have used both experimental and modelling techniques in middle-ear research. Experimental studies in animal models have revealed certain characteristics of the middle ear in response to sound pressure, to static or quasi-static pressure, and to experimentally induced lesions, thereby providing information otherwise unavailable in a normal clinical setting.

Mathematical models are useful in interpreting experimental data and in providing additional insight. Finite-element modelling was first introduced into middle-ear research by Funnell in 1975 and since then it has become a very popular tool in studying middle-ear mechanics. The model parameters have direct relationships to the structure and material properties of the system. Several finite-element models have been developed to gain a quantitative understanding of the TM and ossicles in humans (Wada et al., 1992; Beer et al., 1999; Bornitz et al., 1999; Prendergast et al., 1999; Koike et al., 2002; Sun et

al. 2002) and in other species (Funnell, 1975; Rabbitt and Holmes, 1986; Funnell et al., 1987; Funnell and Ladak, 1996; Elkhouri et al., 2006; Tuck-Lee et al., 2008).

Experimental measurements and mathematical modelling complement one another in developing a quantitative understanding of middle-ear mechanics. Among the many tools used in experimental middle-ear research, laser Doppler vibrometer (LDV) has emerged as a potent, non-invasive tool that permits real-time acquisition of dynamic vibrational data over a wide range of audio frequencies. Many groups have investigated the use of LDV for studying the motion of the middle-ear ossicles in human cadavers (e.g., Vlaming & Feenstra, 1986; Huber et al., 1997; Nishihara & Goode, 1997; Nakajima et al., 2005) and other species (e.g., Buunen & Vlaming, 1981; Doan et al., 1996; Bigelow et al., 1996 & 1998; Akache et al., 2007). Studies have also been conducted on live human ears, indicating plausible diagnostic uses of LDV (Goode et al., 1996; Rodriquez Jorge et al., 1997; Huber et al. 2001; Kenneth et al., 2004; Rosowski et al., 2008).

## **1.2 Research objectives**

The goal of our research is to characterize the mechanics of the gerbil middle ear by acquiring LDV measurements at multiple points on the TM. The Mongolian gerbil in particular has become a popular species for experimental research in auditory sciences. This is in part due to the fact that they have prominent middle-ear structures that allow easy accessibility and manipulation.

Most experimental studies in middle-ear research have involved measurements from relatively few points on the TM and the ossicles. For a complete understanding of the system we need information from more points. In our study we acquired displacement measurements from multiple points on the gerbil TM. The motion of the TM in response to a sound stimulus over a range of frequencies (0.2 to 10 kHz) was measured using a single-point LDV. The frequency responses were then analyzed to study the underlying

mechanics of the system. Measurements at multiple points revealed spatial characteristics of the TM motion that had not been reported for the gerbil. This study also includes the effect of an open middle-ear cavity on the vibrations of the gerbil TM.

### **1.3 Thesis outline**

A brief review of the anatomy and mechanics of the middle ear is presented in Chapter 2. Chapter 3 provides a summary of previous studies relevant to our animal model. The methods and materials used in this study are presented in Chapter 4 followed by our experimental results in Chapter 5. Conclusions and future directions are presented in Chapter 6.

## CHAPTER 2

# THE AUDITORY SYSTEM

### 2.1 Introduction

In this chapter an overview of the auditory system is presented. We begin with the basics of hearing physiology and sound perception in Section 2.2 followed by a brief explanation of the anatomy of the human middle ear in Section 2.3. Structural differences between the gerbil ear and the human ear are presented in Section 2.4, and finally middle-ear mechanics are discussed in Section 2.5.

### 2.2 Overview of hearing

#### 2.2.1 Physics of sound

Sound waves can be defined as a series of compressions and rarefactions caused by mechanical stimuli. They can propagate through almost any material medium, at a speed characteristic of that medium. Sound is typically generated by mechanical vibrations of a sound source such as human vocal cords, strings of a guitar, a vibrating tuning fork or the membrane of an audio speaker. A vibrating object displaces the particles of the surrounding medium. This results in alternations of sound pressure, causing the sound wave to travel through the medium.

#### 2.2.2 Perception of sound

In humans, sound waves are perceived when mechanical vibrations are converted into electrical impulses that are then interpreted by the brain. Perception depends on characteristics of the sound waves such as frequency, wavelength, amplitude, intensity, speed and direction. As shown in Figure 2.1, the human ear has three components: (i) outer ear, (ii) middle ear, and (iii) inner ear. The **outer ear** consists of the externally visible part (pinna) and the auditory canal (external ear canal). The pinna is designed to collect the sound and funnel the sound energy into the auditory canal. The second

component, the **middle ear**, consists of an air-filled chamber, a tympanic membrane (TM, or eardrum) and a chain of three interconnected ossicles (malleus, incus and stapes), as well as ligaments and muscles. The **inner ear** consists of the liquid-filled cochlea and the vestibular system. A sound wave from the external ear canal induces a mechanical stimulus on the TM. The vibrational displacement of the TM and the ossicles results in propagation of the sound energy through the middle ear to the oval window, the boundary with the inner ear. The inner ear is responsible for the conversion of the mechanical energy of the sound waves to electrical impulses which are sent by the auditory nerve to the brain. The brain then interprets these signals as sound.

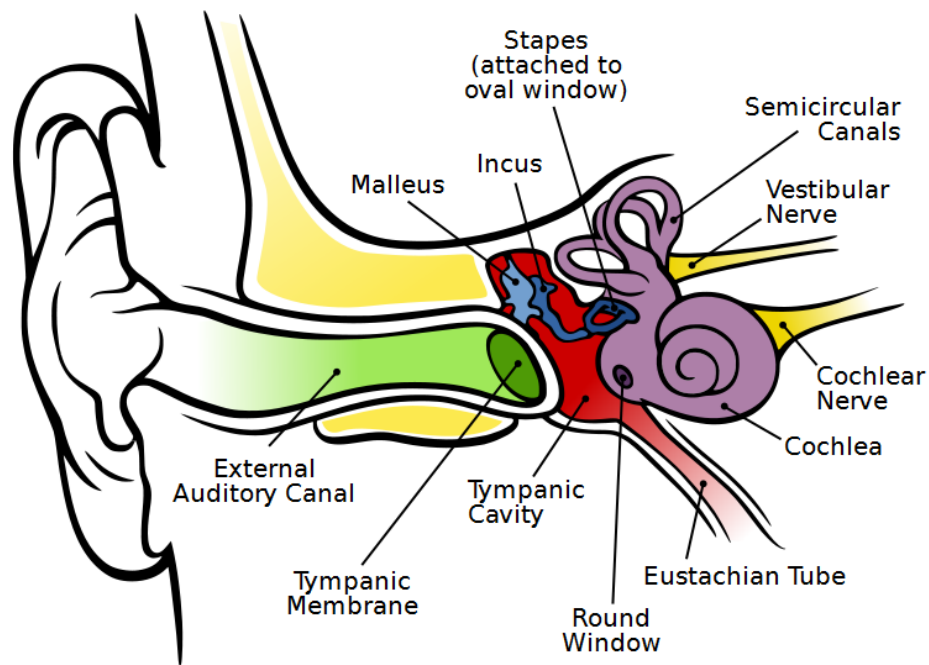


Figure 2.1: Anatomy of the human ear (Source: <http://en.wikipedia.org/wiki/Ear> as of 14 Dec 2009)

## 2.3 Human middle ear

### 2.3.1 Tympanic membrane

The TM is a roughly conical, thin membrane that separates the external ear from the tympanic cavity. As shown in Figure 2.2, in humans the TM consists of the pars tensa and the pars flaccida. The latter is located superior to the pars tensa. The pars tensa region occupies most of the TM. The manubrium (handle) of the malleus is attached to the medial side of the TM and extends down to the umbo (Figure 2.2). The TM is anchored to a bony ring (also known as the tympanic annulus) by the fibrocartilaginous ring. Kuypers et al. (2005) estimated the thickness of human TM using confocal microscopy (Figure 2.3). They concluded that the TM had maximum thickness near the annulus and near the manubrium, and that the overall thickness of the remaining portion was approximately constant. They studied three human TMs and found mean thickness values of 120, 50, and 40  $\mu\text{m}$ , indicating the presence of a large inter-specimen variation.

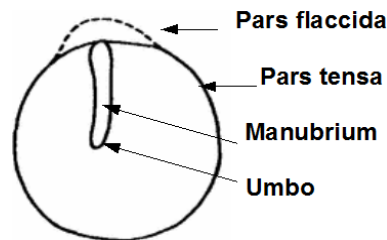


Figure 2.2: Human tympanic membrane (Modified after: [http://audilab.bmed.mcgill.ca/~funnell/AudiLab/teach/me\\_saf/me\\_saf.html](http://audilab.bmed.mcgill.ca/~funnell/AudiLab/teach/me_saf/me_saf.html))

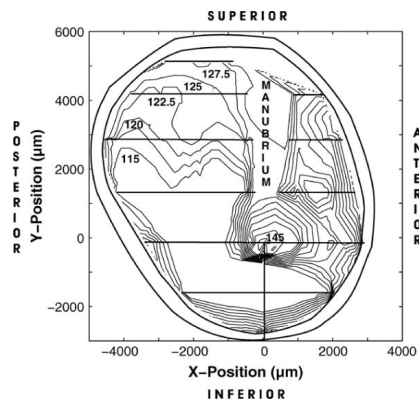


Figure 2.3: Contour map of the thickness distribution of a human TM (From Kuypers et al., 2005)

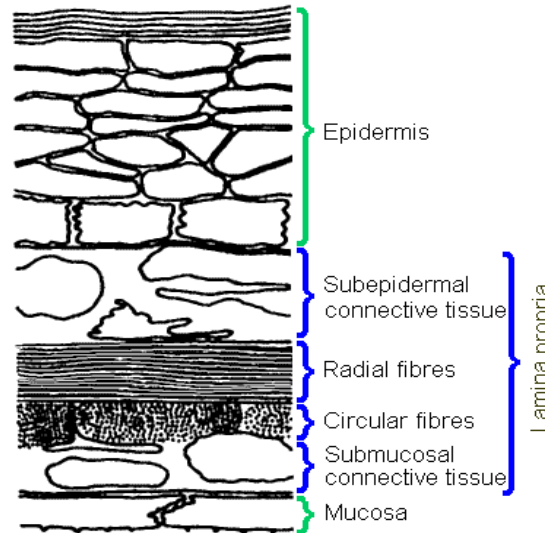


Figure 2.4: Structure of the tympanic membrane.  
 (Source: [http://audilab.bmed.mcgill.ca/~funnell/AudiLab/teach/me\\_saf/me\\_saf.html](http://audilab.bmed.mcgill.ca/~funnell/AudiLab/teach/me_saf/me_saf.html))

As shown in Figure 2.4, the pars tensa consists of multiple layers (Lim 1968 & 1970):

- i. **Mucosal** layer on the medial side
- ii. **Epidermal** layer on the lateral side
- iii. **Lamina propria** that forms the intermediate layer and itself consists of four layers

The subepidermal and submucosal connective-tissue layers are found next to the epidermal and mucosal layers respectively. The radial and circular fibrous layers of the lamina propria lie between these loose connective-tissue layers. The radial layer consists of collagen fibrils that radiate outward from the manubrium to the annulus. The circular layer consists of fibres that are more or less concentrically arranged around the manubrium. These fibrous layers are responsible for the mechanical stiffness characteristics of the pars tensa region.

In all species, the pars flaccida is smaller, thicker and floppier than the pars tensa. It lacks the highly organized fibrous layers of the lamina propria.

### 2.3.2 Ossicles

A chain of three small bones (or ossicles) is attached at one end to the TM and at the other end to the cochlea. This chain consists of the malleus, the incus and the stapes. The malleus is so named for its resemblance to a hammer and it consists of a head, a neck and three processes: the anterior process, the lateral process and the manubrium (Figure 2.5). The manubrium is attached to the medial side of the TM. Its size decreases towards the inferior end, then it flattens and curves slightly towards the ear canal. This region corresponds to the umbo. A portion of the head of the malleus connects to the incus. The incus, or anvil, so named because it is acted upon by the hammer, has two processes: a short process and a long process (Figure 2.6). At the inferior end of the long process is the lenticular process, which articulates with the head of the stapes. The stapes, so called for its resemblance to a stirrup, is the smallest bone in the human body. It consists of a head, a neck, two crura and a base (Figure 2.7). The two crura (anterior crus and posterior crus) connect to the oval-shaped base (or, the footplate).

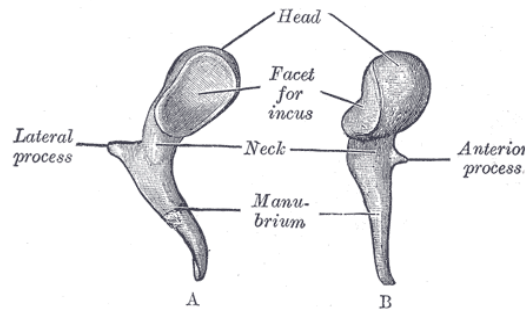


Figure 2.5: Anatomy of the malleus (Source: Gray, 2000)

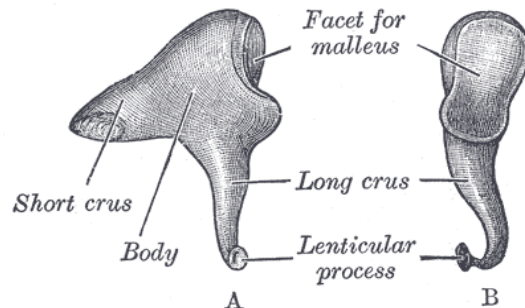


Figure 2.6: Anatomy of the incus (Source: Gray, 2000)

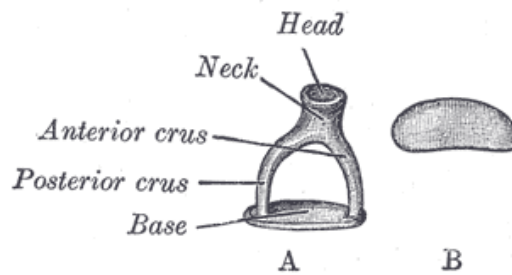


Figure 2.7: Anatomy of the stapes (Source: Gray, 2000)

### 2.3.3 Other middle-ear structures

Middle-ear joints, muscles and ligaments play important roles in the transmission of sound through the middle ear into the inner ear. The middle-ear ossicles articulate with each other by means of two synovial joints: (i) the incudo-malleolar joint connects anteriorly to the head of the malleus and posteriorly to the incus; (ii) the incudo-stapedial joint connects the convex surface of the lenticular process of the incus with the concave top of the stapes head. In addition to the attachment with the TM, the malleus is suspended by several ligaments of which appear to be variable in humans. The incus is anchored by three ligaments: the posterior incudal ligament, which secures the short crus of the incus to the cavity wall; and the medial and lateral incudomalleolar ligaments (alternatively considered to be part of the joint capsule), which secure the body of the incus to the head of the malleus.

Finally, the malleus also connects to one of the two middle-ear muscles, namely the tensor tympani muscle. This muscle is embedded in the medial wall of the tympanic cavity and its tendon is attached to the medial and anterior portion of the malleus neck and manubrium. The second muscle, the stapedius muscle, is the smallest skeletal muscle in the human body. Its tendon attaches to the posterior aspect of the stapes neck.

In a wide variety of species including human, recent studies have shown that the tympanic ring has an array of contractile elements, either myofibroblasts (Kuypers et al.,

1999) or smooth-muscle fibres (Henson and Henson, 2000; Henson et al., 2001a,b). The elements were found anchored to the cartilaginous annulus at one end, and to the radially oriented fibres of the pars tensa at the other end. Such an arrangement of contractile elements suggests a possible role in controlling blood flow and/or in regulating the tension on the TM (Yang & Henson, 2002).

The middle-ear structures described above are located within an air-filled middle-ear space. The middle-ear cavity can be subdivided into three compartments known as the epitympanum, the mesotympanum, and the hypotympanum. The epitympanum is the upper portion of the tympanic cavity and houses the head of the malleus and the body of the incus. The mesotympanum is the area located medial to the TM, housing parts of the malleus and incus, the stapes and the middle-ear muscles. The hypotympanum is located inferior to the TM.

## **2.4 Gerbil middle ear**

Mongolian gerbils (*Meriones unguiculatis*) have increasingly been used for auditory research over the past few decades (e.g., Cohen et al., 1993; Teoh & Rosowski et al., 1997; Olson, 1998; von Unge et al., 1999; Funnell et al., 1999 & 2000; Dirckx & Decraemer, 2001; Overstreet et al., 2003; Ravicz & Rosowski et al., 2004; Elkhouri et al., 2006; Ellaham et al., 2007). This is in part due to the large middle-ear structures found in these rodents. Although gerbils are relatively small (approximate body weight of 80-100 g), their middle ear is approximately half the size of the comparable structures found in humans (Kenneth et al., 1980). The human TM surface area is approximately 69 mm<sup>2</sup> (Weaver & Lawrence, 1954). For gerbils, Rosowski (1996) calculated the average TM surface area to be 14 mm<sup>2</sup>.

The gerbil middle ear is encased in a hypertrophied bony shell known as the bulla. The volume of the middle-ear air spaces in the enlarged bulla of these desert rodents is comparable to that of its brain case (Legoux and Wisner, 1955; Webster, 1965; Lay,

1972), as shown in Figure 2.8. Several investigators have postulated that the large tympanic membrane and middle-ear air spaces are responsible for the low-frequency hearing sensitivity observed in these animals (Legouix and Wisner, 1955; Webster, 1962; Rosowski et al., 1997). It has been established that this kind of auditory specialization helps the desert rodents to perceive the low-frequency sounds produced by approaching predators (Webster, 1965).

## 2.5 Middle-ear mechanics

### 2.5.1 Axis of rotation

Helmholtz (1868) suggested that the malleus-incus complex of the middle ear rotates around an axis that passes through the posterior incudal ligament (PIL) such that it is perpendicular to the line passing through the umbo and the lenticular process of the incus (Figure 2.9A). Later, Dahmann (1930) regarded the anterior malleolar ligament (AML) and the PIL as fixed points on the axis of rotation (Figure 2.9B). In support of Dahmann (1930), von Békésy (1960) suggested that the ossicles vibrate about their centre of mass, except at low frequencies for which mass effects are small, in which case they vibrate about an axis determined by the PIL and the AML. Studies have shown that the motion of the ossicles becomes more complicated at high frequencies (e.g., Gyo et al., 1987; Decraemer et al., 1991,1994a,b). Some of the complications include shifting of the axis of rotation, flexing of the manubrium, and relative motion between the malleus and incus. Studies related to TM vibrations will be presented in detail in Section 3.2.2.

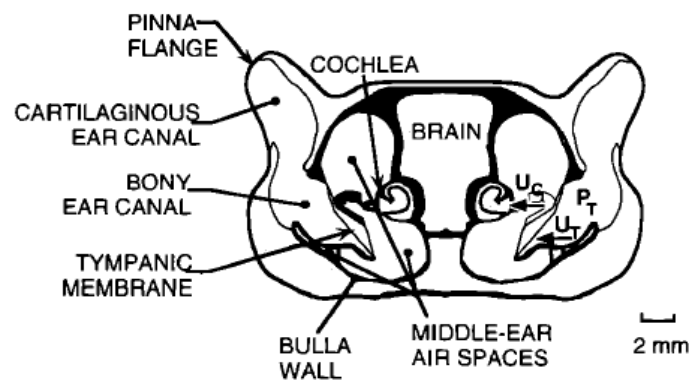


Fig. 2.8: A schematic of the coronal section of the gerbil head. (After Ravicz et al., 1992)

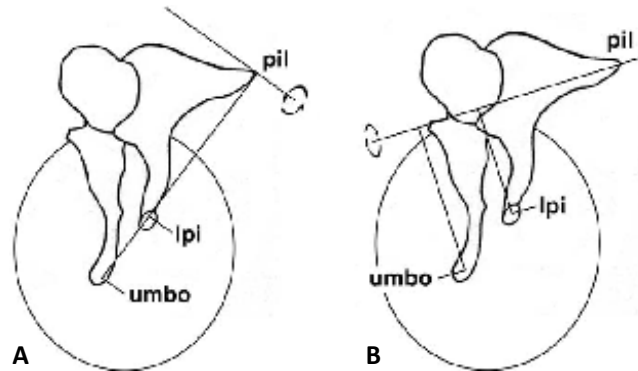


Figure 2.9: Lever ratio as conceived by (A) Helmholtz (B) Dahmann. (After Willi, 2003)

### 2.5.2 Role of the middle ear

As described in section 2.3, the TM is designed to transform air-pressure variations in the external ear canal into mechanical displacements and to transmit these vibrations to the ossicular chain. This transmitted energy is directed to the liquid-filled cochlea. The acoustic impedances of the air and of the cochlear liquid are very different. The acoustic impedance  $Z$  can be defined as the resistance of a medium through which an acoustic wave propagates. Mathematically, the impedance is the ratio of the sound pressure  $P$  to the volume velocity  $U$  (calculated as the particle velocity times a perpendicular surface area):

$$Z = \frac{P}{U}$$

Due to the difference between the acoustic impedances of air and liquid, the sound waves travelling from air to liquid would be partially reflected. The amount of sound energy reflected depends on the ratio of the impedances of the two media. At room temperature, the acoustic impedances of air and water are  $Z_a = 420 \text{ Pa}\cdot\text{s}/\text{m}$  and  $Z_l = 1.5 \text{ MPa}\cdot\text{s}/\text{m}$  respectively. For sound waves travelling from air to water, 99.9 % of the acoustic energy will be reflected back from an air-water interface and only 0.1% will be transmitted to the liquid. The middle ear is designed to overcome this energy-transmission loss by acting as a mechanical impedance-matching transformer that effectively transmits the original signal. This transformation can be thought of as a combination of three mechanical

principles: (i) the surface-area ratio of the TM and footplate, (ii) the lever ratio of the ossicular chain, and (iii) the curvature of the TM.

#### **2.5.2.1 Surface area ratio**

The pressure  $P$  exerted by a force  $F$  in a direction perpendicular to a flat surface of area  $A$  is defined by the ratio:

$$P = \frac{F}{A}$$

For effectively passing on the acoustic pressure from the external auditory meatus into the inner ear, the pressure collected over the tympanic membrane is multiplied by the ratio of the surface areas of the TM and the stapes footplate. Due to the larger surface of the TM and relatively smaller surface area of the stapes footplate, the pressure at the footplate must be greater than that at the TM.

Several investigators have estimated this ratio in humans and found various values in the range of 15 to 26 (Helmholtz, 1868; Fumagalli, 1949; Wever & Lawrence, 1954; Bekesy, 1960). Lay (1972) calculated this ratio to be 27.6 in gerbils. These ratios were estimated based on the geometric areas of the TM and the stapes footplate. However, the effective surface area of the TM contributing to the transformer ratio depends on its displacement distribution (Khanna & Tonndorf, 1972; Tonndorf & Khanna, 1972; Funnell, 1996).

#### **2.5.2.2 Ossicular lever ratio**

At low frequencies, the malleus and incus are assumed to function as a mechanical lever system rotating around a fixed axis of rotation as described earlier. As shown in Figure 2.9, the ossicular lever ratio is calculated as the ratio of the orthogonal distance from the axis of rotation to the umbo and the distance from the same axis to the lenticular process of the incus. This ratio has been estimated to be 1.31 in humans (Wever & Lawrence, 1954) and 3.32 in gerbils (Lay, 1972).

### 2.5.2.3 Tympanic-membrane curvature

Helmholtz (1868) proposed the outward convexity of the tympanic membrane as a mechanism for sound amplification. A slight change in the air pressure over the TM produces a slight change in its curvature leading to a change in the tension of the radial fibres that in turn generates a large force on the umbo (Figure 2.10). This theory was later supported by other studies (Esser, 1947; Guelke & Keen, 1949; Khanna & Tonndorf, 1972). Funnell (1996) found that certain regions of the TM were more effective than they would be without the curvature.

All three factors – TM/footplate area ratio, ossicular lever-arm ratio, and curvature-related transformation ratio – are interrelated and hence it is difficult to separate the force-transformation behaviour into distinct mechanisms (Funnell, 1996). The effective surface area of the TM and the curvature-related lever mechanism both depend on the geometry and material properties of the TM. All three types of mechanism are, thus, involved in determining the characteristics of the overall pressure-to-force transformation.

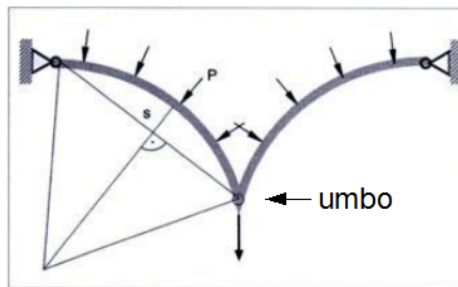


Figure 2.10: Mechanism of sound amplification as described by Helmholtz.  
(Modified after: Jahnke, 2004)

## CHAPTER 3

### PREVIOUS STUDIES

#### 3.1 Introduction

Various experimental techniques and mathematical models have been used to study middle-ear mechanics in both live and *post mortem* ears in a number of species. Our research involves the *post mortem* study of tympanic-membrane vibrations in gerbils. In this chapter a review of previous studies relevant to our research is presented. In Section 3.2, a review of human and other non-gerbil studies is presented. Section 3.3 addresses the experimental and modelling research that has been conducted on the Mongolian gerbil. Finally, Section 3.4 sums up some of the important conclusions derived from both experimental and modelling research on the vibrational motion of the gerbil tympanic membrane.

#### 3.2 Non-gerbil studies

##### 3.2.1 Introduction

Early studies on tympanic-membrane (TM) vibrations used a variety of different methods ranging from visual observations using a magnifying glass, mechanical and capacitive probes, high-speed cinematography, stroboscopic techniques and interferometric methods such as laser holography, speckle pattern interferometry and scanning laser interferometry. A comprehensive review of early experimental observations was presented by Funnell and Laszlo (1982). A brief overview of various techniques used to measure TM vibrations and ossicular motion in human and other species is presented in the sections below.

##### 3.2.2 Tympanic membrane vibration patterns

The mode of vibration of the eardrum was measured by Békésy (1941). He used a capacitive probe to map vibration amplitudes point-by-point over the face of a human TM

for an acoustic stimulus of 2000 Hz. Since then many studies have employed various techniques to explore eardrum vibration patterns in both human and animal models. Optical interferometry has emerged as a powerful tool to visualize and quantify spatial patterns of the entire eardrum. In 1972, Tonndorf and Khanna used time-averaged laser holography, a type of optical interference method, for the first time rendering a full-field picture of eardrum vibration patterns. In their study, holographic reconstructions characterize the vibration patterns of the human eardrum over a frequency range of 400 to 6000 Hz (Figure 3.1). Dark and bright fringes resulting from the holographic interference define iso-amplitude contours of vibration. In Figure 3.1, we see that the contours at low frequencies indicate a maximum vibration amplitude in the posterior region and another maximum of lower magnitude in the anterior region. As the frequency increases, the vibration patterns of the TM become much more complex. A similar study in cats revealed that the transition from simple to complex vibration patterns occurred at around the same frequencies as seen in the human ears (Khanna & Tonndorf, 1972).

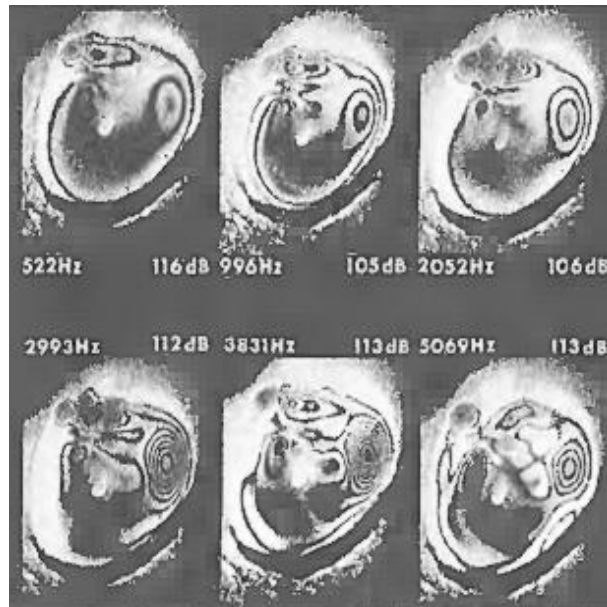


Figure 3.1: Time-averaged holograms for six frequencies between 500 and 5000 Hz. TM of left ear. Orientation: right = posterior, left = anterior. (Source: Tonndorf and Khanna, 1972)

Decraemer et al. (1997) reported vibration profiles of the cat TM measured with a laser interferometer, in response to pure tone acoustical stimulation over a frequency range of 0.2 to 23 kHz. They confirmed that at the lowest frequencies points on the TM vibrate in phase and the manubrium moves with an amplitude that is smaller than neighbouring points in the anterior and posterior regions of the TM. At higher frequencies (above 2.5 kHz) the vibration pattern breaks up into sectional zones of vibrations. Laser Doppler vibrometer measurements on the rat eardrum have been reported by our group (Akache et al., 2007). Of the multiple points measured on the eardrum, the displacements were found to be largest in the posterior region and smallest at the manubrium (Figure 3.2). Recently, Rosowski et al. (2009) used computer-assisted opto-electronic holography (OEH) to measure the vibrational patterns of TM motion in *post-mortem* human, cat and chinchilla ears. The holographic measurements were performed in two modes: time-averaged mode for fast characterization of frequency dependent TM vibration patterns, and stroboscopic mode for determination of the magnitude and phase of the motion of the entire surface of the TM. In all three species, the authors observed that the time-averaged holograms contained simple, complex and ordered fringe patterns depending on the sound frequency (500 to 20000 Hz).

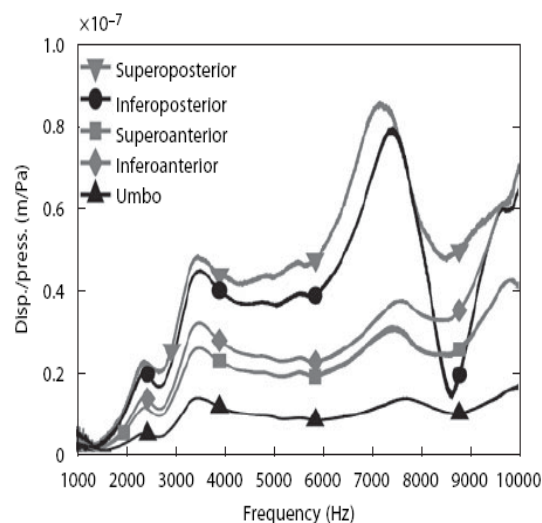


Figure 3.2: Tympanic membrane displacements in a rat model. Disp./press. = Displacement/Pressure. (Source: Akache et al., 2007)

Phase-shift moiré topography, another type of interferometric method, was first used by Dirckx and Decraemer (1991) to observe full-field shape deformations of the human TM in response to large static pressures. Similar to vibration patterns in response to sound pressure, the authors observed displacement maxima in both the anterior and posterior regions of the TM. Their study also demonstrated a strong asymmetry between medial and lateral movements of the eardrum, which is not observed in small-amplitude vibrations.

### **3.2.3 Ossicular motion**

The motion of the incudo-malleal complex was traditionally described as a simple rigid rotation around a fixed axis (e.g., Dahmann, 1930; Stulhman, 1937; Bárány, 1938; Békésy, 1939; Wever & Lawrence, 1954; Tonndorf and Khanna, 1972). Using time-averaged holographic measurements on human TM's, Gundersen and Høgmoen (1976) concluded that the movement of the ossicles was like that of a lever moving about a frequency-dependent axis of rotation. [Buunen and Vlaming (1981) used LDV to measure the umbo vibrations in response to a pressurized ME cavity. It does not fit the context here, so I have removed the ref.] Using a stroboscopic illumination technique along with a video measuring system, Gyo et al. (1987) observed that the measured ossicular-lever ratio increased at higher frequencies ( $> 2$  kHz), which they attributed to a shifting of the axis of rotation. Using a superconducting quantum interference device (SQUID) magnetometer, Brenkman (1987) measured displacement responses of human temporal bones and found that the transformer ratios varied across frequencies. They concluded that such a discrepancy might be due to a frequency-dependent change in the rotational axis or to some energy loss in the malleus-incus joint. Decraemer et al. (1991) used heterodyne laser interferometry to investigate the motion of the malleus in anaesthetized cats. They measured displacements at four points along the manubrium using glass microbeads to increase optical reflectivity, and reported the frequency responses shown in Figure 3.3. They showed that the manubrium has pure translational motion at some frequencies, rotational at others and mixed at most frequencies, thereby

indicating that the rotational axis shifts with frequency. They also suggested the possibility of bending of the manubrial tip at higher frequencies. Decraemer et al. (1994) used the same technique to measure malleus movement at several points on the manubrium in both cat and human. Their results were consistent with the previous findings that indicated a frequency-dependent shift in the rotational axis. They also noted that the modes of vibrations were complex, indicating that there were additional vibrational components along other axes that needed to be addressed. Decraemer & Khanna (1996, 1997) further investigated manubrial motion with 3-D measurements at multiple points on the cat manubrium. They concluded that “the instantaneous axis of rotation changes within each cycle of oscillation and the pattern of change is different for each frequency”. Decraemer & Khanna (2001) carried out a similar experiment on human temporal bones. A 3-D geometrical model was constructed from the recorded data points and the model was animated with rigid-body parameters. Based on the animation results, they concluded that neither malleus nor incus vibrated about a fixed axis. Moreover, they found a substantial amount of slippage between malleus and incus even at very low frequencies.

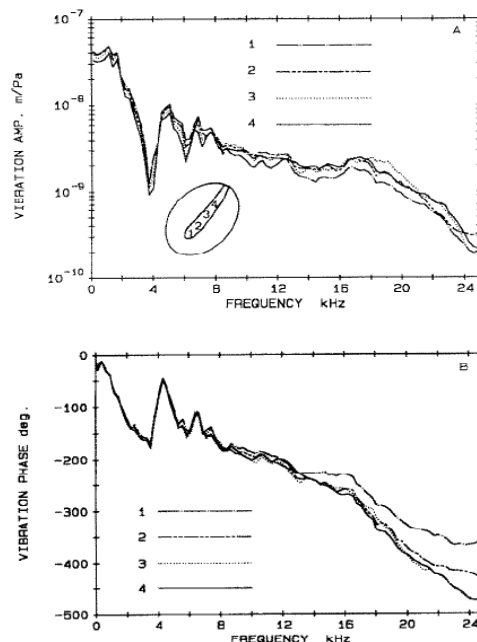


Figure 3.3: Normalized displacements along the manubrium measured by Decraemer et al. (1991). The 4 line styles represent 4 different beads.

### 3.2.4 Middle-ear cavity

In the past, investigators from several disciplines, including comparative anatomy and animal psychophysics, have postulated that the range of frequencies audible to humans and other mammals is shaped by the properties of the middle-ear structures such as area of the TM, middle-ear cavity volume, specializations of the ossicles, etc. (e.g., Legoux & Wisner, 1955; Webster, 1961 & 1962; Webster & Webster, 1972, 1975, 1984; Lay, 1972, 1974; Plassmann & Brandle, 1992). The increased sensitivity to sounds below a few kHz among some desert rodents, relative to others of comparable body size, has been shown to be closely associated with the relatively large middle-ear structures found in those rodents (Webster 1962; Webster & Webster, 1972, 1975, 1984). Direct evidence indicating a connection between middle-ear volume and low-frequency hearing in small rodents was first presented by Webster (1962) and Webster & Webster (1971, 1972). In their study, they reduced the middle-ear cavity volume in kangaroo rats and observed a reduction in the recorded cochlear microphonics (Webster, 1962). They also observed an elevation of the behavioural threshold (Webster & Webster, 1971, 1972). When they reduced the middle-ear volume by 75%, a threshold elevation of approximately 10 dB was observed for frequencies below 2 kHz. Moreover, they observed that the animals whose ME volume was reduced were more susceptible to predation, especially during the dark nights when vision was less useful (Webster & Webster, 1971). Another study by Ravicz & Rosowski (1997) estimated the effect of variations in middle-ear cavity size on the auditory thresholds of some rodents (hamster, kangaroo rat and gerbil) using measurements of the middle-ear input impedance and mathematical models (Ravicz & Rosowski, 1992, 1996). They observed that greater reductions of ME cavity volume produced larger threshold elevations and vice versa. They also found that the threshold predictions for ME volumes equal to those found in the hamster, kangaroo rat and gerbil resembled the threshold functions measured in those animals.

### **3.3 Gerbil studies**

Early gerbil studies mainly focussed on measurements pertaining to auditory thresholds. Finck and Sofouglu (1966) measured the hearing sensitivity of the Mongolian gerbil by recording the cochlear microphonic response at the round window. They found that an auditory response occurs within the range of 200 to 32000 Hz and a maximum sensitivity was observed at low frequencies – 3 to 5 kHz. Similar results were also reported by Lay (1972). However, Ryan (1976) observed that the auditory response of the gerbil fell within the range of 0.1 to 60 kHz, with high sensitivity for tones between 1 and 16 kHz. Furthermore, Henry et al. (1980) studied age-related hearing loss in gerbil and found results in agreement with the findings of Ryan (1976).

#### **3.3.1 Static pressure deformations**

It has been well established that static pressure variations affect middle-ear function. Inward or outward bulging of the TM caused by pressure gradients is often observed in acute stages of chronic middle ear disease (von Unge et al., 1993). Tympanometry is commonly used to assess the condition of the middle ear by applying static-pressure gradients across the TM. However, this technique only measures the acoustic volume displacement of the TM integrated over the entire surface. Studies of the spatial displacement patterns in response to static pressure are discussed in this section.

Using a real-time differential moiré interferometer, von Unge et al. (1993) measured the displacement patterns of the gerbil eardrum in response to static (or quasi-static) pressure gradients. From the interferometric displacement recordings, they observed two points of maximum displacement on the pars tensa: one on the anterior side superior to the umbo, and a smaller one on the posterior side at approximately the same level as the other. Figure 3.4 shows the two areas where these maxima occurred in all specimens studied under different positive pressures up to +20 cm H<sub>2</sub>O. The maxima are situated closer to the manubrium of the malleus than to the annulus ring. Later, the same group using the same interferometric technique reported the shape and displacement patterns of the gerbil

eardrum with experimentally-induced otitis media (von Unge et al., 1995). For the control ears, the interferograms presented in this study were consistent with those published in 1993.

Using a similar technique, Dirckx et al. (1997) studied the effect of middle-ear static pressure on the pars flaccida portion of the gerbil eardrum. Pars flaccida volume displacements for both positive and negative pressure gradients were measured. The displacements were found to behave non-linearly as a function of static pressure gradients across the middle ear, with a large increase up to  $\pm 0.4$  kPa and maintaining a rather constant displacement for pressures beyond 0.4 kPa. The authors concluded that pars-flaccida-induced middle-ear pressure regulation was limited to very small pressure changes (on the order of a few hundred Pa).

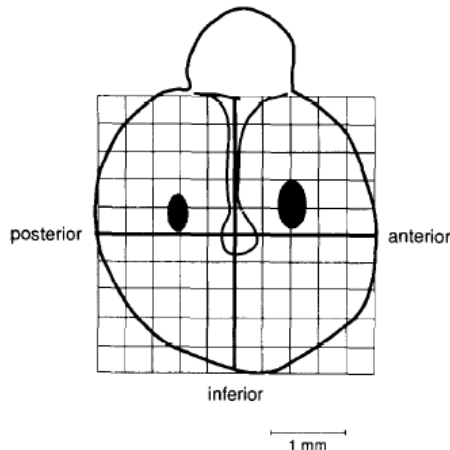


Figure 3.4: A schematic representation of gerbil eardrum. The locations with maximal displacement are marked on both posterior and anterior quadrants. (Source: Von Unge et al., 1993)

Dirckx and Decraemer (2001) used a high-resolution moiré interferometer to observe the shape of the gerbil eardrum at quasi-static pressures. They measured the full-field eardrum deformations while sequentially removing different middle-ear components. The measurement with an intact middle-ear served as a baseline and the rest of the measurements were compared against it. The authors concluded that removing the cochlea and stapes, and cutting the tensor tympani, had no effect on static eardrum deformations.

Studies using static pressures on the eardrum maintain the pressures for some time before shape deformations are recorded. This invokes the viscoelastic characteristics of the eardrum (creep and stress relaxation). The eardrum displacements thus obtained are inherently different from vibrations in response to sound pressure. Such vibration measurements are discussed in the following section.

### **3.3.2 Vibration measurements**

Several groups have investigated middle-ear mechanics in the Mongolian gerbil using sound pressure as stimulus. Ravicz et al. (1992) and Ravicz & Rosowski (1997) presented a series of studies in an effort to quantify sound-power collection by the auditory periphery of the gerbil. Rosowski et al. (1997, 1999), Olson & Cooper (2000), Overstreet & Ruggero (2002), and Ravicz & Rosowski (2004) used laser interferometry to measure the stapes velocity transfer function. To date, four studies have reported gerbil eardrum measurements: Cohen et al. (1993), Rosowski et al. (1997), Olson & Cooper (2007) and Ellaham et al. (2007). These are discussed in turn in the following four paragraphs.

Cohen et al. (1993) studied the development of the auditory function of gerbils in 8 different age groups: 10, 15, 20, 25, 30, 35 and 42 days after birth (DAB), and adult. Gerbils from the age of 77 to 91 DAB were considered as adults. The authors used heterodyne laser interferometry to measure the peak-to-peak umbo-velocity responses to

a 100 dB SPL stimulus over a wide range of frequencies (0.2 to 40 kHz). Between 4 and 20 kHz the slope of the adult umbo response was approximately  $-6$  dB/octave; it became  $+7$  dB/octave from 20 to 40 kHz (Figure 3.5). The authors speculated that the adult velocity responses might be affected by the surgical procedure wherein they drilled a hole in the bulla to position the laser beam at the tip of the umbo. Unlike the situation in younger gerbils, in the adult drilling a hole where they did opens the enlarged bullar cavity, thus affecting sound transmission in the adult middle ear.

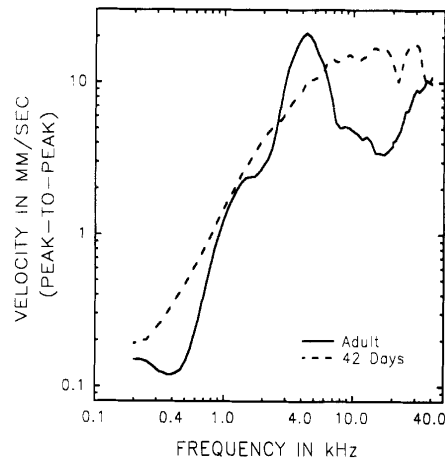


Figure 3.5: Averaged peak-to-peak umbo amplitude response from adult and 42-day-old gerbils. (Source: Cohen et al. 1993)

Rosowski et al. (1997) reported single-point velocity measurements at the umbo and on the pars flaccida using a laser Doppler velocimeter and investigated the functional implications of the pars flaccida on the hearing sensitivity of the gerbil. The normal, removed and stiffened pars flaccida measurements were compared and analysed in both intact and open middle ears. They demonstrated that in an open-bulla configuration, stiffening of the pars flaccida had no effect on the umbo velocity responses. Furthermore, they found that in the case of an intact middle-ear, a stiffened pars flaccida decreased the input admittance at low frequencies and had no significant effect at frequencies above 1 kHz. Umbo velocity responses of both open and closed middle-ear configurations are shown in Figure 3.6. The open-cavity response at the umbo seems to have a stiffness-dominated behaviour at low frequencies with a broad peak at around 1.5 kHz. Beyond this frequency, a slope of  $-1$  can be observed as the system becomes mass-controlled. A sharp drop in the velocity response at 3 kHz is attributed to an anti-resonance produced as a result of opening the bulla. The closed-cavity curve shows a sudden change in the magnitude response as well as the corresponding phase response at around 0.45 kHz. The pars-flaccida velocity measurement has a sharp resonance peak at the same frequency. Closing the bullar hole removed the antiresonance effect at 3 kHz and decreased the umbo-velocity at frequencies less than 2 kHz.

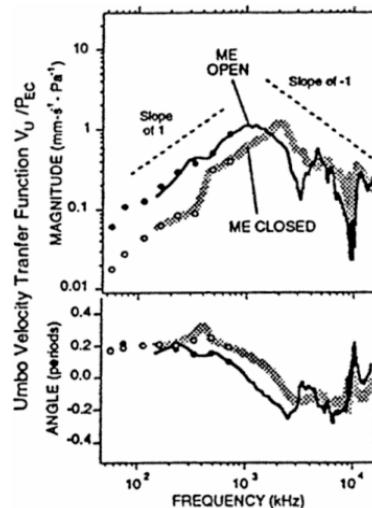


Figure 3.6: Normalized umbo response with the middle-ear cavity open (black line) and closed (grey line). (Source: Rosowski et al. 1997)

The umbo velocity responses reported by Cohen et al. are shown in Figure 3.7 along with those of Rosowski et al. (1997). In this figure, the peak-to-peak velocity measurements presented by Cohen et al. have been divided by  $4\sqrt{2}$  to obtain an appropriately scaled velocity response (a factor of 2 to scale the response from 100 dB SPL to 1 Pa, a factor of 2 to obtain a zero-to-peak response and a factor of  $\sqrt{2}$  to obtain the RMS response). Compared with the results of Rosowski et al., the low-frequency amplitudes of Cohen et al. are lower; the first peak is at a higher frequency and has a larger magnitude; and there are other differences in the details of the curves.

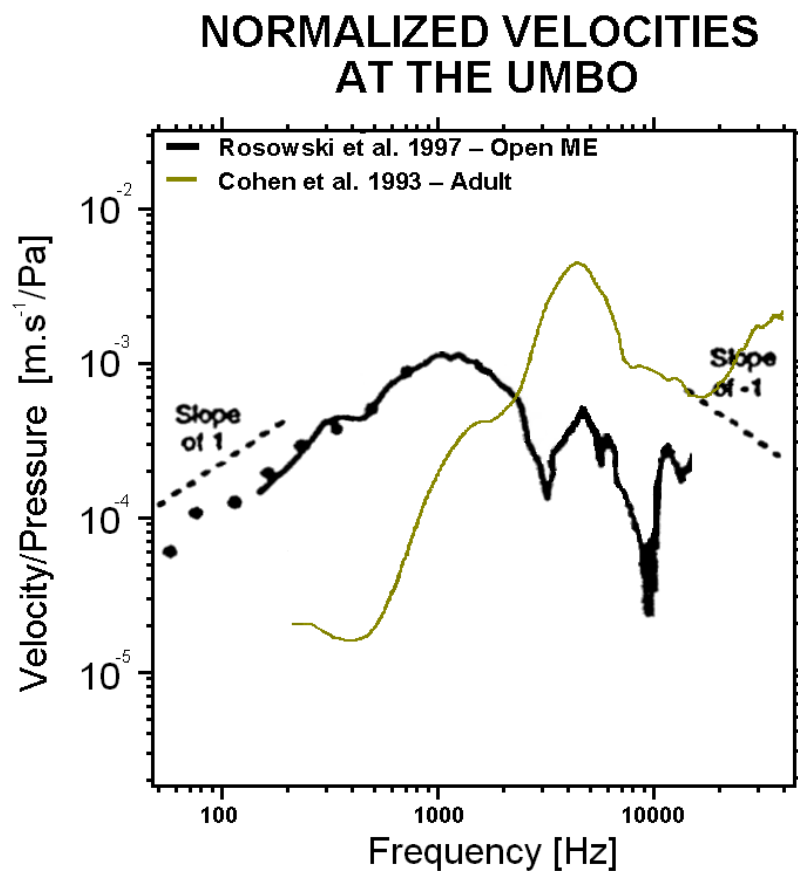


Figure 3.7: Umbo velocity responses in adult gerbils (After: Cohen et al. (1993) and Rosowski et al. (1997)).

De La Rochefoucauld and Olson (2007, 2009) investigated middle-ear delays in gerbils. They measured the middle-ear velocity at different locations along the sound transmission path (from the ear canal to the stapes), including at multiple points on the TM, using a wide range of frequencies (up to 50 kHz). Their measurements were performed using an open-field sound excitation and were normalized with respect to the sound pressure measured at the entrance of the ear canal. In order to compare their results with the other studies mentioned in this section or to our measurements, the overall transmission characteristics that are produced in the ear canal would have to be measured and corrected for in order to estimate the sound pressure near the eardrum.

Vibration patterns at multiple points on the gerbil eardrum were first reported from our group by Ellaham et al. (2007). The study provided a detailed longitudinal tracking of the effects of drying of middle-ear structures on vibration measurements. Figure 3.7 shows a spectrogram representing the distribution of mid-manubrium displacements as a function of frequency and time. The magnitudes are expressed using a logarithmic colour scale normalised to approximately the maximal displacement. Passive rehydration of middle-ear structures was achieved using a moist cotton ball placed on the bulla. The peaks observed in the magnitude response of the eardrum shifted towards higher frequencies as the ear dried. The maximum displacement clearly shifts back towards its initial frequency upon hydration. The red squares indicate the time of rehydration. These results quantitatively support the results reported by Voss et al. (2000): by remoistening the middle ear, *post mortem* effects of drying of the middle ear can be partially reversed. Comparison with the results of Rosowski et al. (1997) suggest that the measurements of both Cohen et al. (1993) and Ellaham et al. (2007) were made on middle ears that were too dry to be representative of their normal state.

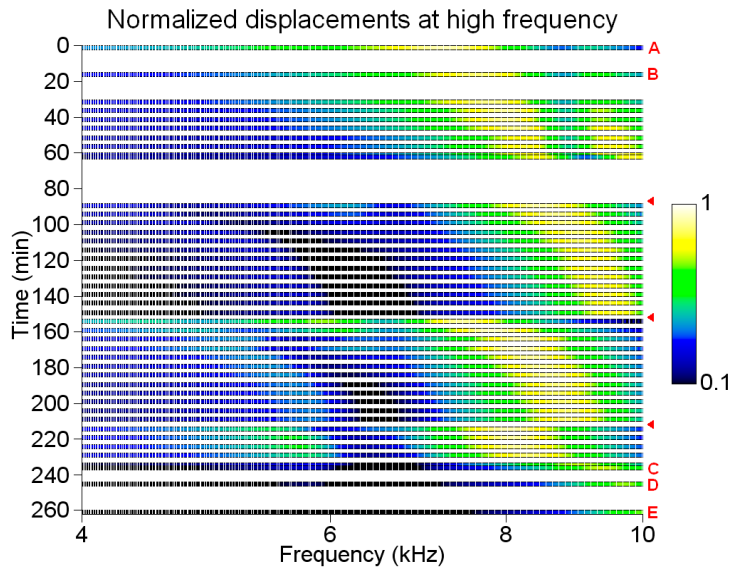


Figure 3.8: Tracking TM frequency shifts over time in the gerbil. The input stimulus frequency ranges from 4 to 10 kHz. The colour scale is normalized to 90 nm/Pa. (Source: Ellaham et al. 2007)

### 3.3.3 Finite-element models

First introduced for the middle ear by Funnell (1975), finite element (FE) modelling has emerged as a very popular tool in middle-ear research. Since then several groups have used the FE method to study the mechanics of the eardrum and ossicles in humans (e.g., Wada et al., 1992; Beer et al., 1999; Bornitz et al., 1999; Prendergast et al., 1999; Koike et al., 2002; Sun et al., 2002; Gan et al., 2006) and in cats (Funnell & Lazlo, 1978; Funnell et al., 1987; Ladak & Funnell, 1996; Funnell et al., 2005).

The first FE model of the gerbil middle ear was developed by Funnell et al. (1999 & 2000). The geometry of the gerbil eardrum in this model was based on images from phase-shift moiré topography in collaboration with Decraemer's group. The ossicular geometry was first based on a high-resolution magnetic resonance microscopy (MRM) dataset obtained from Duke University Center for In Vivo Microscopy (Henson et al., 1994, 1996). X-ray micro-CT data and serial histological images were used to supplement the MRM data. Figure 3.9 shows low-frequency simulation results obtained

from the model for the normal middle ear and the fixed-malleus middle ear. The pars flaccida displacements are about the same in both conditions but the pars tensa displacements decrease by about half in comparison with the mobile-malleus case. Figure 3.10 shows low-frequency simulations of ossicle displacements. The low-frequency ossicular motion is consistent with the classical notion of a simple rotation around a fixed axis defined by the anterior malleolar ligament (AML) and the posterior incudal ligament (PIL). Manubrial displacements are maximal at the umbo and decrease towards the short process.

Elkhouri et al. (2006) enhanced the previous model by incorporating X-ray micro-CT images with a voxel size of 5.5  $\mu\text{m}$ , which allowed a more precise reconstruction of the thin stapedial annular ligament and also of the tiny bony pedicle between the long process and the lenticular process of the incus. Figure 3.11 shows low-frequency simulation results of the ossicle displacements.

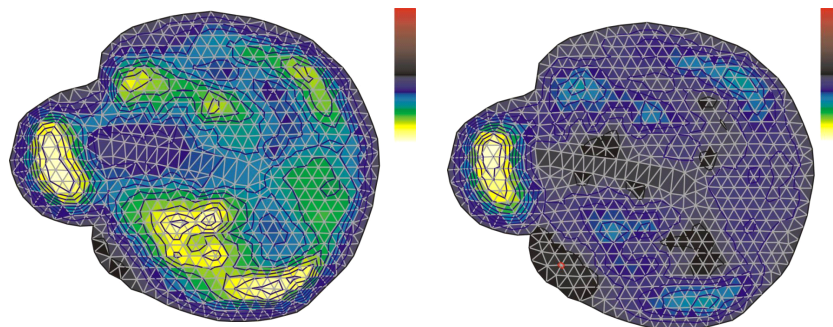


Figure 3.9: Low-frequency vibration pattern with (A) mobile ossicles and (B) fixed ossicles. (After Funnell et al., 1999)

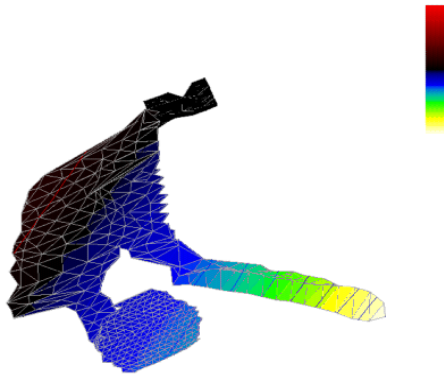


Figure 3.10: Simulated low-frequency vibration patterns of the ossicles.(After Funnell et al., 2000)

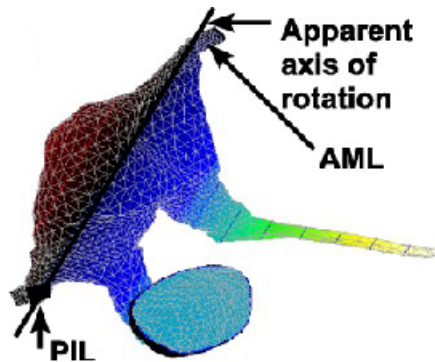


Figure 3.11: Simulated low-frequency displacement patterns of the ossicles. (After Elkhouri et al., 2006)

### 3.4 Conclusion

We have presented a review of studies relevant to our research work. These studies employed various techniques to measure TM vibrations in humans and other species. Experimental measurements of low-frequency TM vibrations are in qualitative agreement about the locations of maximum displacements. Middle-ear structures display frequency-dependent modes of vibration. The eardrum vibrations break up into sectional vibrations which become more complex with frequency.

Several studies have reported experimental measurements of gerbil stapedial and umbo motion, but there is a lack of experimental data to characterize the vibration of the gerbil

eardrum. Measurements at multiple points on the eardrum would help in characterizing gerbil eardrum vibrations at higher frequencies and also be useful to validate mathematical models of the middle ear.

## CHAPTER 4

# MATERIALS AND METHODS

### 4.1 Introduction

This Chapter includes the experimental methods employed in our study. Specimen preparation is presented in Section 4.2. In Section 4.3 a detailed discussion of the experimental set-up is presented. Finally, an overview of the specific types of measurements made is presented in Section 4.4.

### 4.2 Specimen preparation

The measurements were made in Mongolian gerbils (*Meriones unguiculatus*) supplied by Charles River Laboratories (St-Constant, Québec). Twelve gerbils with body weights between 70 and 100 g were used in this study.

The animal was first euthanised by anaesthetic overdose (CO<sub>2</sub> gas) followed by a cervical dislocation. The bone of the bulla was exposed by surgically removing the skin and other soft tissues over it. The bone lateral to the tympanic membrane was drilled away, widening the opening of the ear canal. Figure 4.1 (A & C) shows the surgically exposed portions of the gerbil TM. For the eardrum to vibrate normally, the air pressure on both sides must be the same. In a living animal a pressure mismatch can be equalised through the opening of the Eustachian tube, which connects the middle ear to the nasopharynx. In a *post mortem* study, like ours, the animal cannot equilibrate the middle-ear pressure and the external air pressure. In almost all the specimens, because of the build-up of a negative middle-ear pressure during the surgery, the pars flaccida was observed to be sucked in to form a bowl-like shape such that part of it was in contact with the head of the malleus. Once the overlying tissue had been removed, a ventilation hole was drilled in the bulla, away from the TM, for the release of any built-up pressure in the middle-ear cavity. In three specimens two ventilation holes were drilled in different parts of the bulla in order to check for location-dependent effects of bullar opening. The pars flaccida

returned to its normal shape (flat and almost circular) as soon as the hole was drilled, indicating an equalisation of air pressure between the bulla and the external environment. Since a ventilation hole changes the acoustical response of the system, a long narrow polyethylene tube (diameter < 1 mm, length = 15 cm) was inserted into the hole. The tube served to provide a shunt at very low frequencies but effectively blocked the hole in the auditory frequency range.

An ultrasonic humidifier was used during the surgical preparation in order to minimize the *post mortem* effects of drying of the gerbil middle-ear structures. Glass-coated plastic beads of diameter 90 – 150 microns (Sigma-Aldrich, model G4519) were placed along and across the TM and manubrium. A representative image of the gerbil TM with glass beads placed at measurement locations is shown in Figure 4.1 (B).

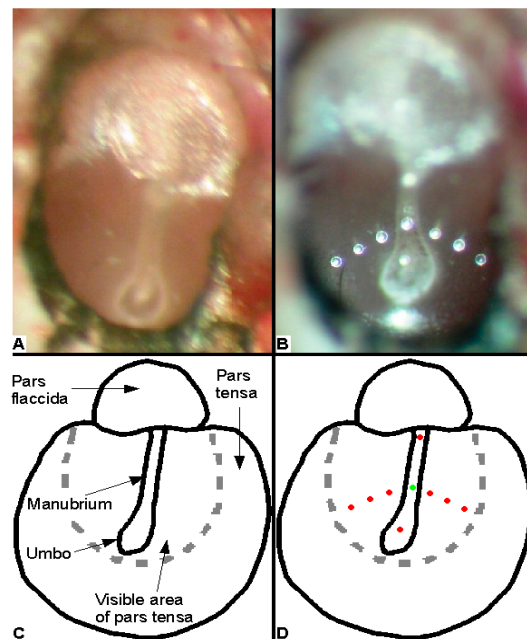


Figure 4.1: A. Photograph of the gerbil eardrum under the microscope. B. Photograph of the gerbil eardrum with glass microbeads. Corresponding schematic illustrations are shown in C & D.

### **4.3 Experimental set-up**

The basic components of the specimen-fixation device and of the measurement system and its peripherals are discussed in this section. The experimental set-up can be categorised into three parts: (a) acoustical system, (b) fixation device, and (c) laser Doppler vibrometer.

#### **4.3.1 Acoustical system**

The acoustical system consisted of an acoustic driver and a microphone coupled together in a sound chamber. Sound was delivered into the coupler by an acoustic transducer (ER-2 Tubeophone, Etymotic Research) and the sound pressure was monitored by a probe-microphone system (ER-7C, Etymotic Research) that was placed 2 to 3 mm from the eardrum. Figures 4.2 and 4.3 show the frequency responses of the transducer and the probe microphone respectively. Both the frequency responses were quite flat between 0.1 and 10 kHz.

The Tubeophone cannot produce large volume velocities and hence the sound administered to the middle ear needs to be confined to a small volume. For this purpose an aluminum coupler, previously designed in our lab (Ellaham, 2007), was used in our study. Figure 4.4 shows the coupler dimensions. The coupler had three holes, two of which allowed insertion of the speaker and the probe microphone respectively. The third hole allowed insertion of a 15-cm PE-50 tube (inner diameter = 0.58 mm, outer diameter = 0.96 mm). This tube acted as a vent, serving the same purpose as the middle-ear ventilation tube described in Section 4.2. Silicon rubber was used to attach the specimen to the bottom of the coupler so that a good acoustic seal was obtained between the coupler and the metal washer that had been fixed to the ear canal. The top of the cavity was covered with an antireflection-coated glass window (T47-518, Edmund Optics) to provide an acoustic seal.

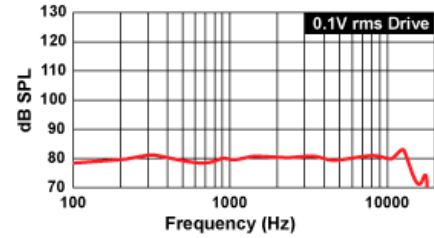


Figure 4.2: The ER-2 Tubephone, and its frequency response. (Source: <http://www.etymotic.com/pro/er2-ts.aspx>)



**Frequency response:**  
 Equalized to flat beyond 10 kHz.  
 Top curve: probe tube inlet open.  
 Bottom curve: probe tube inlet closed.

**Probe tube (silicone):**  
 OD = 0.95mm, ID = 0.5mm,  
 Length: 76mm

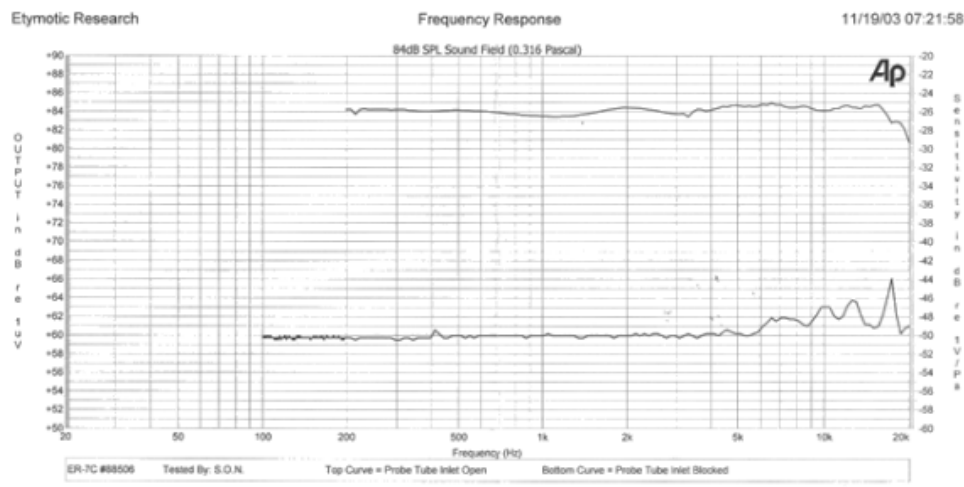


Figure 4.3: The ER-7C probe microphone and its frequency response curve provided by the manufacturer.

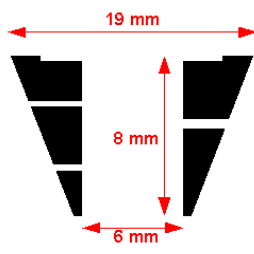


Figure 4.4: Coupler dimensions (After Ellaham, 2007)

The range of audible frequencies extends from 0.2 to 20 kHz in humans (Vander et al., 2004) and from 0.1 to 60 kHz in gerbils (Ryan, 1976). Ideally measurements should be performed over the entire range of audible frequencies. However, some experimental factors limited the range of frequencies used in our measurements. Noise sources that affect the quality of the measured signals include noise signals produced within electrical devices, optical noise due to the laser signal, and mechanical vibrations picked up from the environment. The eardrum vibration measurements were performed inside a double-walled audiometric examination room (model C-24, Genie Audio, St-Laurent, QC) which attenuates acoustical noise. Figure 4.5 shows a picture of the sound-proof room along with its dimensions. A graph characterising the sound transmission loss of the room is shown in Figure 4.6.

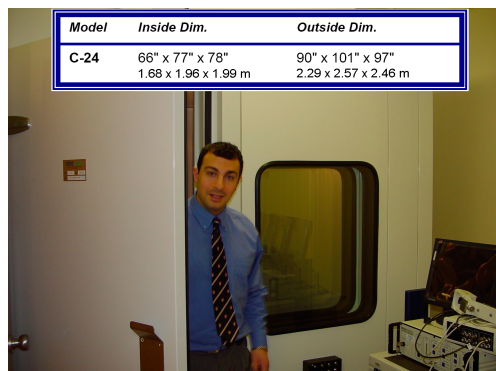


Figure 4.5: The sound-proof room (After Ellaham, 2007).

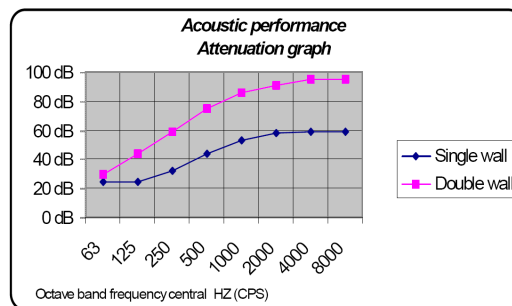


Figure 4.6: Acoustic performance attenuation graph of the sound-proof room as per ASTM E596-96 tests. (Source: Génie Audio)

The choice of an appropriate acoustic stimulus is extremely important in order to achieve a desired frequency resolution and signal-to-noise ratio (SNR). A series of sinusoidal excitations (pure tones) gives a very high SNR but individual measurements at many frequencies would be very time consuming, so it would be practically impossible to achieve a high frequency resolution (Ellaam, 2007). Sinusoidal sweep and white noise signals can be used as alternatives to pure tones since they provide a broad spectrum with high frequency resolution in a single measurement. A sinusoidal sweep is a signal whose frequency ‘sweeps’ through the range of interest. The most common types of sweep signals are linear and logarithmic. A linear sweep has a linear rate of change of frequency while a logarithmic sweep has a logarithmic rate of change of frequency. White noise, unlike sinusoidal sweep signals, consists of random signals. In our experimental set-up, the vibrometer software (VibSoft 4.3, Polytec Inc.) allows the selection of several types of input signals, namely, sine, triangle, rectangle, ramp, linear sweep, chirp, white noise and user-defined signals. We found that white noise results in an output with low SNR even after averaging over 100 realizations. However, a single realization obtained with a sweep stimulus often had a higher SNR. Similar results were also observed by Ellaam (2007). Moreover, the use of linear sweep signals was previously validated in our lab by Akache (2005). In this study, we used 128-msec-long linear-sweep excitation signals over the range of 0.2 to 12.5 kHz. According to the Nyquist criterion, the sampling frequency to be chosen should be equal to or more than 25 kHz; a sampling frequency of 25 kHz was used for data acquisition. The vibrometer software uses a 1600-line FFT to compute the frequency-domain signal. The corresponding frequency resolution is 7.8125 Hz (12.5k/1600).

### **4.3.2 Fixation device**

The fixation device was specifically designed to provide a rigid coupling between the aluminum coupler and the specimen under study. A metal washer (size M4) was attached to the bony rim of the ear canal by means of dental cement (IRM, Dentsply Caulk) to achieve a good acoustic seal. A wooden block (approximate length, thickness and width:

2 cm, 1 cm and 1cm respectively) with two holes was glued to the gerbil skull. The gerbil was then placed under an operating microscope (OPMI 1-H, Zeiss) to which the vibrometer head was attached. An optimal view of the surgically exposed area on the gerbil TM was achieved by adjusting the orientation of an aluminum rod, of which one end was screwed onto the wooden block attached to the gerbil head and the other end slid into a fixation device. The desired field of view was maintained by tightening the clamp of the fixation device. The specimen was placed directly below an aluminum coupler, the design and dimensions of which were presented in Section 4.3.1. Any air gap between the metal washer and the coupler was sealed with dental cement. A schematic illustration of this set-up is shown in Figure 4.7.

The set-up allowed the degrees of freedom necessary to spatially adjust the orientation of the eardrum with respect to the laser Doppler vibrometer. A 3-D computer model of the set-up is shown in Figure 4.8.

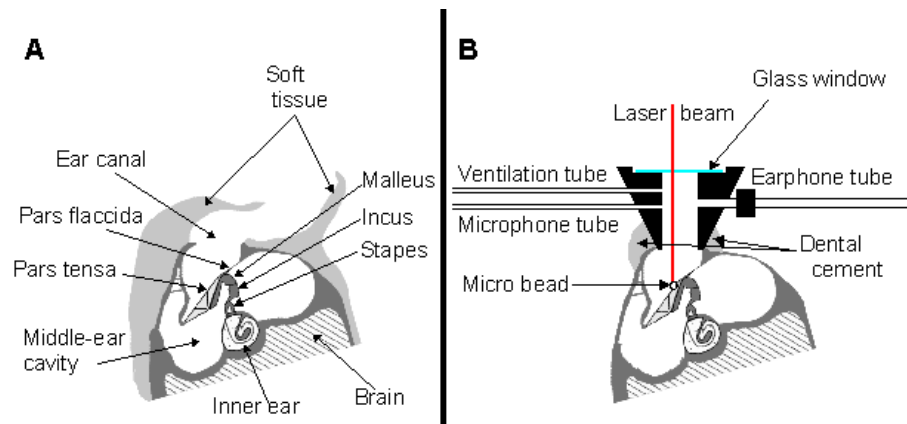


Figure 4.7: Schematic illustrations of A. the gerbil middle ear B. the experimental preparation. (After Rosowski et al., 1997)

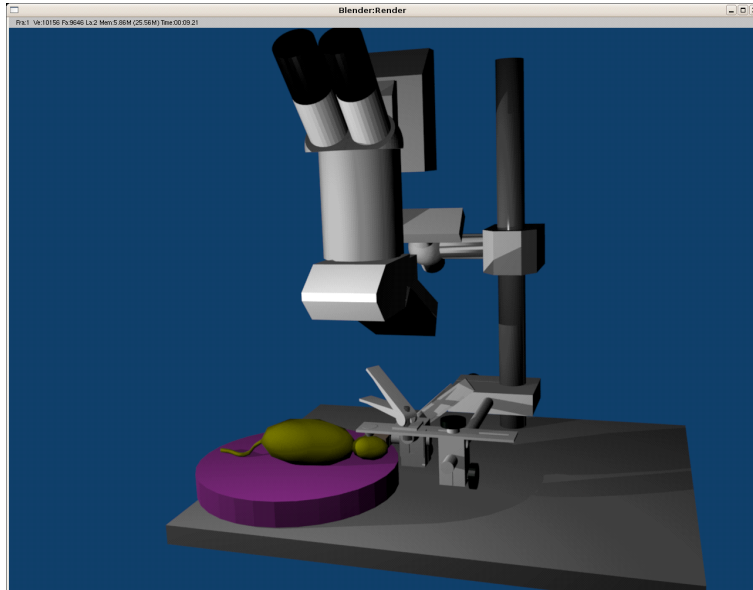


Figure 4.8: A 3-D computer model of the fixation device. The specimen head is attached to the device and placed under the operating microscope and the laser head.

### **4.3.3 Laser Doppler vibrometer**

A variety of different optical techniques can be employed to measure the displacement of a surface or a structure without the loading effects produced by attached transducers. Laser Doppler vibrometry (LDV) is one such non-contact vibration-measurement technique. It uses the Doppler effect to measure deflections of mechanical structures. The displacement sensitivity that can be recorded by the LDV is on the order of nanometres.

We used the hearing laser vibrometer (HLV-1000, Polytec) which is a special version of single-point compact laser vibrometer developed by Polytec. A brief description of the principles of operation is given in Section 4.3.3.1 and the components associated with the laser Doppler vibrometer are presented in Section 4.3.3.2.

#### **4.3.3.1 Principles of LDV**

The following description is based primarily on an interferometry book by P. Hariharan (2007) as well as on the technical overview from the “Polytec Vibrometer University”

Website. The basic principle behind LDV is the Doppler effect. When a coherent laser beam is projected onto a vibrating object, the observed frequency of the laser decreases when the surface moves away from the laser head and increases when it moves toward the laser head. This is called the Doppler effect. The light (of wavelength  $\lambda$ ) scattered back from the surface of the object moving with velocity  $v$  is shifted in frequency by an amount proportional to the relative velocity of the surface. This shift in frequency is called the Doppler shift ( $f_D$ ):

$$f_D = \frac{2v}{\lambda} \quad (\text{Eq. 4.1})$$

Optical interferometry is measurement based on the interference that occurs when two or more light waves are superimposed. According to the principle of superposition, two or more waves that are in phase reinforce one another, whereas when they are out of phase they tend to cancel each other. A phase difference between the interfering light waves results in the formation of an interference pattern which consists of alternating dark and bright fringes. This idea of superposition is the underlying basis of operation of interferometers. There are different types of optical interferometers. Of these, the laser Doppler vibrometer falls into the category of heterodyne interferometers.

Figure 4.9 shows a schematic diagram of a typical Polytec laser Doppler vibrometer, a single-point heterodyne interferometric device. A He-Ne laser beam is first divided into a reference beam and a signal beam. The reference beam of frequency  $f_0$  is allowed to pass through an acousto-optic modulator (also known as a Bragg cell). The Bragg cell shifts the reference signal by a frequency  $f_B$  (where  $f_B = 40$  MHz in our vibrometer) and generates a carrier frequency of  $(f_0 + f_B)$ . The electric field of the resultant beam,  $E_R(t)$ , at time  $t$  is given by

$$E_R(t) = E_r \cos(2\pi(f_0 + f_B)t + \Phi_1) \quad (\text{Eq. 4.2})$$

The measurement beam is directed onto the vibrating object and the reflected light undergoes a Doppler frequency shift ( $f_D$ ). The electric field of the measurement beam,  $E_M(t)$ , at time  $t$  is given by

$$E_M(t) = E_m \cos(2\pi(f_0 + f_D)t + \Phi_2) \quad (\text{Eq. 4.3})$$

When the target object moves, interference between the reference beam and the measurement beam leads to intensity modulation of the resultant beam. This intensity modulated signal,  $I(t)$ , is sensed by the photodetector. The total intensity can be calculated from the electric fields:

$$I(t) = \frac{(E_R + E_M)^2}{2} \quad (\text{Eq. 4.4})$$

Substituting equations 4.2 and 4.3 in equation 4.4, we get

$$I(t) = \frac{[(E_r \cos(2\pi(f_0 + f_B)t + \Phi_1)) + (E_m \cos(2\pi(f_0 + f_D)t + \Phi_2))]^2}{2} \quad (\text{Eq. 4.5})$$

where  $f_1 = f_0 + f_B$

and  $f_2 = f_0 + f_D$

According to the formula  $(a+b)^2 = a^2 + b^2 + 2ab$ , Eq. 4.5 can be written as

$$I(t) = \left(\frac{E_r^2}{2} \cos(2\pi f_1 t + \Phi_1) \cdot \cos(2\pi f_1 t + \Phi_1)\right) + \left(\frac{E_m^2}{2} \cos(2\pi f_2 t + \Phi_2) \cdot \cos(2\pi f_2 t + \Phi_2)\right) + (E_r E_m \cos(2\pi f_1 t + \Phi_1) \cdot \cos(2\pi f_2 t + \Phi_2)) \quad (\text{Eq. 4.6})$$

Applying the trigonometric formula  $\cos A \cdot \cos B = \frac{1}{2} [\cos(A-B) + \cos(A+B)]$  in Eq. 4.6, we obtain

$$I(t) = \frac{(E_r^2 + E_r^2 \cos(4\pi f_1 t + 2\Phi_1))}{4} + \frac{(E_m^2 + E_m^2 \cos(4\pi f_2 t + 2\Phi_2))}{4} + \frac{(E_r E_m \cos(2\pi(f_1 - f_2)t + (\Phi_1 - \Phi_2)) + \cos(2\pi(f_1 + f_2)t + (\Phi_1 + \Phi_2)))}{2}$$

Since the photodetector has a low-pass filter, its sensitivity is dependent only on the difference between  $f_B$  and  $f_D$ . The resultant intensity at the detector is thus given by

$$I(t) = I_r + I_m + 2\sqrt{I_r I_m} \cos(2\pi(f_B - f_D)t + (\Phi_1 - \Phi_2)) \quad (\text{Eq. 4.7})$$

Eq. 4.7 can also be written as

$$I(t) = I_r + I_m + 2\sqrt{I_r I_m} \cos((2\pi(r_1 - r_2)/\lambda) + (\Phi_1 - \Phi_2)) \quad (\text{Eq. 4.8})$$

where  $r_1$  and  $r_2$  represent the path length of the measurement beam and the reference beam respectively. As the path length of the reference beam is constant over time, any motion of the object under investigation ( $r_1 = r(t)$ ) generates a pattern of dark and bright fringes at the detector. The Bragg cell provides the information about the direction of motion of the vibrating object: when the object is at rest, a fringe pattern with a modulation frequency of  $f_B$  (40 MHz) is generated; when the object moves towards the interferometer the frequency detected is less than the modulation frequency, and when it moves away from the vibrometer the detector records a frequency higher than the modulation frequency. Digital demodulation techniques are then employed to retrieve the velocity of the moving object.

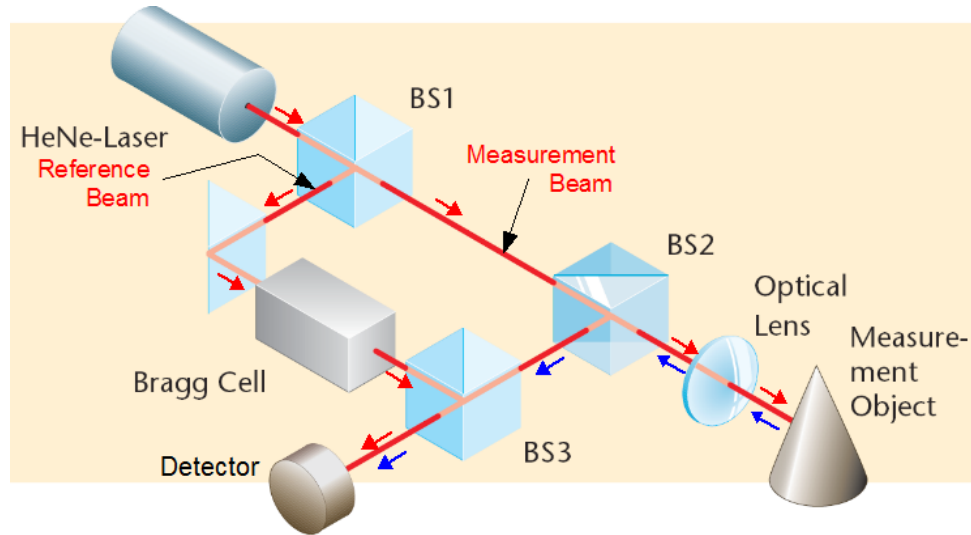


Figure 4.9: Schematic diagram of the laser Doppler vibrometer. Three beam splitters (BS1, BS2, and BS3) are used to split, redirect, and combine the laser beams. (Source: polytec.com)

#### **4.3.3.2 Hardware and software**

The laser Doppler vibrometer (HLV-1000, Polytec) is attached to various components that work together to acquire and process the measured signals. The HLV-1000 is specifically designed to study the acoustics of the middle ear and hearing devices. It consists of a vibrometer controller unit and a laser sensor head connected with a fibre-optic cable. The sensor head is attached to a beam-positioning device and the assembly is mounted onto a clinical microscope stand. The operating microscope (OPMI 1-H, Zeiss) magnifies the surface of the target object, thereby allowing precise positioning of the laser beam onto a desired point on the vibrating object. The beam positioning device has a handle which allows a user to deflect the laser beam. The vibrometer controller unit is also connected to a junction box (VIB-Z016, Polytec) which serves as a communication interface to the acoustical system and the Data Management System (DMS). The DMS workstation has a 1.9 GHz AMD processor, 512 MB RAM and 80 GB of hard disk space. It can generate signals that drive the sound-delivery system, and also acquire and process signals detected by the microphone and the laser sensor head. The software used for signal processing is VibSoft 4.3 (Polytec). It provides a user interface that allows manipulation and visualization of the measured signals, namely sound pressure level (SPL), velocity and displacement in both time and frequency domains. The acoustic signal used as input stimulus in our study is produced by the software-controlled signal generator. The signal type (sinusoidal sweep, periodic chirp, white noise, pure tone, user defined, etc.), the frequency resolution and the frequency range can be specified within the software settings.

The hardware and software settings, present in the junction box and VibSoft 4.3 respectively, can be used to set one or more reference signals (e.g., the SPL signal picked up by the microphone) to which the vibrometer signal can be normalised.

#### **4.4 Overview of measurements**

Experimental details of the twelve Mongolian gerbils used in our study are summarized

in Table 4.1. Because of possible temporal effects on the measurements, the time intervals between the start of measurement and the time of sacrifice are included in the table. The measurements were all performed on the right ear to maintain consistency. The displacement frequency responses (displacement divided by sound pressure) were recorded at multiple points along the manubrium and at points on the pars tensa region of the eardrum. A schematic of the arrangement of the glass micro beads generally used in all specimens is shown in Figure 4.10. Multiple sets of consecutive measurements were collected at all points on the eardrum. Such measurements allow assessment of consistency and time-dependent variability within a given experiment. Vibration responses were acquired in two types of experimental configurations: open and closed middle ear. Measurements with an intact middle-ear were recorded in all specimens. In gerbils C, D and E, the middle-ear cavity was gradually opened by widening the two ventilation holes one at a time. Open-bulla measurements at the umbo were acquired at each step.

In gerbils H to L, displacements at a point located approximately at the centre of the pars flaccida were also measured. For all specimens, each of the displacement measurements presented in the next chapter is a single realization, that is, no averaging was performed unless explicitly stated otherwise.

Table 4.1: Experimental details of all specimens

Gerbil	Weight (g)	Gender	Start of measurement with respect to the time of sacrifice
A	71.8	F	1 hr 38 min
B	58.9	F	3 hrs 25 min
C	67	F	2 hrs 35 min
D	72	F	3 hrs 28 min
E	72	F	4 hrs
F	74.7	F	3 hrs 50 min
G	87.9	F	3 hrs 10 min
H	73.2	F	3 hrs 37 min
I	103.3	F	5 hrs
J	66	M	5 hrs 15 min
K	64.8	M	2 hrs 25 min
L	70	M	1 hr 45 min

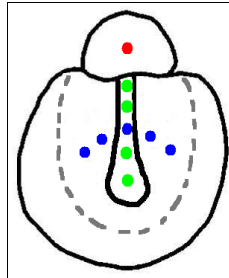


Figure 4.10: A schematic of the arrangement of the glass micro-beads on a gerbil eardrum. The dotted grey lines indicate the visible region of the eardrum.

#### 4.4.1 Sound pressure level

Figure 4.11 shows the sound pressure level (SPL, relative to 20  $\mu$ Pa) measured near the eardrums of gerbils A to L. The SPL was measured with the probe microphone in response to a sinusoidal sweep excitation signal over the frequency range of 0.2 to 10 kHz. The shape of the responses is consistent among all specimens and the responses are observed to be within  $\pm 4$  dB of the mean. In most of the animals, the SPL below 6 kHz is within the range of 70 to 80 dB. At 7 kHz the mean SPL magnitude is about 70 dB, and it

gradually drops with increasing frequency to a value of about 55 dB at 10 kHz. The curves are smooth enough and reproducible enough to provide reliable normalization. All vibration measurements are normalized by the SPL values.

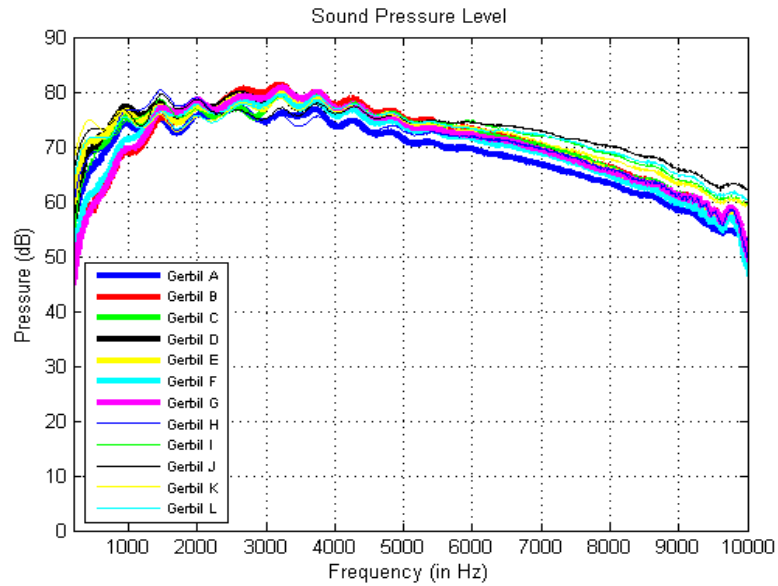


Figure 4.11: Sound pressure level measured near the eardrum of all specimens.

## CHAPTER 5 RESULTS

### 5.1 Introduction

Vibration measurements performed at multiple locations on the gerbil eardrum are presented in this chapter. In Section 5.2 we present the frequency responses measured at the umbo for both open and closed middle-ear configurations; address the variability and repeatability of the measurements; and provide a comparison with previously reported results. Frequency responses at multiple points on the manubrium and on the pars-flaccida are presented in Sections 5.3 and 5.4 respectively. Pars tensa frequency responses are presented in Section 5.5.

### 5.2 Vibrations at the umbo

#### 5.2.1 Displacement frequency response

Measurements were taken at the umbo for all the specimens used in our study. In this section we present umbo displacements normalized by sound pressure level. Two types of experimental configurations, intact and open middle-ear cavity, were employed in our study. Closed bulla measurements taken at the umbo of gerbils A to L are shown in Figure 5.1. Of all the umbo measurements recorded in each specimen, the responses shown in Figure 5.1 are the first ones. In gerbils H and J, the first umbo measurements were obtained 217 min and 315 min, respectively, after the start of measurements which probably explains why their curves are shifted with respect to those of the other gerbils. The repeatability and temporal variability observed in the umbo measurements are discussed in detail in Sections 5.2.3.

The displacement curves in Figure 5.1 show a more or less flat response at low frequencies (200 Hz to approximately 400 Hz) indicating that the middle ear behaves as a stiffness-dominated system at these frequencies. At frequencies greater than 400 Hz, a dip

followed by a sharp rise in the magnitude suggests that mass effects start to become more significant. The peak is followed by a plateau that extends to about 2–3 kHz. Beyond this frequency, we see a gradual drop in the magnitudes of the umbo displacement curves. The average high-frequency roll-off is about  $-10$  dB/octave, which is close to the slope for mass-dominated behaviour ( $-12$  dB/octave).

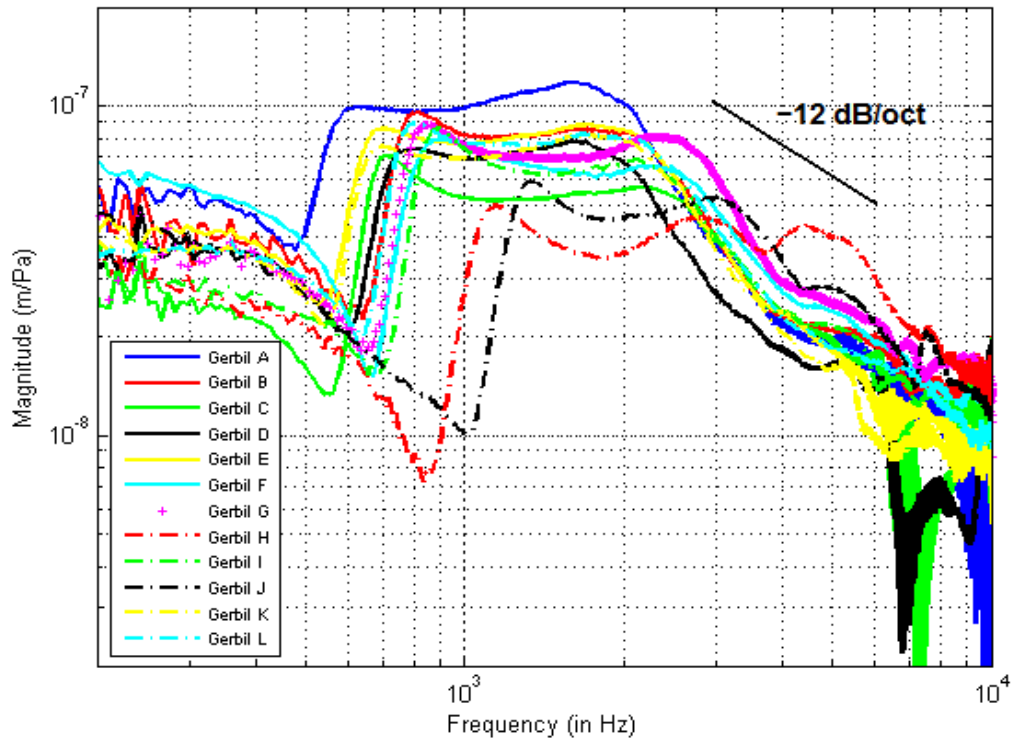


Figure 5.1: Normalised displacement measurements at the umbo in all 12 gerbils. The slope ( $-12$  dB/oct) at the higher frequencies indicates mass-dominated behaviour.

### **5.2.2 Inter-specimen variability**

Variability observed in experimental measurements remains one of the main concerns when it comes to drawing conclusions about the function of the middle ear. The overall shapes of the curves shown in Figure 5.1 are comparable at both low and mid frequencies. However, some large discrepancies are observed at frequencies greater than 6 kHz. At low and mid frequencies (below and above the region of the sharp rise), the umbo displacement responses fall within a range of approximately  $\pm 5$  dB. The normalised umbo displacements at the high frequencies are presented in Figure 5.2 in decibel units for easier comparison between the measurements. At frequencies above 6 kHz, the responses for gerbils B, E, F, G, I, J, K and L fall within the same range of  $\pm 5$  dB. However, in gerbils A, C, D and H the magnitude difference is about 20 to 30 dB. This discrepancy may be due in part to high-frequency noise.

The magnitude variability observed in our measurements is comparable to the variability observed in studies performed by other groups on both gerbil ears and human temporal bones. Cohen et al. (1993) reported a variability of 6 to 16 dB estimated from the averaged umbo displacements measured from 5 or 6 gerbils belonging to each of 8 age groups. In humans, the measurements of Goode et al. (1993) from 15 temporal bones and those of Voss et al. (2000) from 18 temporal bones had variabilities of approximately 20 dB. Finally, Whittemore et al. (2004) reported 95% confidence intervals of about 20 dB for umbo velocity measurements conducted in 56 subjects.

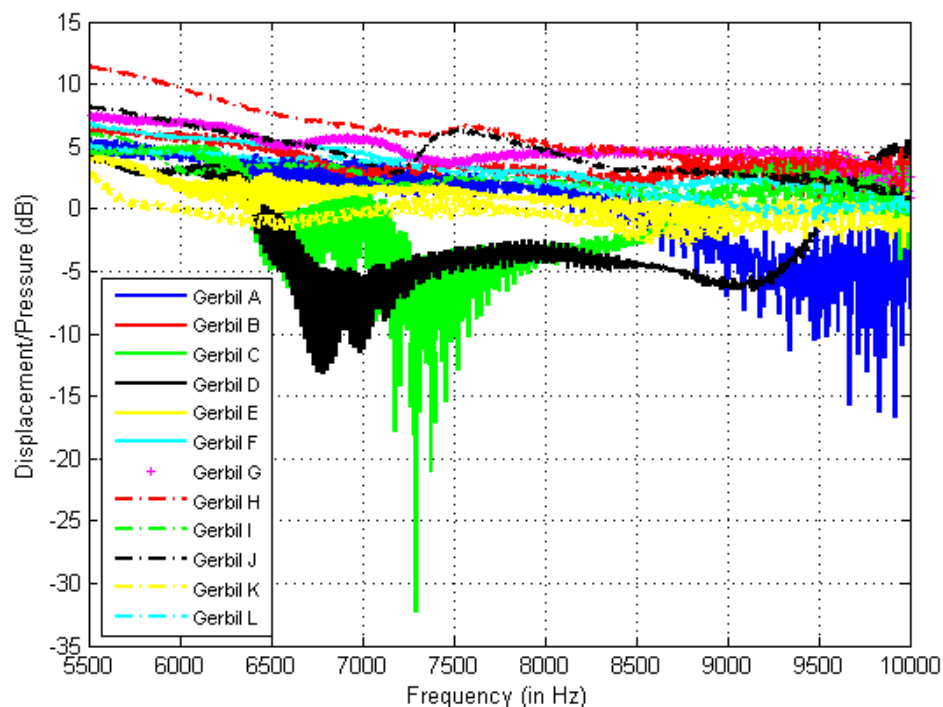


Figure 5.2: Normalised displacement measurements at the umbo expressed in dB (re  $10^{-8}$  m/Pa) over a frequency range of 5.5 to 10 kHz.

### 5.2.3 Repeatability

Since the middle-ear response changes over time, it is important to investigate the consistency of measurements within a given experiment. Measurements in *post mortem* studies are especially vulnerable to dehydration of middle-ear structures that occurs during the course of the experiment. Such temporal effects lead to changes in the material properties of the middle-ear structures. Different groups have employed various strategies to rehydrate the middle ear by remoistening its structures (Lynch et al., 1982; Rosowski et al., 1990; Merchant et al., 1996; Voss et al., 2000 & 2001; Huber et al., 2003). In our study, pieces of moist tissue paper were placed on the outer walls of the bulla to provide passive hydration to the gerbil middle ear.

Short-term repeatability of the umbo measurements recorded in each animal is illustrated by the consecutive magnitude responses in gerbils A, B, C, D, E, F and G shown in

Figures 5.3 to 5.9 respectively. In each gerbil, these umbo responses were all recorded within an interval of 30 min and thus the changes due to the drying effects are small. The observed variability is on the order of 10–20 % (1–2 dB) except at the lowest and highest frequencies.

Table 5.1: Number of consecutive measurements used to assess umbo-displacement repeatability

<b>Gerbil studies</b>	<b># of consecutive measurements</b>
Gerbil A	6
Gerbil B	8
Gerbil C	20
Gerbil D	21
Gerbil E	11
Gerbil F	7
Gerbil G	13

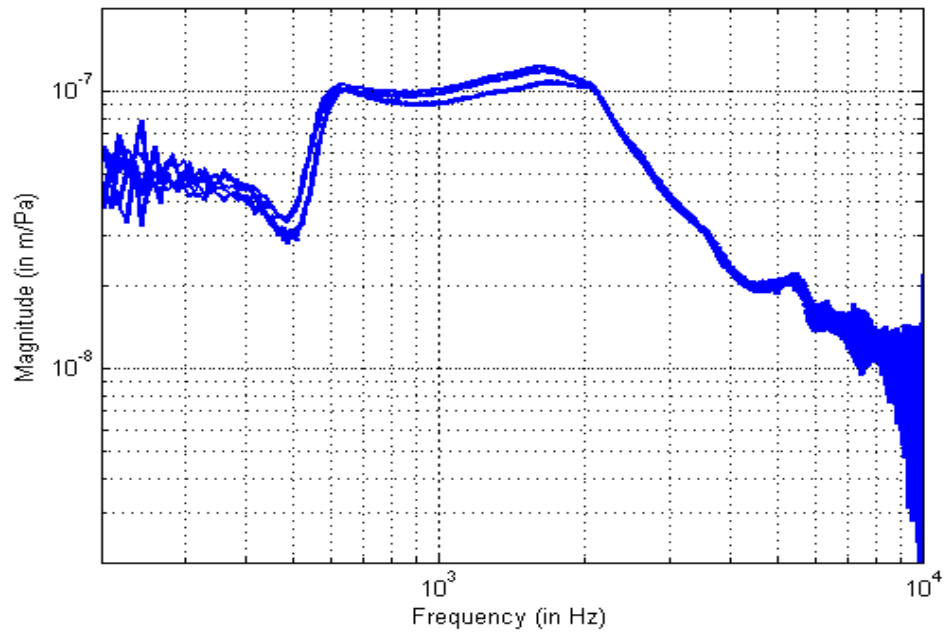


Figure 5.3: Assessing measurement repeatability at the umbo in gerbil A (6 measurements).

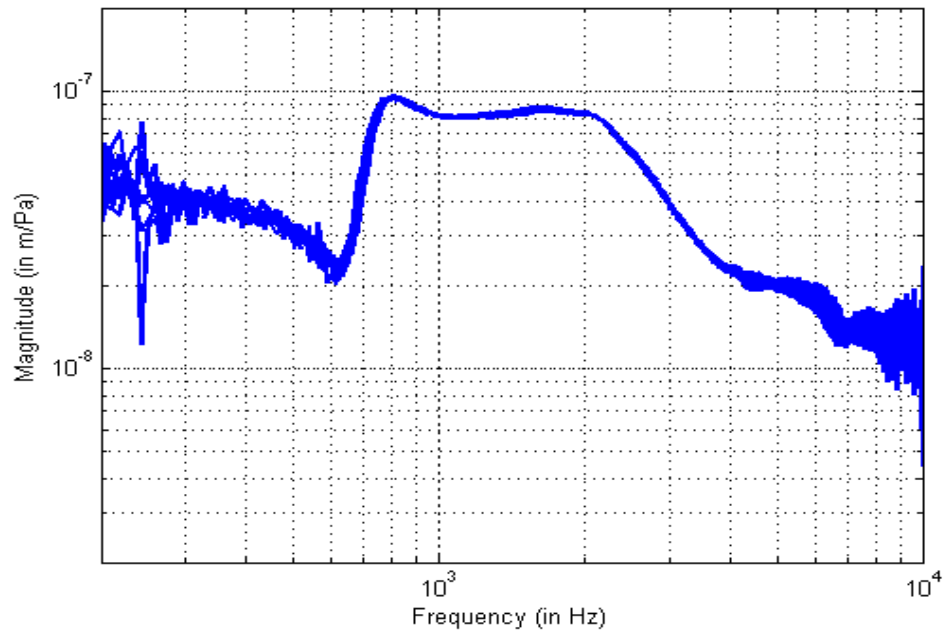


Figure 5.4: Assessing measurement repeatability at the umbo in gerbil B (8 measurements).

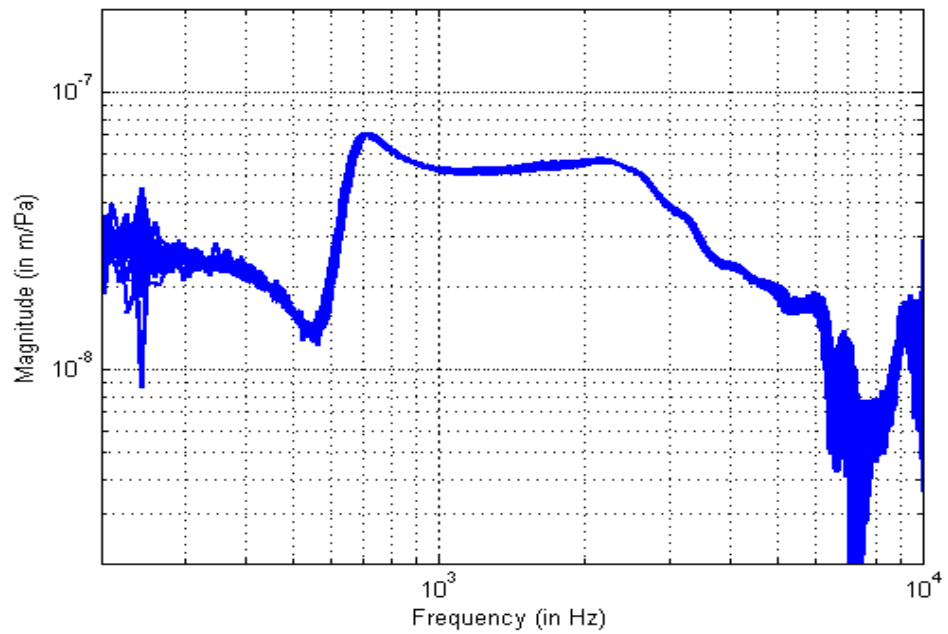


Figure 5.5: Assessing measurement repeatability at the umbo in gerbil C (20 measurements).

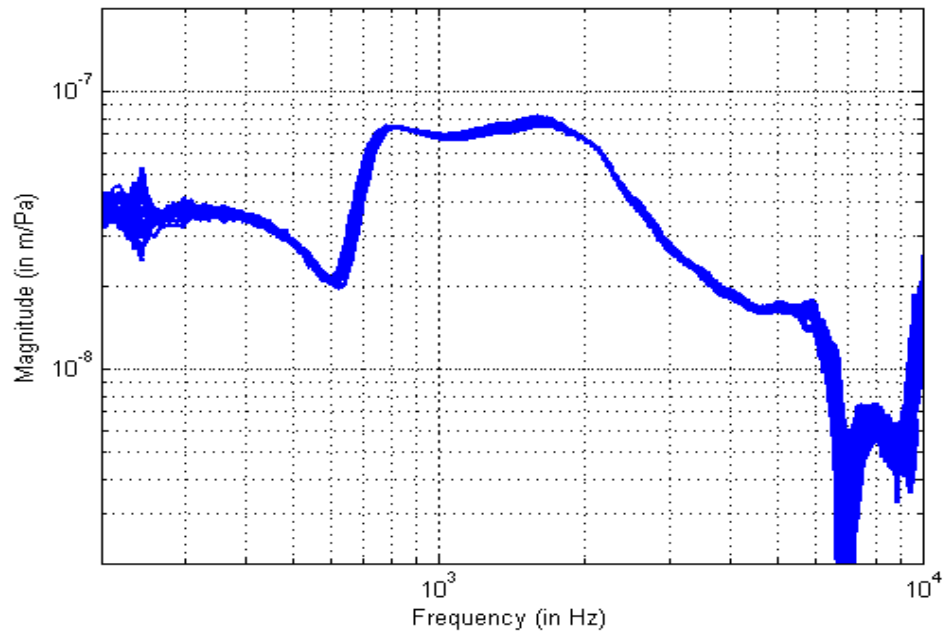


Figure 5.6: Assessing measurement repeatability at the umbo in gerbil D (21 measurements).

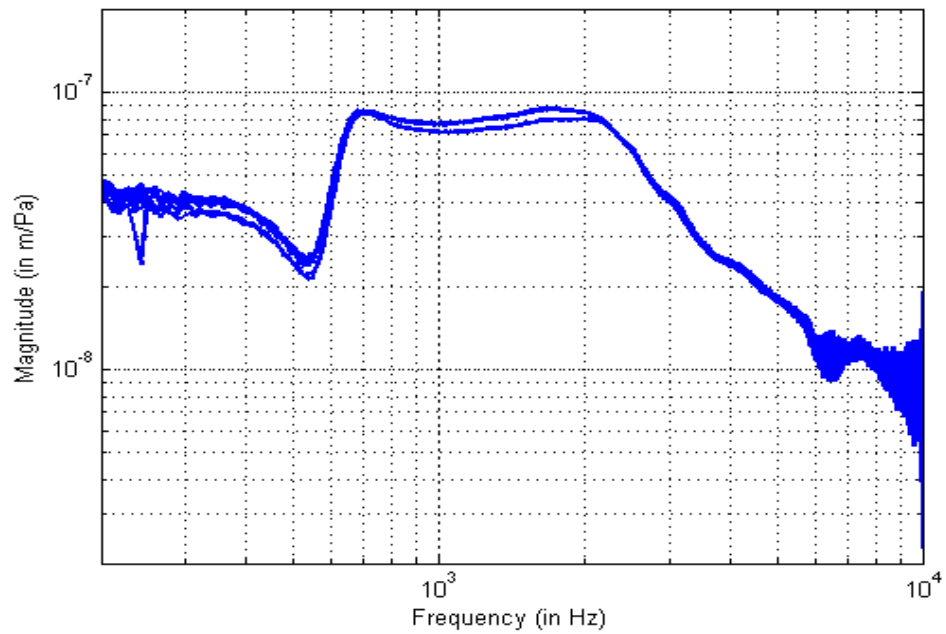


Figure 5.7: Assessing measurement repeatability at the umbo in gerbil E (11 measurements).

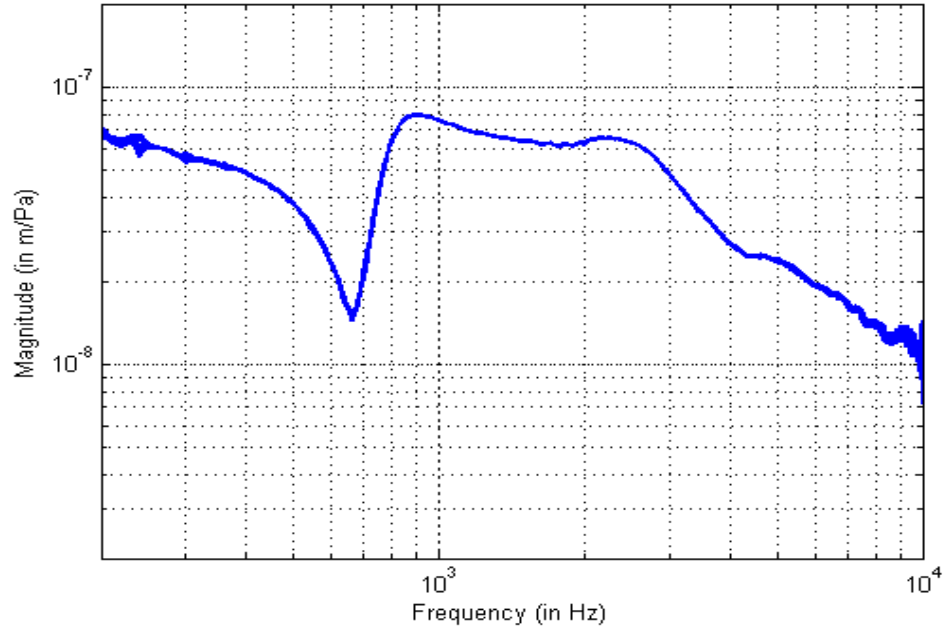


Figure 5.8: Assessing measurement repeatability at the umbo in gerbil F (17 measurements).

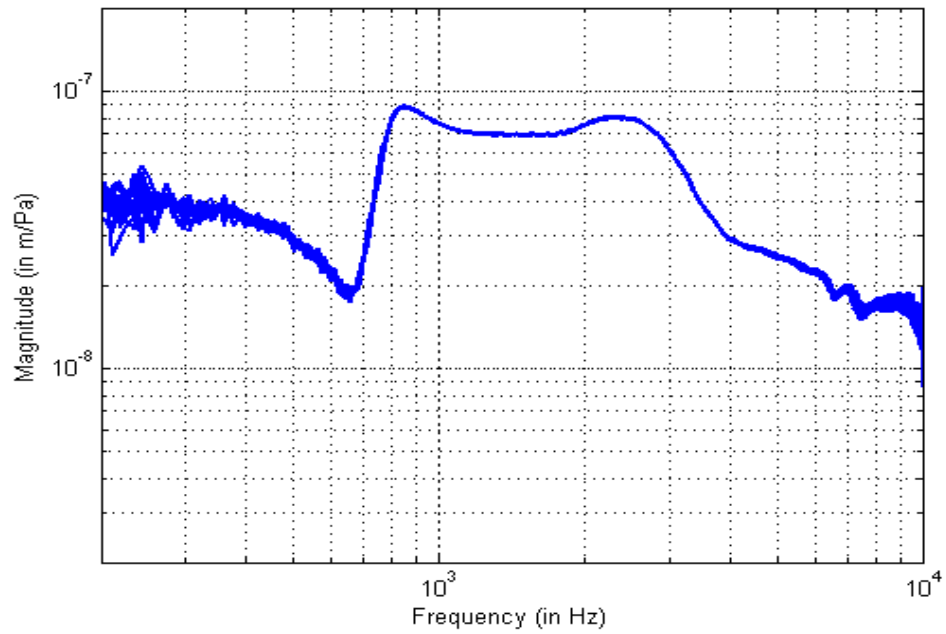


Figure 5.9: Assessing measurement repeatability at the umbo in gerbil G (13 measurements).

As an indication of longer-term repeatability, Figures 5.10 to 5.15 show umbo magnitude responses of gerbils A, B, D, G, I and K recorded at more widely spaced time points within each experiment. Time of euthanasia is considered as a reference time point. When a series of consecutive umbo measurements was taken in a given experiment, they are averaged and shown as a single curve here, with the time shown as a range. Gerbils C, E, F, H, J and L are not considered in this section since their umbo measurements were not acquired for 3 or more time points. From these figures, we observe that the umbo displacements over the frequency range of 0.3 to 2.2 kHz decrease with time. Moreover, in all the gerbils we observe a rightward frequency shift of the peaks with time, causing an increase in the displacement at higher frequencies. These effects (a decrease in magnitude response and a positive shift in frequency) can be attributed to the drying of the TM and other middle-ear structures. In gerbil G, a change of shape is observed in the umbo displacements at frequencies greater than 3.5 kHz.

Although the time differences between the individual umbo-response measurements in gerbils A (Figure 5.10) and D (Figure 5.12) are similar, the magnitude drop in the umbo responses of gerbil A is smaller than that of gerbil D. Moreover, the frequency shift between the first two umbo responses of gerbil A is significantly less than that observed in gerbil D. In all specimens, moist tissue paper placed on the bulla at the start of the experiment was used to reduce the drying effects. However, the tissue paper dries out during the course of the experiment. The tissue paper was re-moistened for a longer period of time in the case of gerbil A, resulting in better passive hydration of its middle-ear structures and possibly reducing the drying effects of the middle ear. Such effects have also been observed in the rehydration studies reported by Ellaham et al. (2007). In each of Figures 5.11 to 5.15 we observe that the drying effects generally increase with increasing time interval between the measurements. For example: in gerbil B, the time intervals between the first and the second measurement, and between the second and the third measurements are 162 min and 28 min respectively. Here we observe that the larger the time difference, the more pronounced the frequency shift and the drop in the overall magnitude.

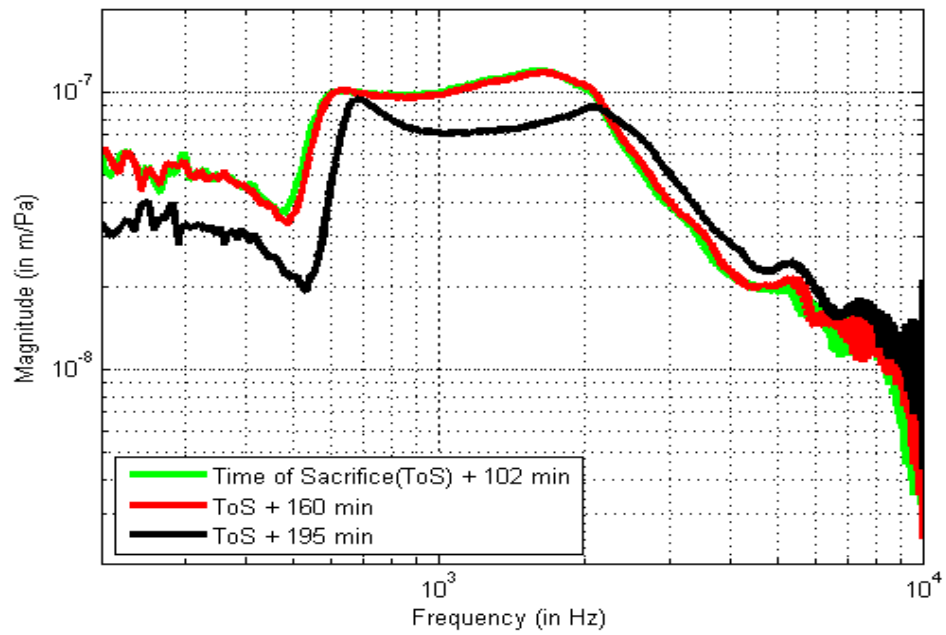


Figure 5.10: Tracking temporal effects of normalised umbo measurements in gerbil A.

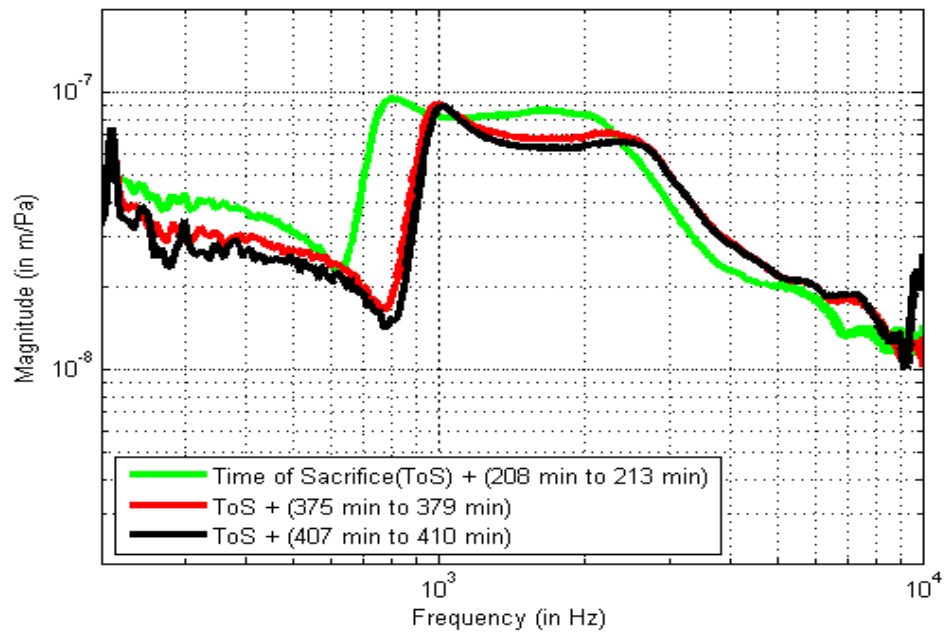


Figure 5.11: Tracking temporal effects of normalised umbo measurements in gerbil B.

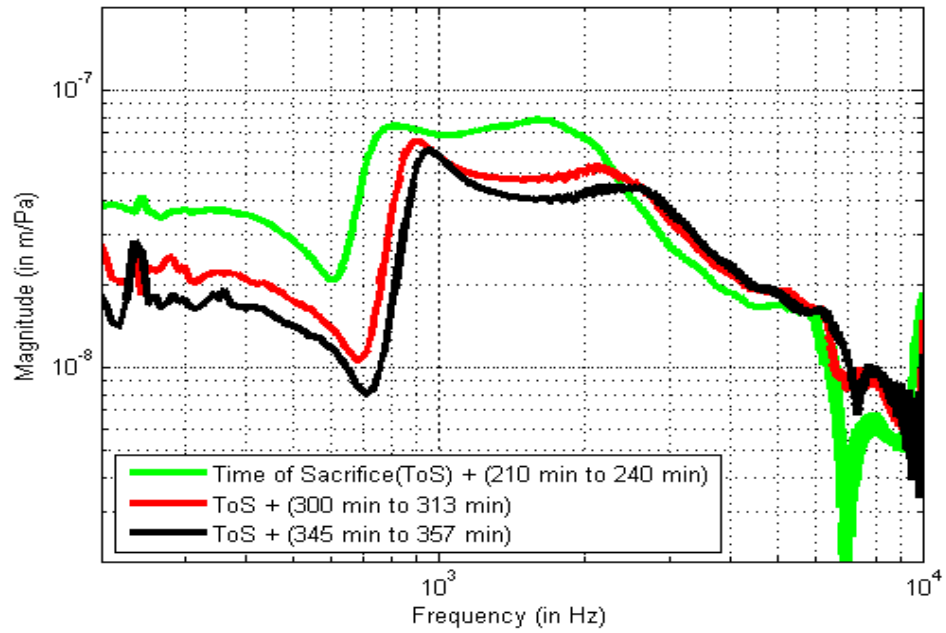


Figure 5.12: Tracking temporal effects of normalised umbo measurements in gerbil D.

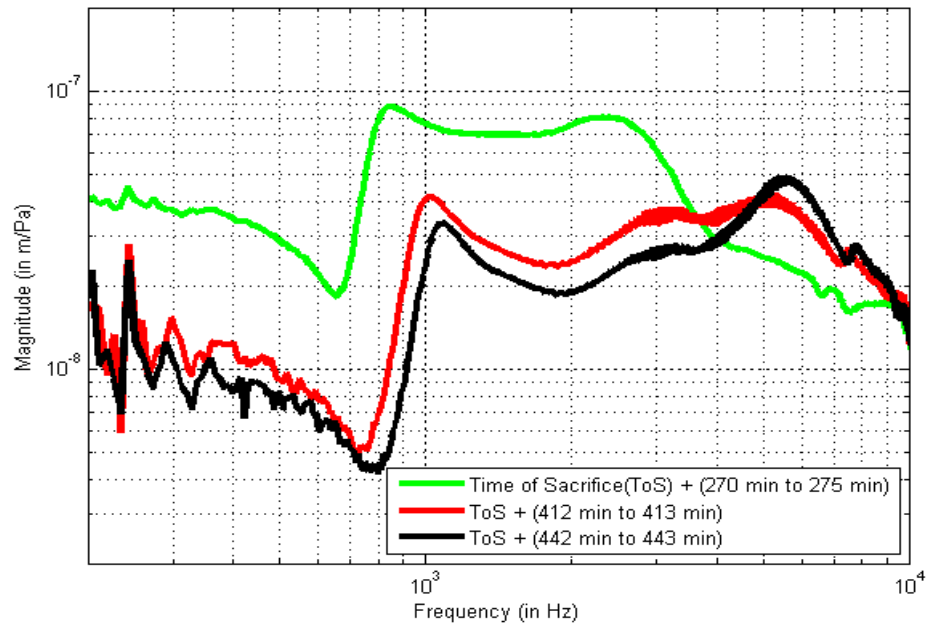


Figure 5.13: Tracking temporal effects of normalised umbo measurements in gerbil G.

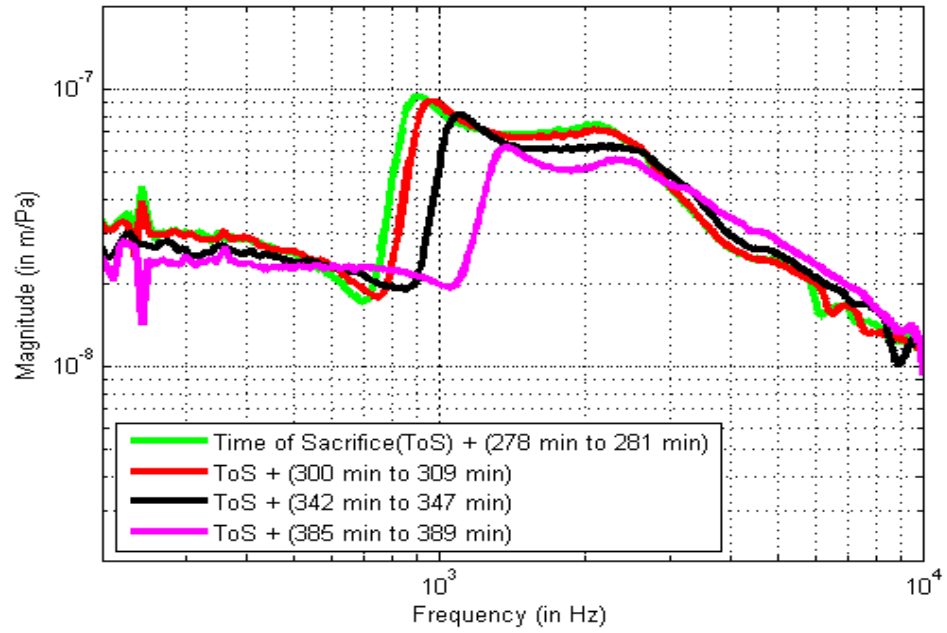


Figure 5.14: Tracking temporal effects of normalised umbo measurements in gerbil I.

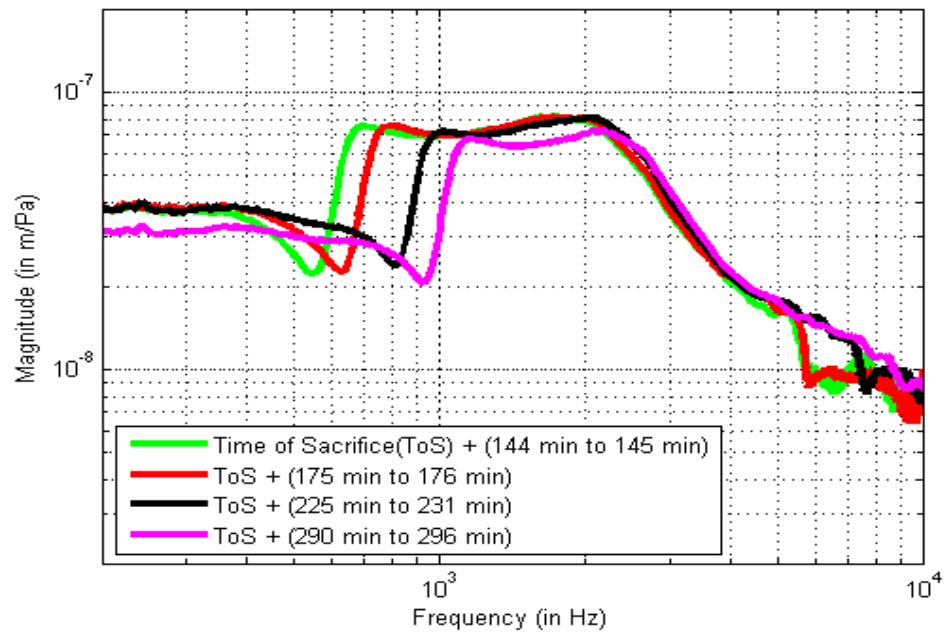


Figure 5.15: Tracking temporal effects of normalised umbo measurements in gerbil K.

### 5.2.4 Open/closed bulla configuration

Gerbils A, C, D and E were used to assess the effects of opening the middle-ear cavity. The closed configuration has a ventilation hole that is effectively closed (except for very low frequencies) by a ventilation tube. The ventilation tubes were removed and the ventilation hole or holes were widened. Two ventilation holes were drilled in the bullae of gerbils A, D and E: one posterior to the pars flaccida and another inferior to the umbo (Figure 5.16). In the case of gerbil C only one ventilation hole, located posterior to the pars flaccida, was drilled and later widened.

The ventilation holes (vent 1 and vent 2) were gradually widened in stages such that the anatomical integrity of the middle-ear structures was maintained, and the umbo frequency responses were acquired at each stage. In order to assess the repeatability of such measurements, umbo displacement responses were recorded in gerbil E without the ventilation tube (at vent 2) and then with the tube placed back in. The removal of the ventilation tube (vent 2) led to increased displacements below 1.5 kHz and a sharp anti-resonance at 2.3 kHz (Figure 5.17).

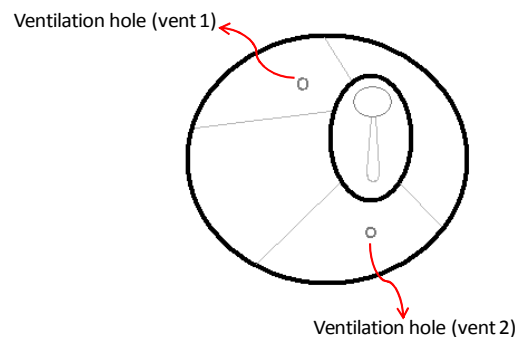


Figure 5.16: A schematic illustration of the gerbil bulla (lateral view) with the two ventilation holes.

Figures 5.18 to 5.21 show the umbo measurements in gerbils A, C, D and E, respectively, with approximate hole diameters specified in the legends. We observe that the presence of either one of the ventilation holes or of both resulted in an anti-resonance. In all specimens, we see that when the ventilation tube (at vent 1) was first removed, there was a sudden increase in the umbo displacement at low frequencies. Except in gerbil A, the responses below 1.5 kHz subsequently remained almost the same as the bulla hole (vent 1) was widened. In all animals, we also observed a rightward shift of the anti-resonance as the hole (vent 1) was widened. In gerbils A and D, introduction of another opening (vent 2) in the bulla resulted in an overall increase in the umbo magnitudes at frequencies below the anti-resonance but this change is not seen in the umbo response of gerbil E. In all three animals there was a significant rightward shift of the anti-resonance when vent 2 was opened. Possible explanations for differences among animals might be changes in the mechanical properties of the TM (drying effects) or bone debris accidentally blocking the ventilation hole while the bulla was drilled.

An open bulla increases the effective volume of the middle-ear cavity, thereby reducing the TM load impedance and increasing the displacement response. Our low-frequency data are consistent with this, and suggest that the smallest hole is equivalent to a wide opening. More specimens need to be studied to draw a more reliable conclusion.

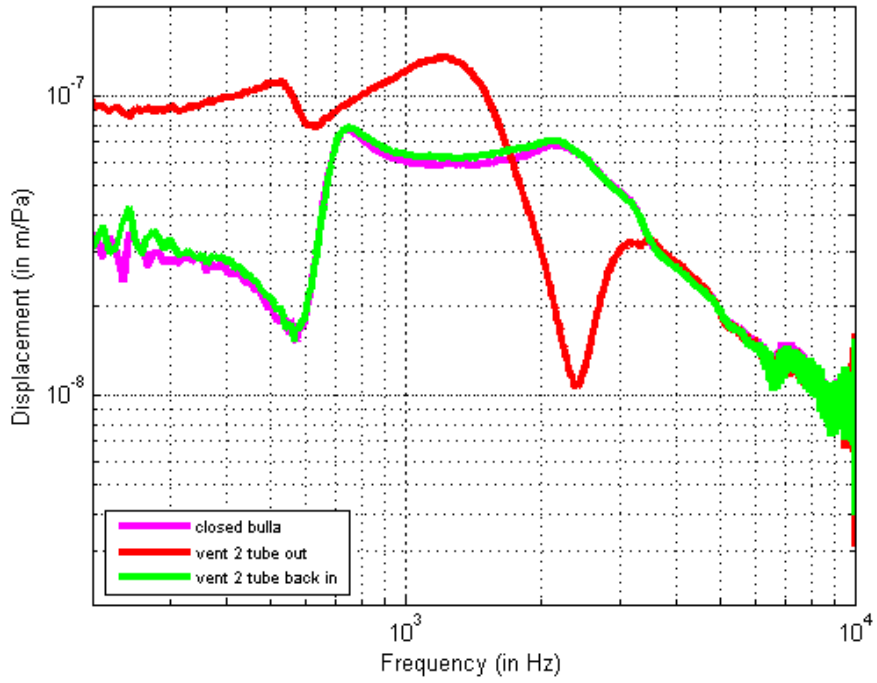


Figure 5.17: Assessing the effect of ventilation hole on the umbo frequency response in gerbil E.

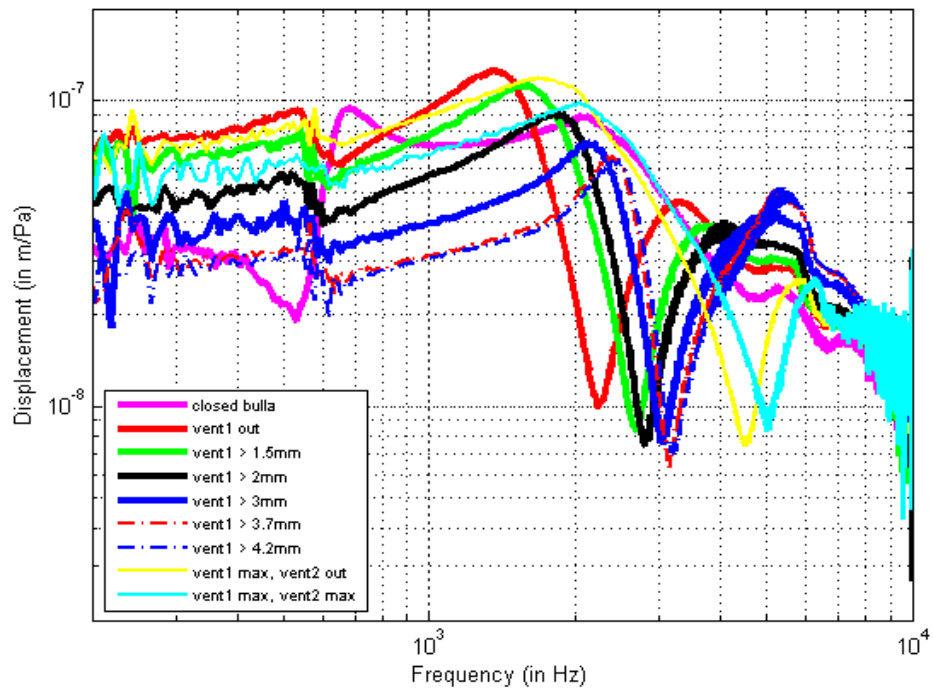


Figure 5.18: Assessing the effect of bullar hole on the umbo frequency responses in gerbil A.

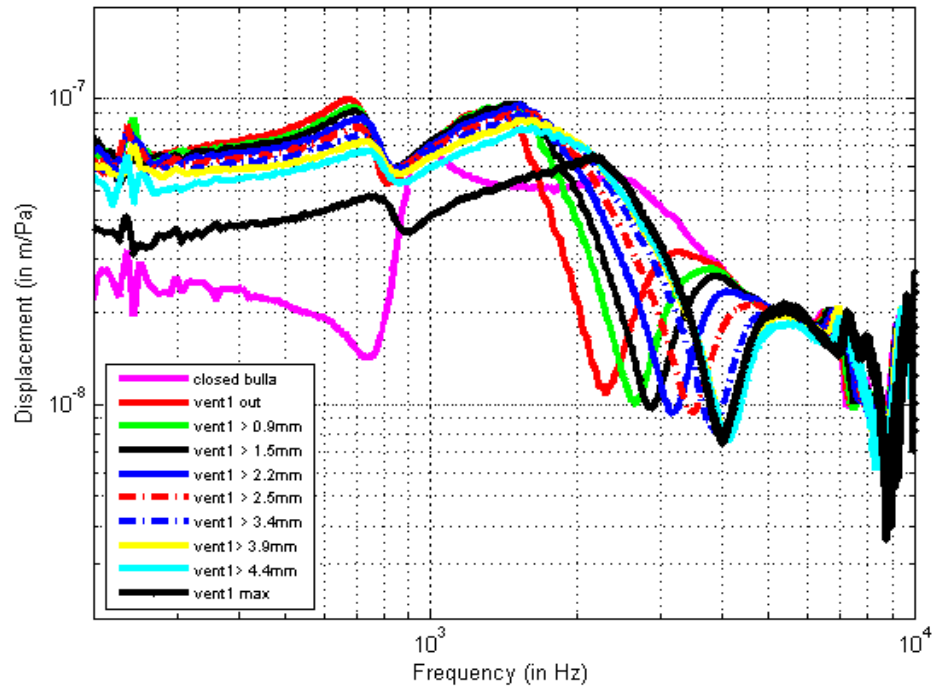


Figure 5.19: Assessing the effect of bullar hole on the umbo frequency responses in gerbil C.

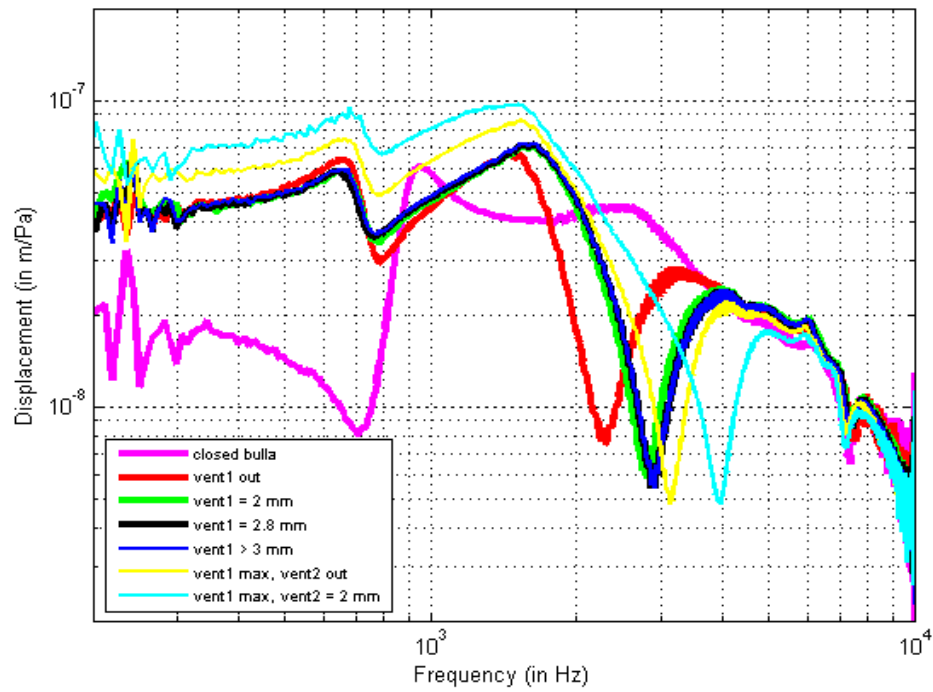


Figure 5.20: Assessing the effect of bullar holes on the umbo frequency responses in gerbil D.

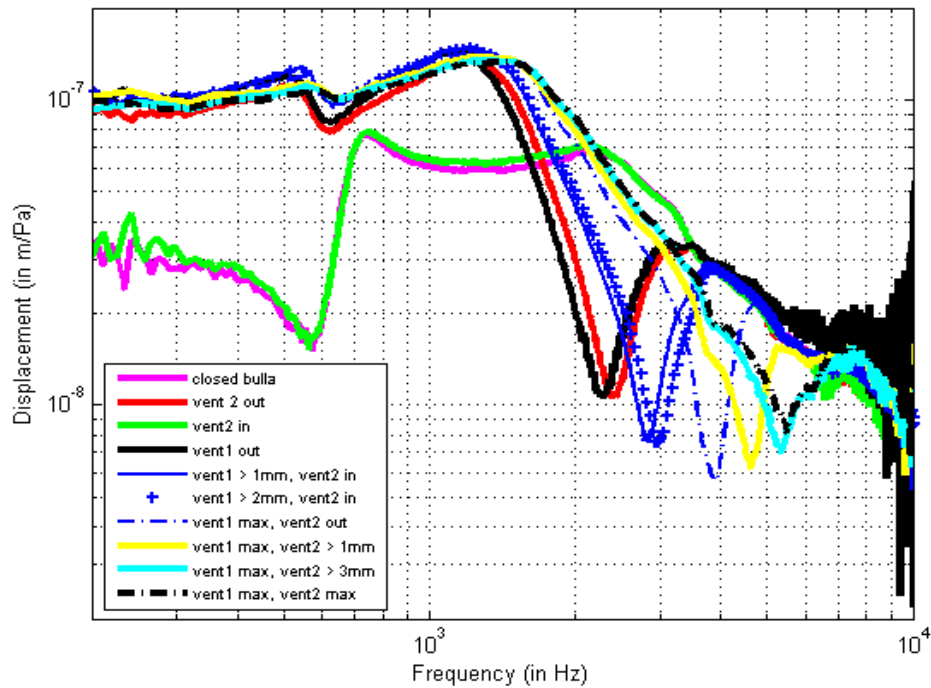


Figure 5.21: Assessing the effect of bullar holes on the umbo frequency responses in gerbil E.

### 5.2.5 Comparison with previous studies

In this section, our umbo measurements are first compared with those reported by Rosowski et al. (1997) for both closed and open middle-ear configurations. We then briefly compare our results with the studies of Cohen et al. (1993) and Ellaham (2007).

Figure 5.22 shows the closed-bulla umbo measurements reported by Rosowski et al. (1997) and those recorded in our gerbils A to L, excluding gerbils H and J since their umbo responses are not comparable to the others with respect to the time of measurement (see Section 5.2.1). The displacement values corresponding to the velocity data reported by Rosowski et al. (1997) were calculated by manually choosing points from their umbo velocity response and dividing those velocities by the corresponding angular frequencies.

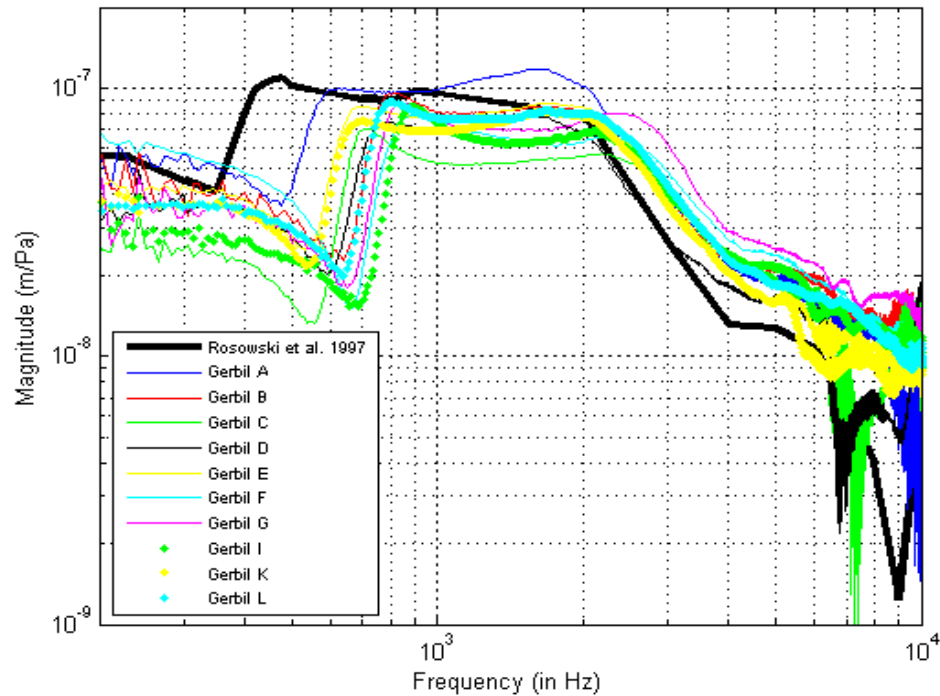


Figure 5.22: Comparison of umbo displacements with those of Rosowski et al. (1997)

In Figure 5.22 we observe that the shapes of our responses are similar to those obtained by Rosowski et al.. At low frequencies our displacement responses are flat, similar to those of Rosowski et al., indicating that the system is stiffness-dominated at these frequencies. However, some differences can be observed in the low-frequency resonance structures. The resonance peak, referred to as a pars-flaccida resonance by Rosowski et al., can be seen at approximately 650 Hz for gerbil A and >650 Hz for the other animals. This is higher than the 450 Hz observed by Rosowski et al.. Such differences between the two studies might be due to temporal effects such as dehydration of the middle-ear structures. The differences seen among our umbo measurements may also be due in part to different drying effects. Although each of these measurements was taken at the start of the experiment, the duration between the time of sacrifice and the start of the actual recording varied according to the surgical preparation time and other experimental factors. Furthermore, even for the same delay, the amount of drying may have differed from ear to ear.

In all of our animals, the displacements become flat at frequencies above the pars-flaccida resonance and remain flat until  $\sim 2$  kHz. This is also seen in the results of Rosowski et al. Although somewhat obscured by irregularities and/or noise, a high-frequency roll-off of about  $-12$  dB/octave above 2 kHz can be observed in our gerbils A, C, D, I, K and L. This again agrees with the displacement response of Rosowski et al. and indicates that the system has become mass-dominated.

Table 5.2 compares our closed-bulla displacement measurements with the data reported by Rosowski et al. (1997). The values in the table represent the maximum displacement observed at the tops of the sharp rises in the umbo magnitude responses. In most of the specimens, our umbo displacement measurements are smaller, with 6 of them being within 25% of the value observed by Rosowski et al.

Table 5.2: Maximum umbo displacements, together with the result of Rosowski et al. (1997)

<b>Gerbil studies</b>	<b>Displacements (nm/Pa)</b>
	Maximum displacement
Gerbil A	98
Gerbil B	95.17
Gerbil C	70.6
Gerbil D	74.2
Gerbil E	85.4
Gerbil F	79.5
Gerbil G	88.06
Gerbil I	85.24
Gerbil K	75.37
Gerbil L	88.5
Rosowski et al. (1997)	111

The overall shapes of our open-bulla umbo measurements (Section 5.2.4) are similar to those reported by Rosowski et al. In both cases, an increase in the magnitude of low-frequency vibrations is seen. Moreover, an antiresonance valley at 2-5 kHz can be observed in our results similar to the one at 3 kHz observed by them.

Compared with the umbo responses reported by Cohen et al. and those obtained by Ellaham (2007), our results and those of Rosowski et al. differ in both magnitude and resonant frequencies. The lower low-frequency displacements and the shifts to higher frequencies (of both Cohen et al. and Ellaham) are consistent with much drier middle ears. All our measurements were obtained by maintaining the body of the gerbil intact after euthanasia as opposed to the decapitation technique used by Ellaham (2007), which apparently led to considerable drying.

### **5.3 Manubrial vibrations**

Figure 5.23 shows the points at which we made measurements on the manubrium. Figures 5.24 to 5.33 show the displacements measured at multiple points on the manubrium in all the animals except gerbils D and H. Because of experimental difficulties, measurements were not taken at some nodes in gerbil D; in the case of gerbil H, the measurements were too far apart in time. For each specimen, the location of measurements are indicated with a schematic diagram at the top-left corner of the graph. Each curve presented here is an individual unaveraged measurement recorded at a given location on the manubrium.

From Figures 5.24 to 5.33, we can observe that there is an overall increase in the magnitude at points further down the manubrium, with the maximum displacement attained at the umbo. However, the temporal effects complicate the responses. This is especially observed in gerbil B where the measurements were widely separated in time and clearly show the effects of drying of the middle-ear structures.

The bottom panel of Figure 5.24 shows the displacement at each point normalised to the displacement measured at the short process of the malleus in gerbil A. These displacement ratios are indicative of the manubrial mode of vibration. Amplitude ratios greater than 1 indicate that the displacement at the measured point is greater than that at the short process. At low frequencies (ignoring the low-frequency noise) and mid frequencies, an increase in the amplitude ratio can be observed as we travel downward along the manubrium from the short process of the malleus to the umbo. The amplitude ratios and the similarity of the shapes of the frequency responses over most of the frequency range suggest that the motion of the manubrium follows a simple vibration pattern. This is in agreement with the classical concept of a rigid manubrium and a malleus-incus complex rotating around a fixed axis. Studies on the cat middle-ear (e.g., Decraemer and Khanna, 1994) have indicated that there is a shifting of the axis of rotation and perhaps a bending at the tip of the manubrium at mid and high frequencies. Temporal effects due to drying would need to be carefully taken into consideration before ruling out these possibilities in our data.

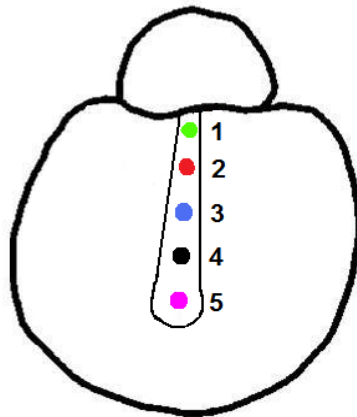


Figure 5.23: A schematic of the gerbil TM showing the points of measurement on the manubrium.

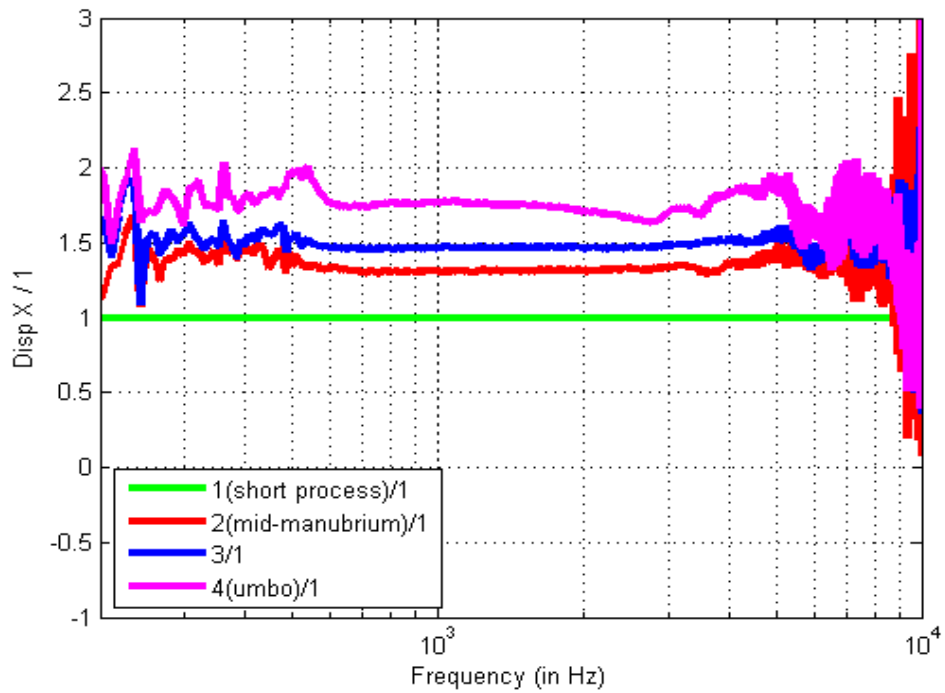
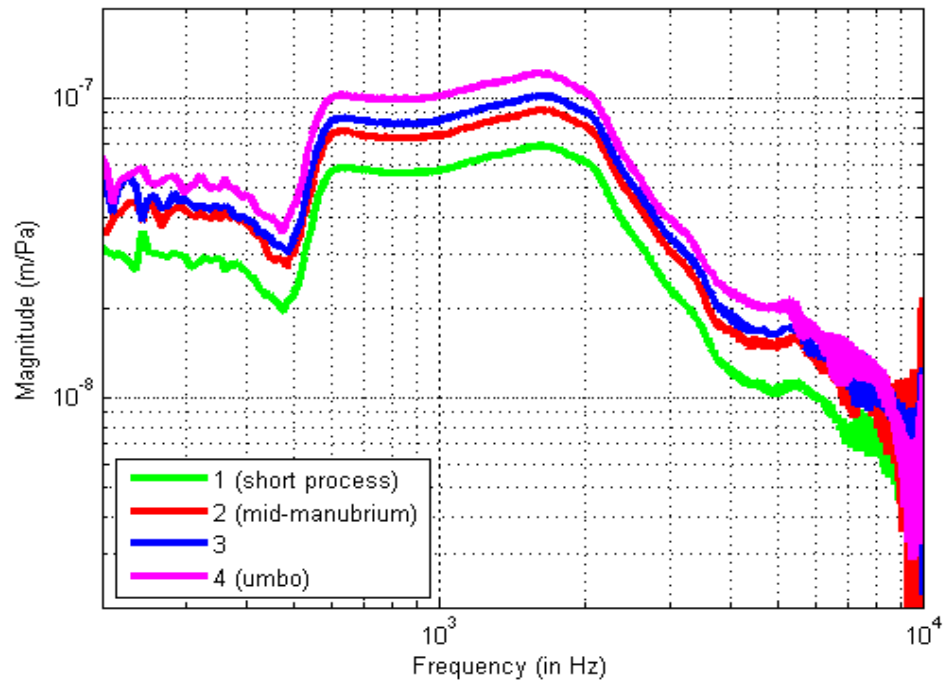


Figure 5.24: Normalised displacements along the manubrium in gerbil A.

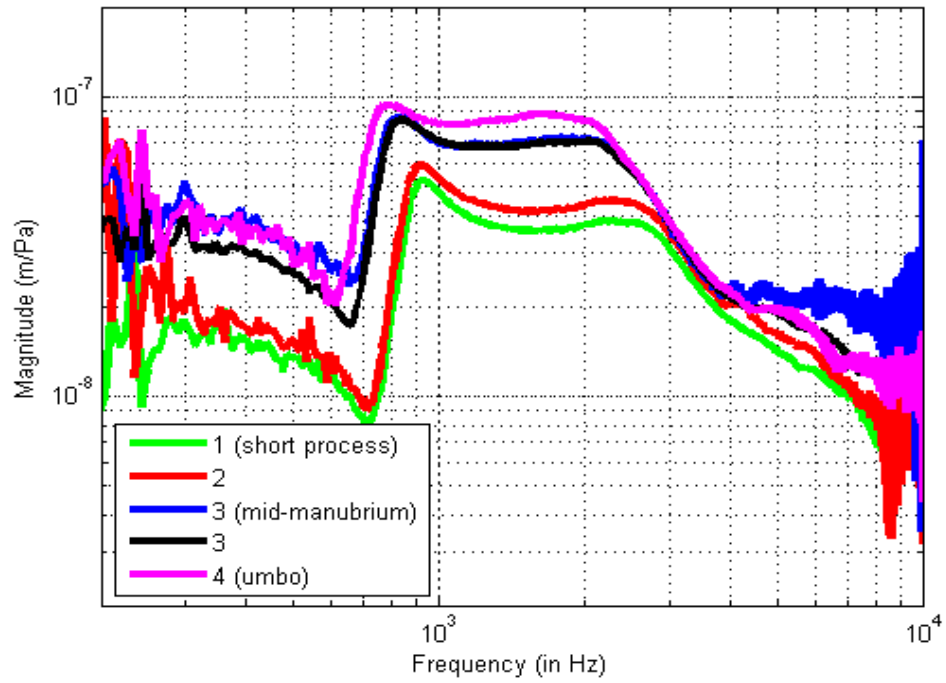


Figure 5.25: Normalised displacements along the manubrium in gerbil B.

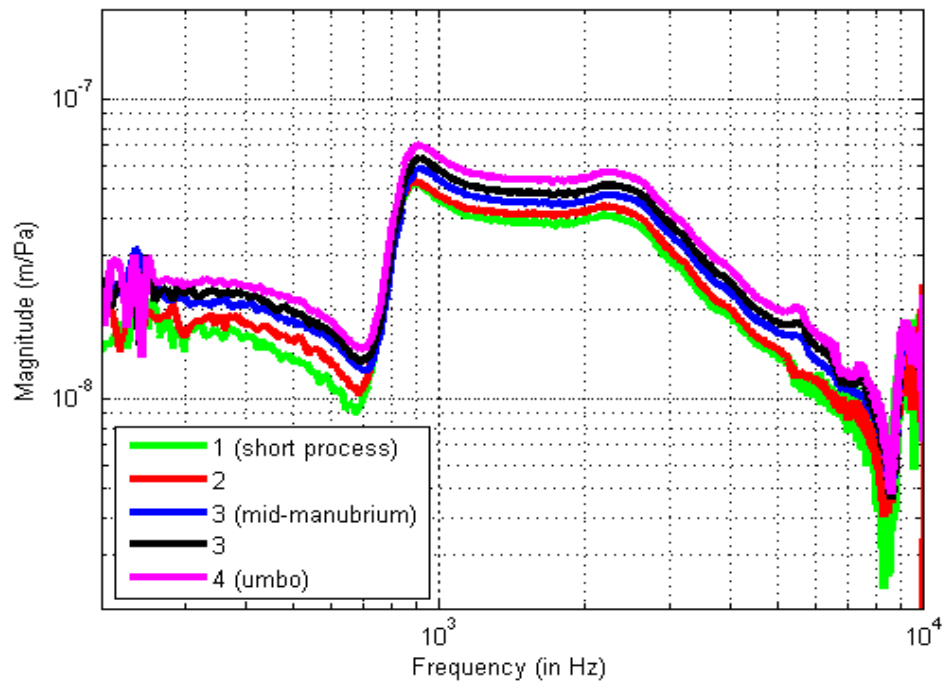


Figure 5.26: Normalised displacements along the manubrium in gerbil C.

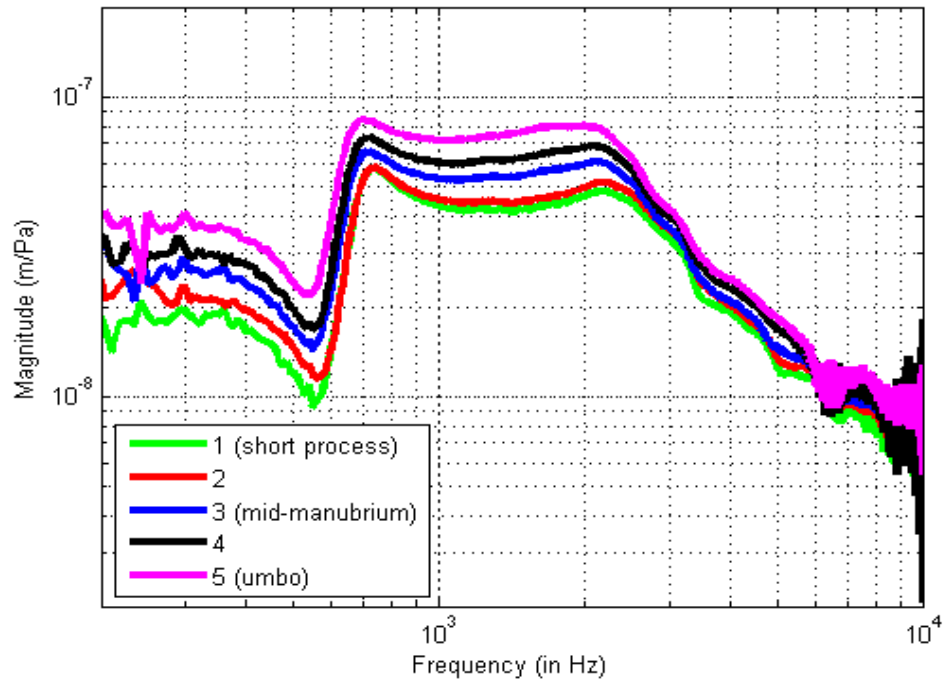


Figure 5.27: Normalised displacements along the manubrium in gerbil E.

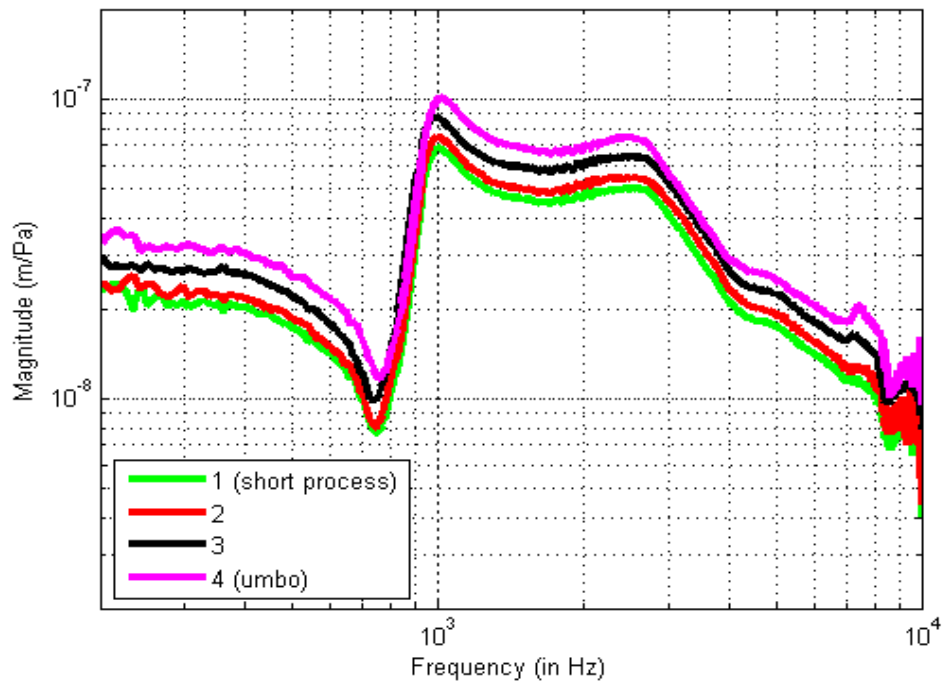


Figure 5.28: Normalised displacements along the manubrium in gerbil F.

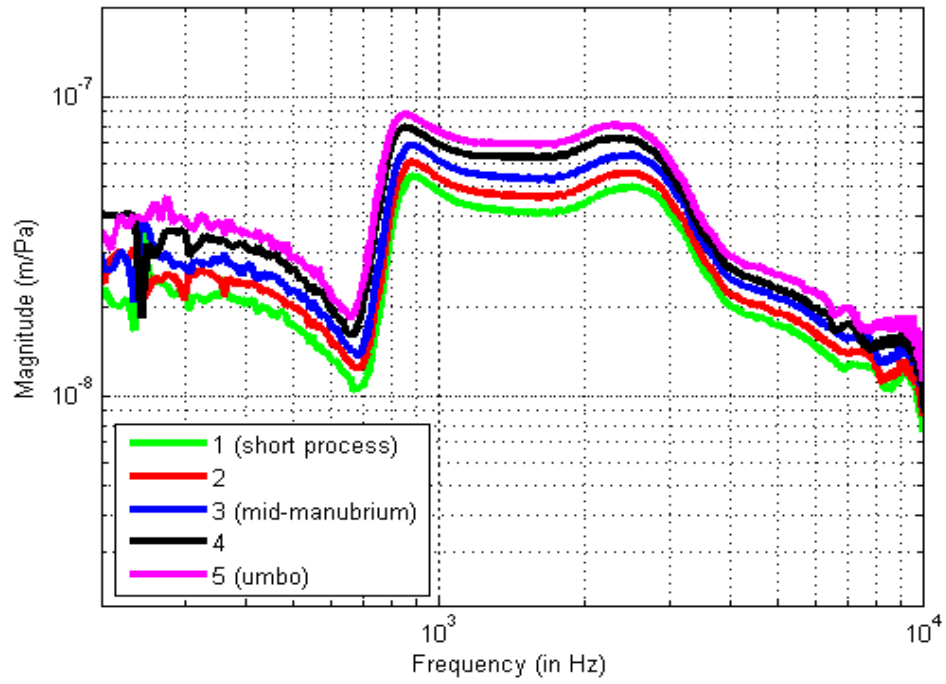


Figure 5.29: Normalised displacements along the manubrium in gerbil G.

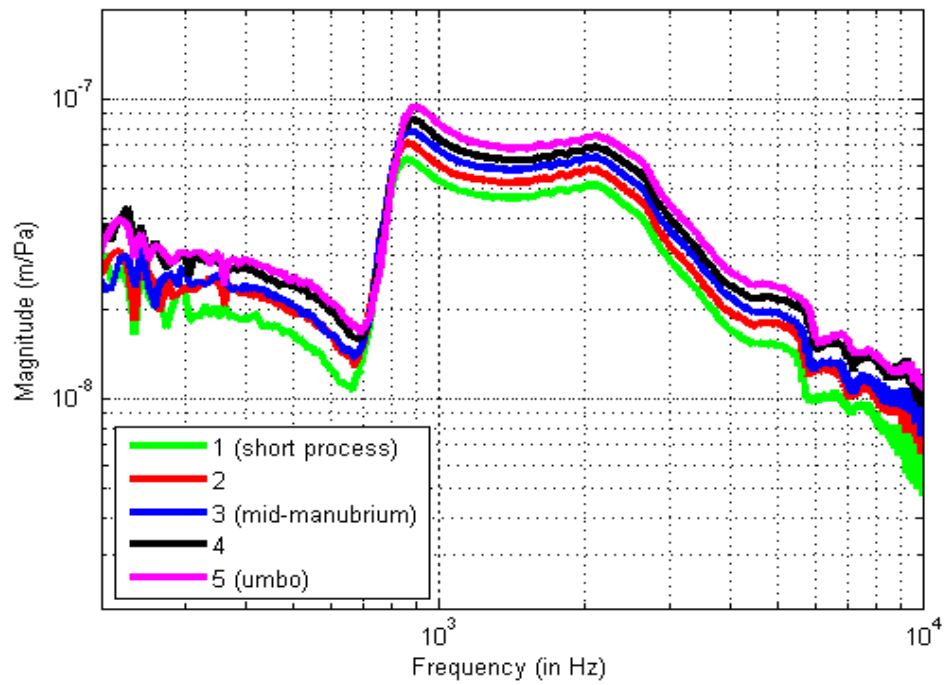


Figure 5.30: Normalised displacements along the manubrium in gerbil I.

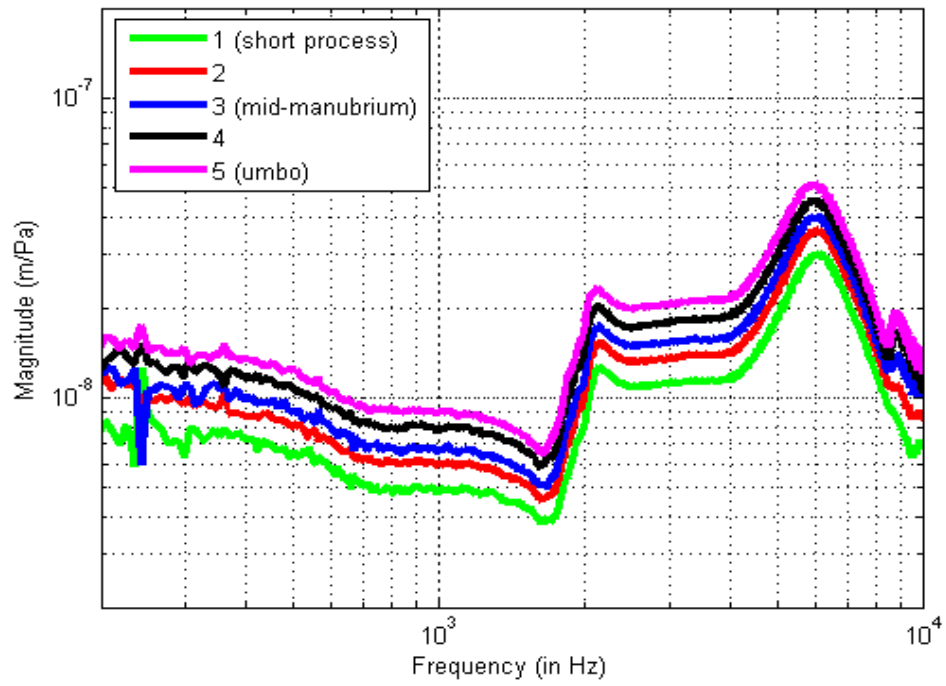


Figure 5.31: Normalised displacements along the manubrium in gerbil J.

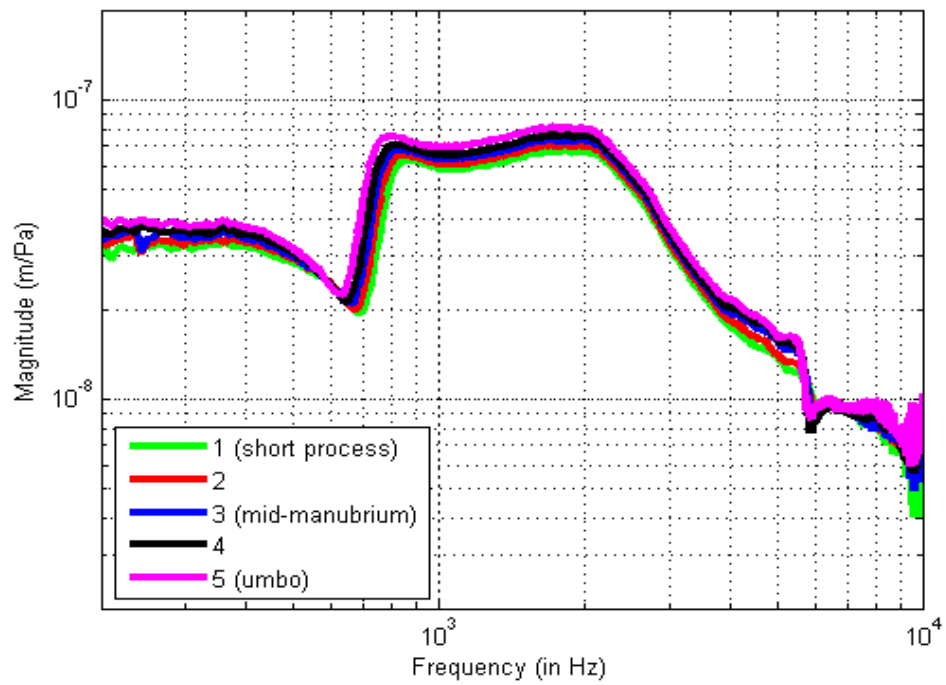


Figure 5.32: Normalised displacements along the manubrium in gerbil K.

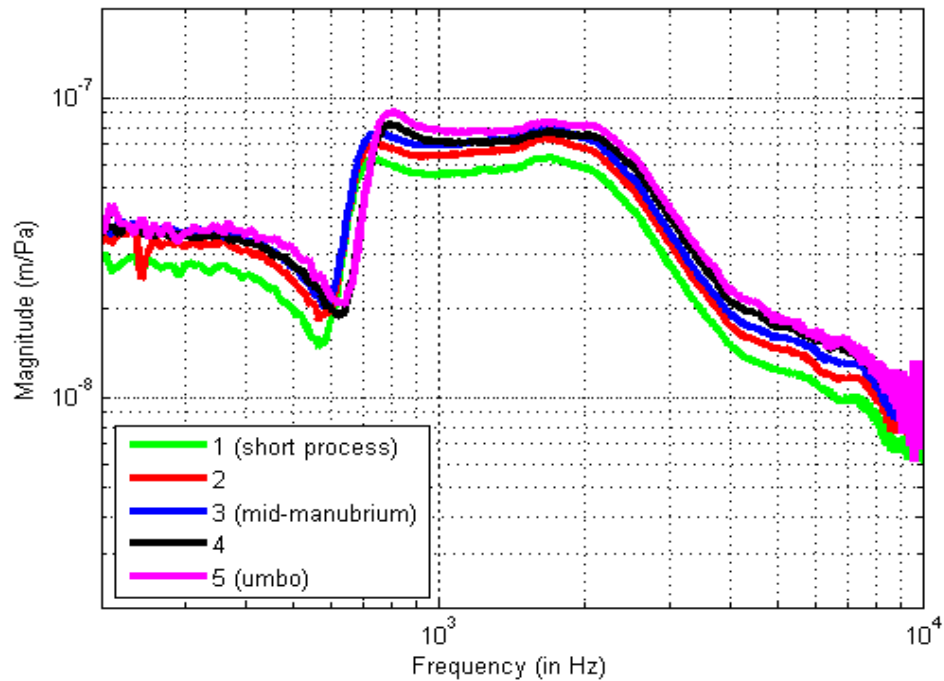


Figure 5.33: Normalised displacements along the manubrium in gerbil L.

## 5.4 Pars-flaccida vibrations

Vibrations were measured at approximately the centre of the pars flaccida in gerbils H to L. The data are presented in Figure 5.34 (top panel). Umbo displacements measured in the same animals are shown for comparison in the bottom panel. For both sets of data the bulla was closed. The amplitudes of the pars-flaccida measurements are on the order of 30 times greater than those of the umbo displacement measurements. The pars-flaccida magnitude response in each specimen has a pronounced resonance peak followed by a smaller peak about an octave higher in frequency, followed in some cases by a third peak. In each gerbil, an increase in the umbo magnitude can be observed at frequencies above the first resonance frequency present in the pars-flaccida magnitude response. These data suggest that the pars flaccida has an important role in the low-frequency hearing sensitivity found in gerbils (Rosowski et al. 1997). In Figure 5.34, inter-specimen discrepancies are observed in the pars flaccida displacements. This variability may be attributable in part to the temporal effects resulting from variations in measurement

timings with respect to the time of sacrifice of the animal.

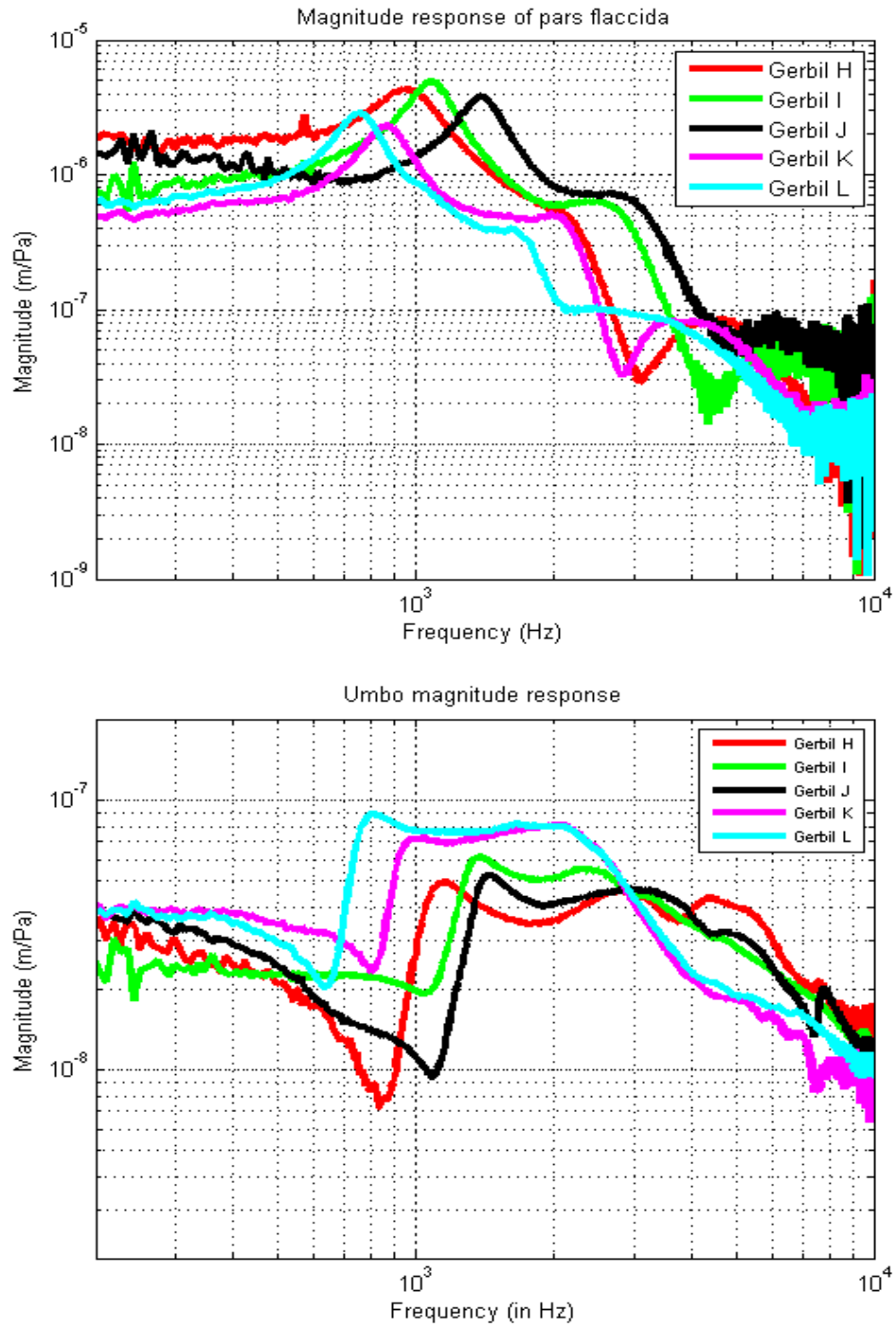


Figure 5.34: Normalised displacements on the pars flaccida (top panel) and the umbo (bottom panel) of gerbils H to L.

## 5.5 Pars-tensa vibrations

The measurement points on the pars tensa are shown in Figure 5.35. Figures 5.36 to 5.45 show closed-bulla displacements measured at multiple points across the visible portion of the pars tensa for 10 specimens (gerbils C to L). Vibration profiles at these points were measured by placing the glass micro-beads along lines normal to and about midway down the manubrium. The arrangement of the beads is shown schematically at the top-left corner of each plot. In most specimens, pars-tensa vibrations were recorded at two points on each side of the manubrium. However, in some of the specimens (gerbils D, E and I) only one point could be measured on one side or both sides of the manubrium. In these animals, the experimental set-up was such that the field of view was limited more than usual by the width of the surgically opened ear canal and/or the position of the gerbil head with respect to the laser head, so that the glass beads farthest from the manubrium were not accessible for measurements.

In these figures we observe that the overall shapes of the pars-tensa responses at frequencies below 3 to 4 kHz ( or 6 kHz in gerbil H) are similar to those measured on the manubrium. The high-frequency resonance structures on the pars tensa are larger and more erratic than those observed in the manubrial magnitude responses, and differ greatly from bead to bead. This is consistent with the fact that the high-frequency vibration patterns of the pars tensa have been observed in other species to be spatially complex and very frequency-dependent.

Even though we observe a huge inter-specimen variability in the high-frequency pars-tensa responses, there are some common patterns. In most of the animals in which there were two points in the anterior region of the pars tensa, the two frequency responses have similar shapes over the entire frequency range. In addition, the pars-tensa measurements at points farthest from the manubrium tend to have larger magnitudes than the measurements on the manubrium and at the points closest to it. Finally, in gerbils D, E, G, H, J, K, and L, the high-frequency vibration patterns in the anterior region of the pars

tensa have sharper and larger resonances than those observed in the posterior region.

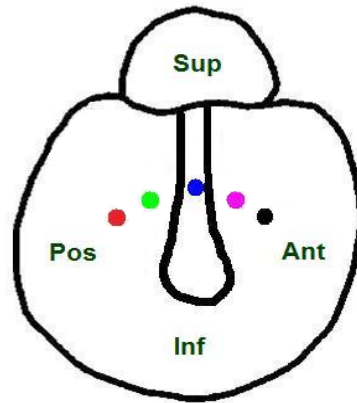


Figure 5.35: A schematic of the gerbil TM showing points of measurement across the pars tensa.

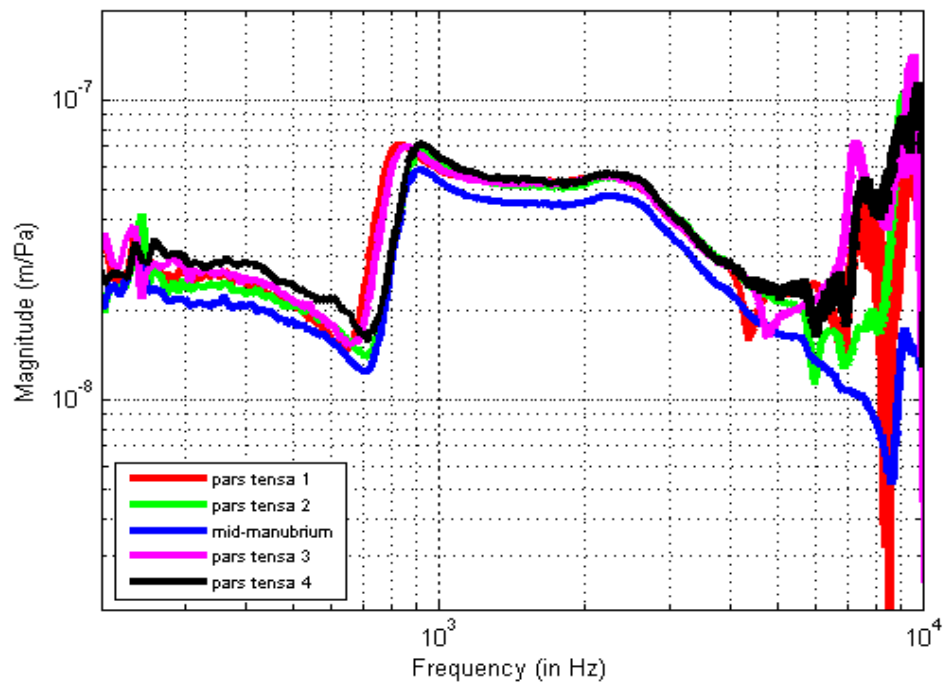


Figure 5.36: Normalised displacements measured on the pars tensa in gerbil C.

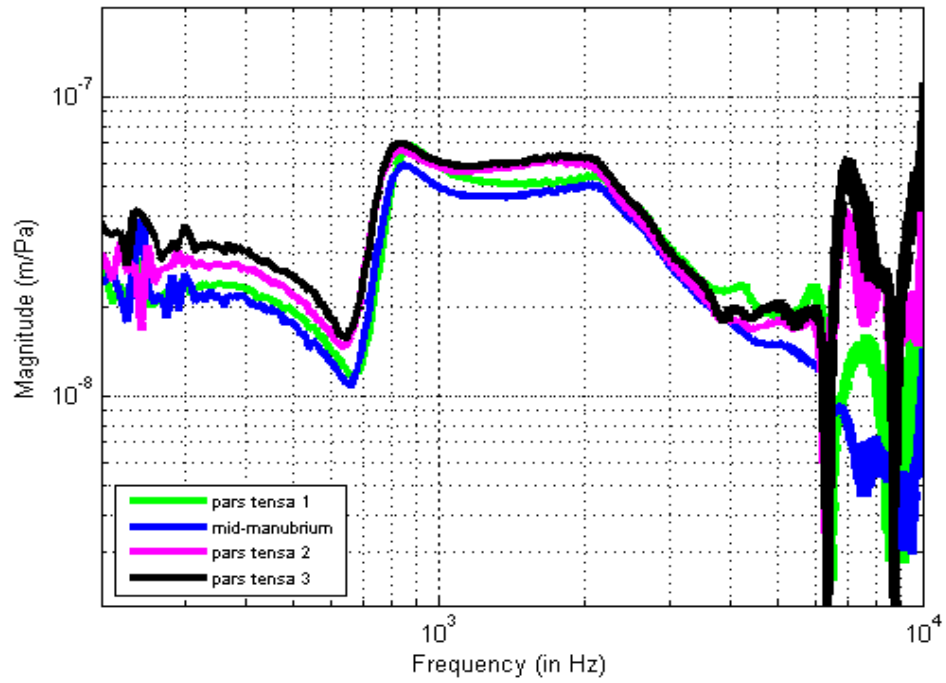


Figure 5.37: Normalised displacements measured on the pars tensa in gerbil D.

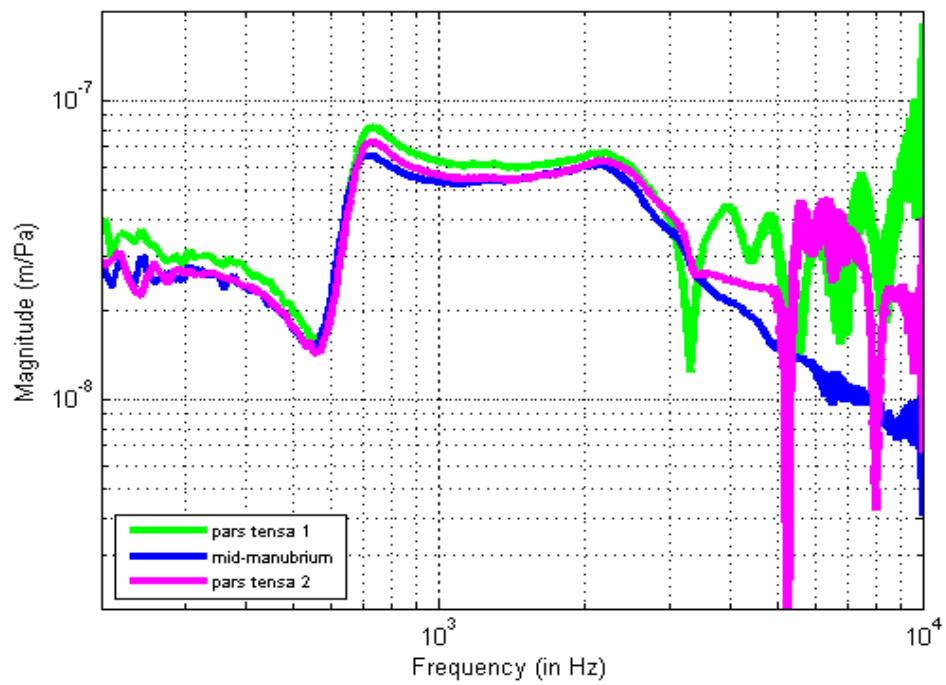


Figure 5.38: Normalised displacements measured on the pars tensa in gerbil E.

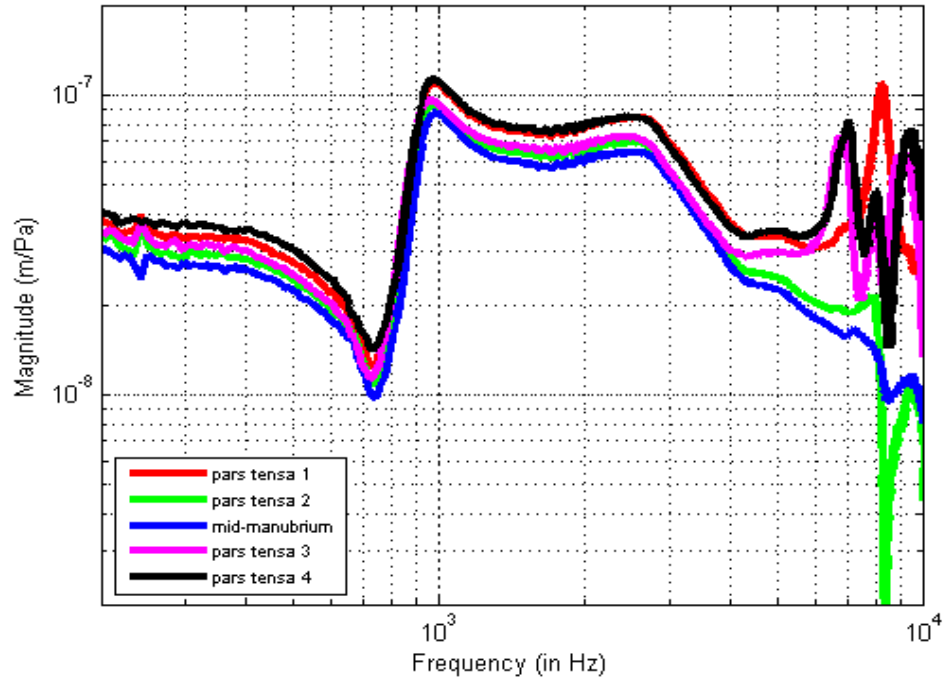


Figure 5.39: Normalised displacements measured on the pars tensa in gerbil F.

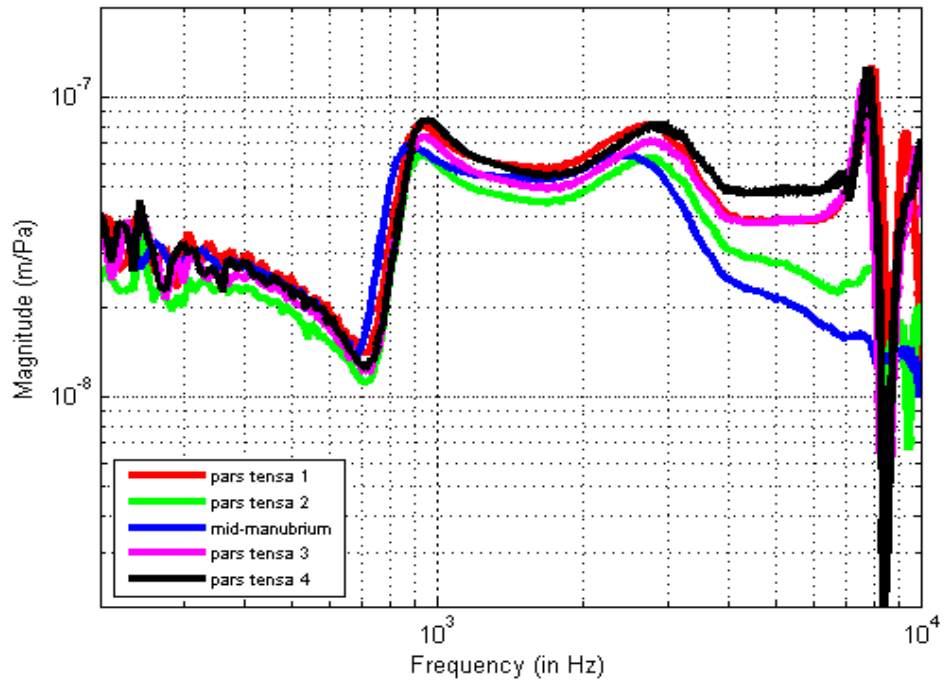


Figure 5.40: Normalised displacements measured on the pars tensa in gerbil G.

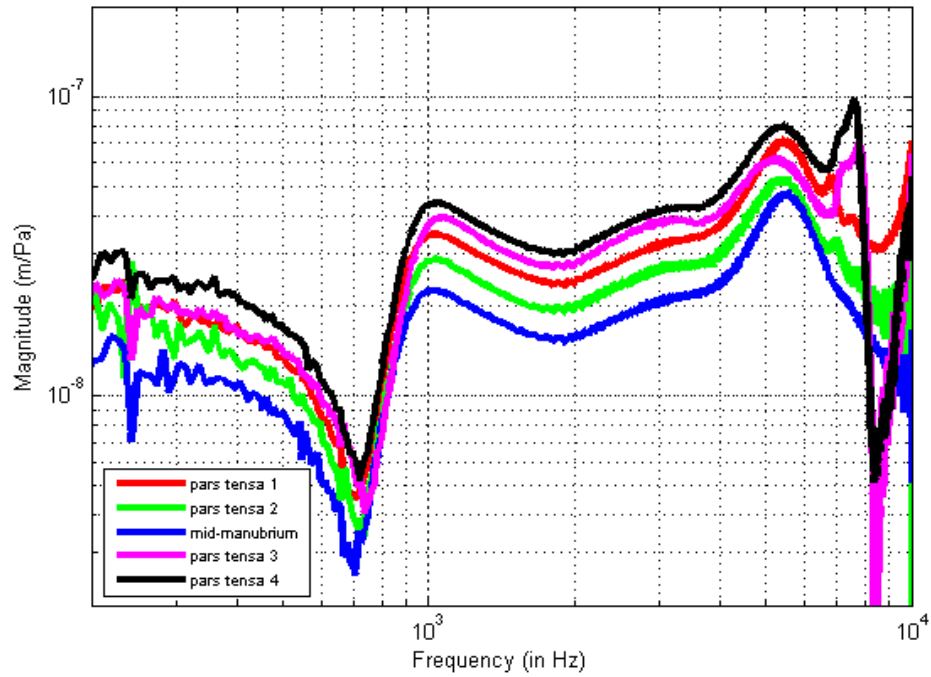


Figure 5.41: Normalised displacements measured on the pars tensa in gerbil H.

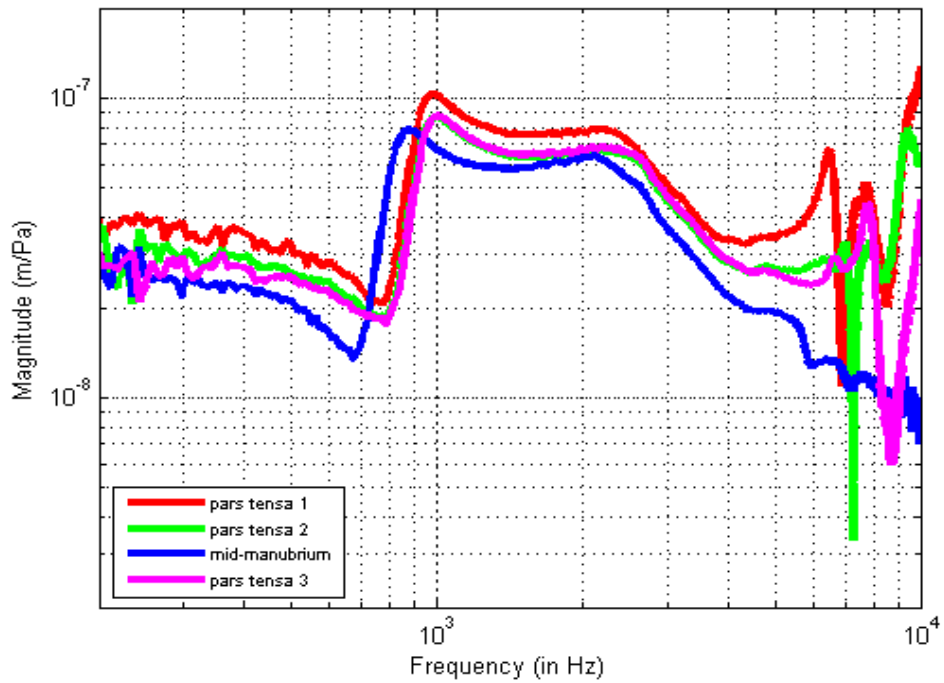


Figure 5.42: Normalised displacements measured on the pars tensa in gerbil I.

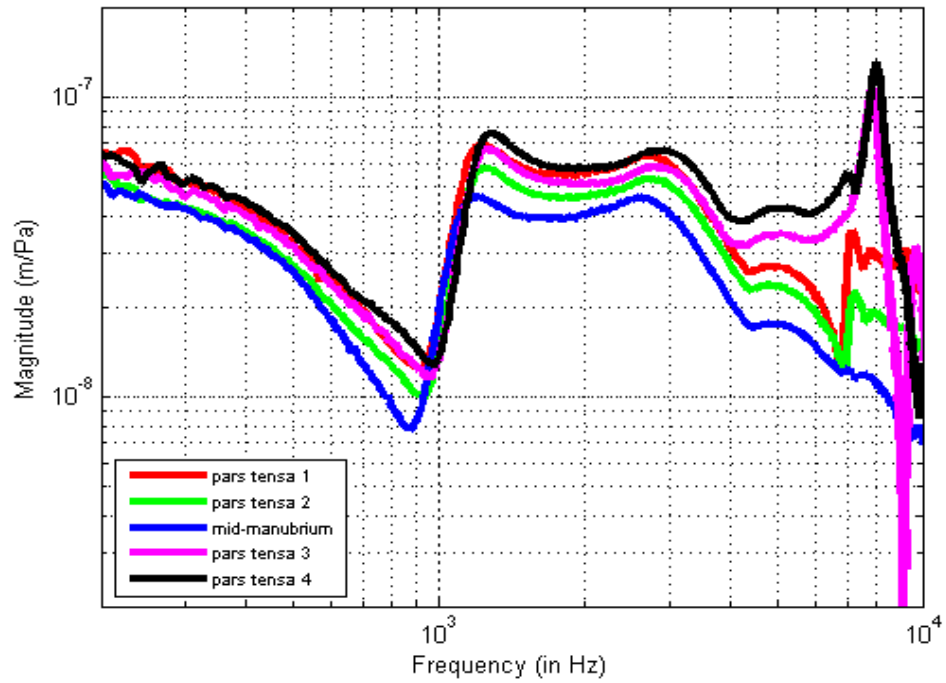


Figure 5.43: Normalised displacements measured on the pars tensa in gerbil J.

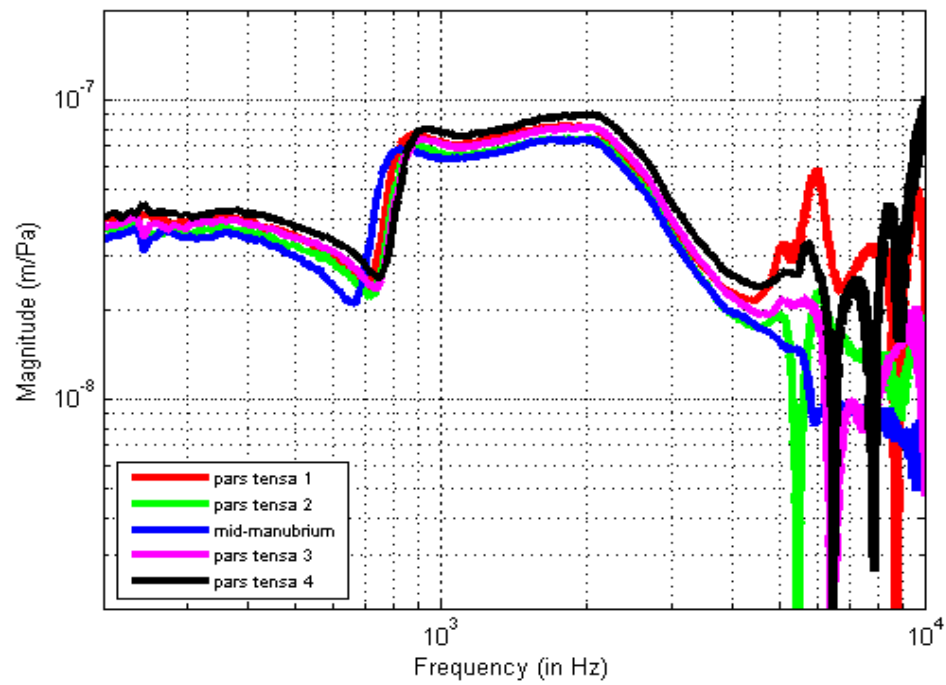


Figure 5.44: Normalised displacements measured on the pars tensa in gerbil K.

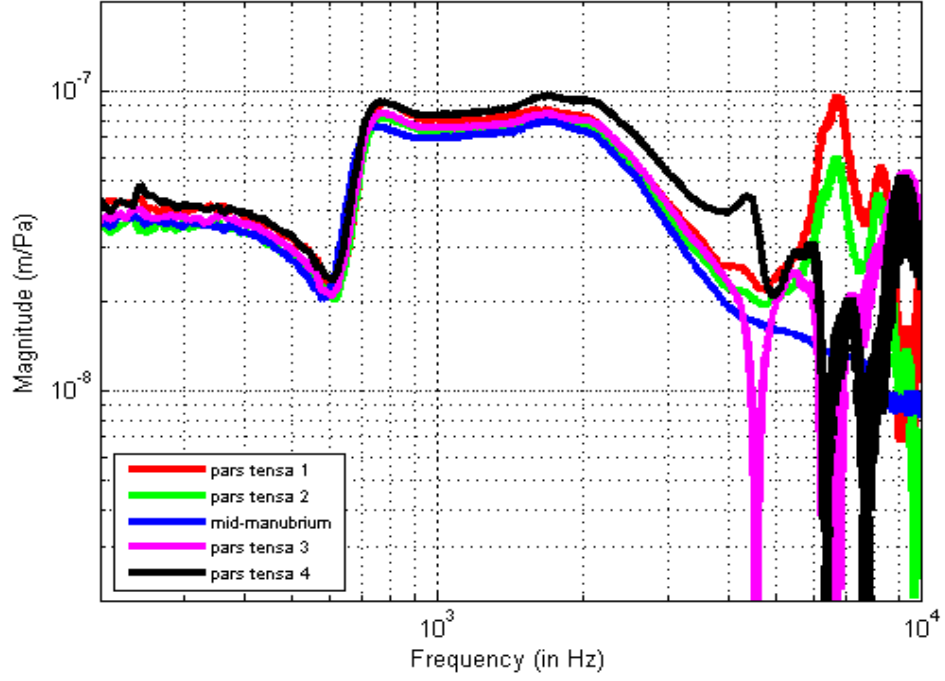


Figure 5.45: Normalised displacements measured on the pars tensa in gerbil L.

## CHAPTER 6 CONCLUSION

### 6.1 Summary

In this work, displacement measurements at multiple points on the gerbil eardrum have been presented with the aim of enhancing our understanding of the mechanics of the gerbil middle ear. Repeatability of these measurements, intra-specimen temporal effects and inter-specimen variability have also been investigated. *Post mortem* displacement frequency responses were acquired using single-point laser Doppler vibrometry (LDV) and analyzed over the frequency range between 0.2 and 10 kHz. All measurements were normalized with respect to the sound pressure level measured near the eardrum.

First, we presented displacement frequency responses measured at the umbo in 12 gerbils. The shape and variability of these responses were studied and a comparison was made with previous measurements presented in other middle-ear studies. Our results match fairly well with the *in vivo* results reported by Rosowski et al. (1997) but show some signs of drying of the middle ear. Time-dependent effects related to drying of middle-ear structures were examined. At low frequencies, reductions in the displacement magnitudes and frequency shifts of the peaks were observed. Magnitude changes also occurred at high frequencies, but were complicated by the frequency shifts of the peaks. To assess the repeatability of our measurements we compared consecutive umbo displacement responses and found that the displacements were quite consistent except at the lowest and highest frequencies. We also investigated the effects of opening the middle-ear cavity in four specimens. As in the case of closed middle-ear measurements, the umbo displacement responses obtained from the open middle ear were similar to those published by Rosowski et al. (1997).

We also studied the spatial vibration patterns along the manubrium of the malleus and at multiple points on the pars flaccida and pars tensa of the tympanic membrane. The vibration characteristics of a point approximately at the centre of the pars flaccida were

presented for 5 gerbils. We found that in all specimens the pars flaccida displacement response showed a sharp resonance peak at a low frequency. Even though some measurement variability was observed, the overall shapes of the curves were similar. We also presented umbo displacement measurements taken at about the same time as the pars flaccida measurements. The magnitude of the umbo response was found to be smaller for frequencies below the pars flaccida resonance frequency. This is consistent with the conclusion by Rosowski et al. (1997) that the pars flaccida vibrations influence low-frequency hearing sensitivity in gerbils.

Characterization of manubrial and tympanic-membrane vibrations at multiple points provides more details than the single-point measurements commonly performed in other middle-ear studies. In this study we have presented the first such multiple-point measurements for the gerbil, apart from two recent studies in which either the sound pressure at the TM was not measured (De La Rochefoucauld & Olson, 2007, 2009) or the middle ear became excessively dry (Ellaham, 2007). The vibration profiles of points along the manubrium (from the short process of the malleus to the umbo) generally showed an overall increase in amplitude. These results are consistent with the traditional notion of a rigid rotation of the incus-malleus complex about a fixed axis. The overall shapes of the manubrial frequency responses were similar at all measurement locations and over most of the frequency range. However, some experiments showed some discrepancies at frequencies ranging from 0.6 to 1 kHz and also at frequencies above 7 kHz, suggestive of temporal effects or frequency-dependent spatial effects or a combination of the two. Further work is required to clarify this issue.

At low and mid frequencies, the shapes of the vibration responses obtained at multiple points on the pars tensa were found to be similar to those measured on the manubrium but the magnitudes were larger (Section 5.5). Gerbil studies using quasi-static moiré interferometry (von Unge et al., 1993; Dirckx & Decraemer, 2001) and low-frequency model simulations (Funnell et al., 2000; Elkhouri et al., 2006) have similarly reported

points of maximum displacement in both anterior and posterior regions of the pars tensa.

We have shown that at frequencies higher than 3 to 6 kHz the frequency responses of points on the gerbil pars tensa become very irregular, indicative of complex frequency-dependent mode of vibrations. The frequency at which such vibration patterns develop is a critical parameter when modelling TM behaviour.

## 6.2 Future Work

An important extension of our study would be to include improved protocols for checking measurement repeatability and temporal effects, particularly associated with the drying of middle-ear structures. One possible way to minimize these *post mortem* effects is to perform *in vivo* measurements. This would in turn help us draw more definitive conclusions related to variability observed in the displacement responses.

The effects of opening the middle-ear space can be further studied by acquiring measurements at all the other points in addition to the umbo. Since the gerbil middle-ear cavity consists of multiple bony compartments, it would be interesting to further study the effects of opening one part of the bulla as opposed to another one. Our results so far for two holes are inconclusive.

Past studies have reported the functional implications of bulla volume in the hearing sensitivity of kangaroo rats (Webster, 1962; Webster & Webster, 1971, 1972). Similar investigations can easily be carried out in the Mongolian gerbil with its enlarged bulla.

It would also be interesting to study the effects of removal or stiffening of the pars flaccida on TM vibration patterns. Such a study was reported by Rosowski et al. (1997) but vibrations were measured only for the umbo.

Extending the study to include more measurement locations on the eardrum would help

to better characterize the mechanics of the middle-ear and thus allow a more complete comparison with model simulations. This, however, would require a larger number of glass micro-beads to be placed on the eardrum, thus requiring a careful study of the effects of these beads.

Dental cement is used to attach the uneven bony rim of the gerbil ear-canal to the fixation device placed under the microscope and the laser head. The angle between the gerbil head and the laser varies between experiments according to the thickness of the dental cement used to achieve the acoustic seal. Slight changes in the angle sometimes limits access to certain points on the eardrum. Moreover, one of the major concerns is that such experimental factors may introduce some unknown variability into the vibration measurements. It might be technically challenging to avoid these issues completely. One plausible solution would be to surgically expose the whole tympanic membrane and to somehow achieve an acoustic seal by attaching the tympanic ring to a coupler. Open middle-ear measurements could then be performed. A widely exposed eardrum would provide easy access to many points for measurements.

Further investigations of manubrial vibrations need to be carried out. In order to fully characterize the motion of the manubrium and to address the issues of manubrial bending and shifting of the ossicular axis of rotation, displacement measurements for a range of observation angles need to be acquired to obtain the 3-dimensional components of the vibrations.

## REFERENCES

- Akache F (2005): *An experimental study of middle-ear vibrations in rats*. Master's thesis, McGill University, Montréal.
- Akache F, Funnell WRJ & Daniel SJ (2007): An experimental study of tympanic membrane and manubrium vibrations in rats. *Audiol NeuroOtol* 12: 59–63.
- Beer HJ, Bornitz M, Hardtke HJ, Schmidt R, Hofmann G, Vogel U, Zahnert T & Hüttenbrink KB (1999): Modelling of components of the human middle ear and simulation of their dynamic behavior. *Audiol NeuroOtol* 4: 156–162.
- Békésy G v (1949): The structure of the middle ear and the hearing of one's own voice by bone conduction. *J Acoust Soc Am* 21: 217–232.
- Békésy G v (1960): *Experiments in Hearing*. McGraw Hill, NY, 745 pp.
- Bigelow DC, Swanson PB & Saunders JC (1996): The effect of tympanic membrane perforation size on umbo velocity in the rat. *Laryngoscope* 106: 71–76.
- Bigelow DC, David K & Saunders JC (1998): Effect of healed tympanic-membrane perforations on umbo velocity in the rat. *Ann Otol Rhinol Laryngol* 107: 928–934.
- Bornitz M, Zahnert T, Hardtke HJ & Hüttenbrink KB (1999): Identification of parameters for the middle ear model. *Audiol NeuroOtol* 4: 163–169.
- Buunen TJF & Vlaming MSMG (1981): Laser-Doppler velocity meter applied to tympanic membrane vibrations in cat. *J Acoust Soc Am* 58: 223–228.

- Cohen YE, Doan DE, Rubin DM & Saunders JC (1993): Middle-ear development V: Development of umbo sensitivity in the gerbil. *Am J Otol* 14: 191–198.
- Dahmann H (1930): Zur Physiologie des Hörens- experimentelle Untersuchungen über die mechanik der Gehörknöchelchenkette, sowie über deren Verhalten auf Ton und Luftdruck. *Z Hals Nasen Ohrenheilkd* 27: 329–367.
- Decraemer WF & Khanna SM (1996): Three dimensional vibrations of the malleus in the cat middle ear. *ARO Midwinter Mtg.*
- Decraemer WF & Khanna SM (1997): Vibrations on the malleus measured through the ear canal. *Middle Ear Mechanics in Research and Otosurgery*. Dresden, Ed. K.B. Hüttenbrink, 32–39.
- Decraemer WF & Khanna SM (2001): Complete 3-dimensional motion of the ossicular chain in a human temporal bone. *ARO Midwinter Mtg.*
- Decraemer WF, Khanna SM & Funnell WRJ (1989): Interferometric measurement of the amplitude and phase of tympanic membrane vibrations in cat. *Hear Res* 38: 1–18.
- Decraemer WF, Khanna SM & Funnell WRJ (1991): Malleus vibration mode changes with frequency. *Hear Res* 54: 305–318.
- Decraemer WF, Khanna SM & Funnell WRJ (1994): Modelling the malleus vibration as a rigid body motion with one rotational and one translational degree of freedom. *Hear Res* 72: 1–18.
- de La Rochefoucauld O & Olson E (2007): Exploring sound transmission through the middle ear by tracing middle ear delay. *ARO Midwinter Mtg.*

- de La Rochefoucauld O & Olson E (2009): A sum of simple and complex motions on the eardrum and manubrium in gerbil. *5th Internat Symp Middle-Ear Mech Res Otol*, Stanford.
- Dirckx JJJ & Decraemer WF (1991): Human tympanic membrane deformation under static pressure. *Hear Res* 51: 93–105.
- Dirckx JJJ & Decraemer WF (2001): Effect of middle ear components on eardrum quasi-static deformation. *Hear Res* 157: 124–137.
- Dirckx JJJ, Decraemer WF, von Unge M & Larsson Ch (1998): Volume displacement of the gerbil eardrum pars flaccida as a function of middle ear pressure. *Hear Res* 118: 35–46.
- Dirckx JJ, Buytaert J & Decraemer WF (2006): Quasi-static transfer function of the rabbit middle ear, measured with a heterodyne interferometer with high-resolution position decoder. *J Assoc Res Otol* 7: 339–351.
- Doan DE, Igic PG & Saunders J (1996): Middle-ear development VII: Umbo velocity in the neonatal rat. *J Acoust Soc Am* 99: 1566–1572.
- Elkhoury N, Liu H & Funnell WRJ (2006): Low-frequency finite-element modelling of the gerbil middle ear. *J Assoc Res Otolaryngol* 7: 399–411.
- Ellaham N (2007): *An experimental study of middle-ear vibrations in gerbils*. Master's thesis, McGill University, Montréal.
- Finck A & Sofonglu (1966): Auditory sensitivity of the Mongolian gerbil. *J Aud Res* 6: 313–319.

- Funnell WRJ (1975): *A theoretical study of eardrum vibrations using the finite-element method*. Ph.D. thesis, McGill University.
- Funnell WRJ (1996): Low-frequency coupling between eardrum and manubrium in a finite element model. *J Acoust Soc Am* 99: 3036–3043.
- Funnell WRJ & Laszlo CA (1978): Modeling of the cat eardrum as a thin shell using the finite-element method. *J Acoust Soc Am* 63: 1461–1467.
- Funnell WRJ & Laszlo CA (1982): A critical review of experimental observations on eardrum structure and function. *ORL* 44: 181–205.
- Funnell WRJ, Khanna SM & Decraemer WF (1992): On the degree of rigidity of the manubrium in a finite-element model of the cat eardrum. *J Acoust Soc Am* 91: 2082–2090.
- Funnell WRJ, Decraemer WFS, von Unge M & Dirckx JJJ (1999): Finite-element modelling of the gerbil eardrum and middle ear. *ARO Midwinter Mtg*.
- Funnell WRJ, Decraemer WFS, von Unge M & Dirckx JJJ (2000): Finite-element modelling of the gerbil eardrum and middle ear. *ARO Midwinter Mtg*.
- Funnell WRJ, Siah TH, McKee MD, Daniel SJ & Decraemer WF (2005): On the coupling between the incus and the stapes in the cat. *J Assoc Res Otolaryngol* 6: 9–18.
- Goode RL, Ball G & Nishihara S (1993): Measurement of umbo vibration in human subjects – method and possible clinical applications. *Am J Otol* 14: 247–251.

- Goode RL, Ball G & Nishihara S (1996): Laser Doppler vibrometer (LDV) – A new clinical tool for the otologist. *Am J Otolaryngol* 17: 813–822.
- Gray H (2000): *Anatomy of the Human Body*. Bartleby.com. www.bartleby.com/107; on-line version of 1918 edition, Lea & Febiger, Philadelphia.
- Gundersen T & Høgmoen K (1996): Holographic vibration analysis of the ossicular chain. *Acta Otolaryngol* 82:16–25.
- Gyo K, Arimoto H & Goode RL (1987): Measurement of the ossicular vibration ratio in human temporal bones by use of a video measurement system. *Acta Otolaryngol* 103: 87–95.
- Hagr AA, Funnell WRJ, Zeitouni AG & Rappaport JM (2004): High-resolution x-ray computed tomographic scanning of the human stapes footplate. *J Otolaryngol* 33: 217–221.
- Hariharan P (2007): *Basics of Interferometry*. 2<sup>nd</sup> Ed. (Academic Press, Sydney)
- Helmholtz HFL (1869): Die Mechanik der Gehörknöchelchen und des Trommelfells, *Pflügers Archiv Physiol* 1, 1–60. English translations — **(1)** Bucks AH, & Smith N (transl.) (1873) *The Mechanism of the Ossicles of the Ear and Membrana Tympani* (Woods, New York), 69 pp. **(2)** Hilton J (transl) (1874). *The Mechanism of the Ossicles and the Membrana Tympani*, (New Sydenham Society, London), 62: 97–155.

- Helmholtz HLF (1877): *Die Lehre von den Tonempfindungen* (Verlag von Fr. Vieweg u. Sohn, Braunschweig), 4<sup>th</sup> ed. English translation — Ellis, AJ (transl.) (1885). *Sensations of Tone* (Longmans, Green & Co., London), 2nd ed. Reprinted (1954). (Dover, New York), 134–135.
- Henry KR, McGinn MD & Chole RA (1980): Age-related auditory loss in the Mongolian gerbil. *Arch Otorhinolaryngol* 228: 233–238.
- Henson OW Jr & Henson MM (2000): The tympanic membrane: highly developed smooth muscle arrays in the annulus fibrosus of mustached bats. *J Assoc Res Otolaryngol* 1, 25–32.
- Henson MM, Rask-Andersen H, Madden VJ & Henson OW (2001a): The human tympanic membrane: Smooth muscle in the region of the annulus fibrosus. *ARO Midwinter Mtg.*
- Henson OW, Henson MM & Cannon J (2001b): Comparative study of smooth muscle and collagen fibers in the attachment zone of the tympanic membrane. *ARO Midwinter Mtg.*
- Huber A, Ball G, Asai M & Goode R (1997): The vibration pattern of the tympanic membrane after placement of a total ossicular replacement prosthesis. In: Hüttenbrink K, ed. *Middle-ear Mechanics in Research and Otosurgery*. Baalsdorf, Germany: UniMedia GmbH, 82–88.
- Huber AM, Schwab C, Linder T, Stoeckli SJ, Ferrazzini M, Dillier N & Fisch U (2001): Evaluation of eardrum laser Doppler interferometry as a diagnostic tool. *Laryngoscope* 111: 501–507.

- Huber AM, Ma F, Felix H & Linder T (2003): Stapes prosthesis attachment: The effect of crimping on sound transfer in otosclerosis surgery. *Laryngoscope* 113: 853–858.
- Jahnke K (2004): *Middle ear surgery – recent advances and future directions*. Thieme, New York, USA.
- Khanna SM & Tonndorf J (1972): Tympanic membrane vibrations in cats studied by time-averaged holography. *J Acoust Soc Am* 51: 1904–1920.
- Kohllöffel LUE (1984): Notes on the comparative mechanics of hearing. III. On Shrapnell's membrane. *Hear Res* 13: 83–88.
- Koike T, Wada H & Kobayashi T (2002): Modeling of the human middle ear using the finite-element method. *J Acoust Soc Am* 111: 1306–1317.
- Kuijpers W, Peters TA & Tonnaer ELGM (1999): Nature of the tympanic membrane insertion into the tympanic bone of the rat. *Hear Res* 128: 80–88
- Kuypers LC, Dirckx JJ, Decraemer WF & Timmermans J (2005): Thickness of the gerbil tympanic membrane measured with confocal microscopy. *Hear Res* 209: 42–52.
- Ladak H, Decraemer WF, Dirckx JJ & Funnell WRJ (2004): Response of the cat eardrum to static pressures: Mobile versus immobile malleus. *J Acoust Soc Am* 116: 3008–3021.
- Lay DM (1972): The anatomy, physiology, functional significance and evolution of specialized hearing organs of gerbilline rodents. *J Morph* 138: 41–120.

- Legoux JP & Wisner A (1955): Role fonctionnel des bulles tympaniques géantes de certains rongeurs (Meriones). *Acustica* 5: 208–216.
- Lim DJ (1968): Tympanic membrane. Electron microscopic observation. Part 1. Pars tensa. *Acta Otolaryngol* 66: 181–198.
- Lim DJ (1968): Tympanic membrane. Electron microscopic observation. Part 2. Pars flaccida. *Acta Otolaryngol* 66: 515–532.
- Lim DJ (1970): Human tympanic membrane. An ultrastructural observation. *Acta Otolaryngol* 70: 176–186.
- Lynch TJ, Nedzelnitsky V & Peak WT (1982): Input impedance of the cochlea in cat. *J Acoust Soc Am* 72: 108–130.
- Lynch TJ, Peake WT & Rosowski JJ (1994): Measurements of the acoustic input impedance of cat ears: 10 Hz to 20 kHz. *J Acoust Soc Am* 96: 2184–2209.
- Merchant SN, Ravicz ME & Rosowski JJ (1996): Acoustic input impedance of the stapes and cochlea in human temporal bones. *Hear Res* 97: 30–45.
- Nakajima HH, Ravicz ME, Rosowski JJ, Peake WT & Merchant SN (2005): Experimental and clinical studies of malleus fixation. *Laryngoscope* 115: 147–154.
- Nishihara S & Goode RL (1997): Measurement of tympanic membrane vibration in 99 human ears. *Proc Internat Workshop Middle-Ear Mech Res Otosurg*, Dresden, Germany, 91–94.

- Oaks E (1967): *Structure and function of inflated middle ears of rodents*. Ph.D. thesis, Yale University, New Haven.
- Olson ES (1998): Observing middle and inner ear mechanics with novel intracochlear pressure sensors. *J Acoust Soc Am* 103: 3445–3463.
- Olson E & Cooper N (2000): Stapes motion and scala vestibuli pressure in gerbil. *ARO Midwinter Mtg.*
- Overstreet EH & Ruggero MA (2002): Development of a wide-band middle-ear transmission in the Mongolian gerbil. *J Acoust Soc Am* 111: 261–270.
- Overstreet EH, Richter CP, Temchin AN, Cheatham MA & Ruggero MA (2003): High-frequency sensitivity of the mature gerbil cochlea and its development. *Audiol NeuroOtol* 8: 19–27.
- Prendergast PJ, Ferris P, Rice HJ & Blayney AW (1999): Vibroacoustic modelling of the outer and middle ear using the finite-element method. *Audiol NeuroOtol* 4: 185–191.
- Rabbitt RD & Holmes MH (1986): A fibrous dynamic continuum model of the tympanic membrane, *J Acoust Soc Am* 80: 1716–1728.
- Ravicz ME, Rosowski JJ & Voigt HF (1992): Sound-power collection by the auditory periphery of the Mongolian gerbil *Meriones unguiculatus*. I: Middle-ear input impedance. *J Acoust Soc Am* 92: 157–177.

- Ravicz ME & Rosowski JJ (1997): Sound-power collection by the auditory periphery of the Mongolian gerbil *Meriones unguiculatus*. III. Effect of variations in middle-ear volume on power collection. *J Acoust Soc Am* 101: 2135–2147.
- Ravicz ME & Rosowski JJ (2004): High-frequency sound transmission through the gerbil middle ear. *ARO Midwinter Mtg*.
- Rodriguez Jorge J, Zenner HP, Hemmert W, Burkhardt C, Gummer AW (1997): Laservibrometrie: ein mittelohr- und Kochelaanalysator zur nichtinvasiven Untersuchung von Mittel- und Innenohrfunktionsstörungen. *Hals Nasen Ohren*, 45:997–1007.
- Rosowski JJ, Davis PJ, Merchant SN, Donahue KM & Coltrera MD (1990): Cadaver middle ears as models for living ears: Comparisons of middle-ear input immittance. *Ann Otol Rhinol Laryngol* 99:403–412.
- Rosowski JJ, Teoh SW & Flandermeyer DT (1997): The effect of pars flaccida on the sensitivity to sound; in Lewis ER, Long GR, Lyon RF, Narins PM, Steele CR, Hecht-Poinar E (eds): *Diversity in Auditory Mechanics*. Singapore, World Scientific, 129–135.
- Rosowski JJ, Ravicz ME, Teoh SW & Flandermeyer D (1999): Measurements of middle-ear function in the Mongolian gerbil, a specialized mammalian ear. *Audiol NeuroOtol* 4: 129–136.
- Rosowski JJ, Brinsko KM, Tempel BI & Kujawa KG (2003a): The aging of the middle ear in 129S6/SvEvTac and CBA/CaJ mice: measurements of umbo velocity, hearing function, and the incidence of pathology. *J Assoc Res Otolaryngol* 4: 371–383.

- Rosowski JJ, Cheng JT, Ravicz ME, Hulli N, Hernandez-Montes M, Harrington E & Furlong C (2009): Computer-assisted time-averaged holograms of the motion of the surface of the mammalian tympanic membrane with sound stimuli of 0.4–25 kHz. *Hear Res* 253: 83–96.
- Rosowski JJ, Furlong C, Ravicz ME, Rodgers MT (2007): Real-time opto-electronic holographic measurements of sound-induced tympanic membrane displacements. In: Huber, A., Eiber, A. (Eds.), *Middle-Ear Mechanics in Research and Otology* 295–305.
- Rosowski JJ, Mehta RP & Merchant SN (2003b): Diagnostic utility of laser-Doppler vibrometry in conductive hearing loss with normal tympanic membrane, *Otol Neurotol* 24:165–175.
- Rosowski JJ, Huber AM, Ravicz ME & Goode RL (2004): Are temporal bones useful models of human middle-ear mechanics?, *ARO Midwinter Mtg.*
- Rosowski JJ, Rodgers MT, Ravicz ME & Furlong C (2007): Preliminary analyses of tympanic-membrane motion from holographic measurements, *ARO Midwinter Mtg.*
- Rosowski JJ, Nakajima HH & Merchant SN (2008): Clinical utility of laser-Doppler vibrometer measurements in live normal and pathologic human ears, *Ear Hear* 29: 3-19.
- Ruggero MA & Temchin AN (2003): Middle-ear transmission in humans: wide-band, not frequency-tuned? *Acoustic Research Letters Online* 4: 53–58.
- Ryan A (1976): Hearing sensitivity of the Mongolian gerbil, *Meriones unguiculatis*, *J Acoust Soc Am* 59: 1222–1226.

- Sun Q, Gan RZ, Chang KH & Dormer KJ (2002): Computer-integrated finite element modeling of human middle ear. *Biomech Model Mechanobiol* 1:109–122.
- Swanepoel, De Wet (2008): Infant hearing loss in developing countries: a silent health priority. *Audiol Today* 20: 16–24.
- Tonndorf J & Khanna SM (1972): Tympanic-membrane vibrations in human cadaver ears studied by time-averaged holography. *J Acoust Soc Am* 52: 1221–1233.
- Vander AJ, Sherman JH & Luciano DS (2004): *Human physiology: The mechanisms of body function*. ninth edition (McGraw Hill, Sydney).
- Vlaming MSMG & Feenstra L (1986): Studies on the mechanics of the normal human middle ear. *Clin Otolaryngol* 11:353–363.
- Vogel U, Zahnert T, Hofmann G, Offergeld C & Hüttenbrink KB (1996): Laser vibrometry of the middle ear: opportunities and limitations. *Middle ear Mech Res Otolaryngol*, edited by K.B. Hüttenbrink (UniMedia GmbH, Dresden), 128–133.
- von Unge M, Bagger-Sjöbäck D & Borg E (1991): Mechanoacoustic properties of the tympanic membrane: a study on isolated Mongolian gerbil temporal bones. *Am J Otol* 12: 407–419.
- von Unge M, Decraemer WF, Bagger-Sjöbäck D & Dirckx JJ (1993): Displacement of the gerbil tympanic membrane under static pressure variations measured with a real-time differential moiré interferometer. *Hear Res* 70: 229–242.

- von Unge M, Decraemer WF, Dirckx JJ & Bagger-Sjöbäck D (1995): Shape and displacement patterns of the gerbil tympanic membrane in experimental otitis media with effusion. *Hear Res* 82: 184–196.
- von Unge M, Decraemer WF, Dirckx JJ & Bagger-Sjöbäck D (1999): Tympanic membrane displacement patterns in experimental cholesteatoma. *Hear Res* 128: 1–15.
- Voss SE, Rosowski JJ, Merchant SN & Peake WT (2000): Acoustic responses of the human middle ear. *Hear Res* 150: 43–69.
- Voss SE, Rosowski JJ, Merchant SN & Peake WT (2001): Middle-ear function with tympanic-membrane perforations. II. A simple model. *J Acoust Soc Am* 110: 1445–1452.
- Wada H, Metoki T & Kobayashi T (1992): Analysis of dynamic behavior of human middle ear using a finite-element method. *J Acoust Soc Am* 92: 3157–3168.
- Weber M (1927): *Die Säugetiere*. Vol. 1, p. 202. Fischer, Jena.
- Webster D & Webster M (1972): Kangaroo rat auditory thresholds before and after middle ear reduction. *Brain Behav Evol* 5: 41–53.
- Wever EG & Lawrence M (1954): *Physiological Acoustics*. Princeton University Press, Princeton, NJ.
- Whittemore KR, Merchant SN, Poon BB, Rosowski JJ (2004): A normative study of tympanic membrane motion in humans using a laser Doppler vibrometer (LDV). *Hear Res* 187:85–104.

Willi UB (2003): *Middle-ear Mechanics: The Dynamic Behavior of the Incudo-Malleolar Joint and its Role During the Transmission of Sound*. Ph.D. thesis, Universität Zürich.

Yang X & Henson OW Jr (2002): Smooth muscle in the annulus fibrosus of the tympanic membrane: physiological effects on sound transmission in the gerbil. *Hear Res* 164: 105–114.

Zimmer WM, Deborah FR & Saunders JC (1994): Middle-ear development VI: Structural maturation of the rat conducting apparatus. *Anat Rec* 239: 475–484.

polytec.com: Polytec Vibrometer University, Retrieved April 1, 2008.

[http://www.polytec.com/usa/158\\_463.asp?highlightSubMenu=Vibrometer%20University](http://www.polytec.com/usa/158_463.asp?highlightSubMenu=Vibrometer%20University)

International Electrotechnical Commission (IEC) in Safety of laser products – Part 1: Equipment classification, requirements and user's guide, IEC 60825-1, Geneva.